Reappraisal of the morphology and phylogenetic relationships of the alligatoroid crocodylian *Diplocynodon hantoniensis* from the late Eocene of the United Kingdom

JONATHAN P. RIO[1*,] PHILIP D. MANNION[2,] EMANUEL TSCHOPP[3,] JEREMY E. MARTIN[4] and MASSIMO DELFINO[5,6]

[1]*Department of Earth Science and Engineering, Imperial College London, South Kensington Campus, London, SW7 2AZ, UK*
[2]*Department of Earth Sciences, University College London, Gower Street, London, WC1E 6BT, UK*
[3]*Division of Paleontology, American Museum of Natural History, Central Park West at 79th Street, New York, 10024–5192, USA*
[4]*Université Lyon, ENS de Lyon, Université Lyon 1, CNRS, UMR 5276 Laboratoire de Géologie de Lyon: Terre, Planète, Environnement, Lyon, France*
[5]*Dipartimento di Scienze della Terra, Università di Torino, Via Valperga Caluso 35, 10125 Torino, Italy*
[6]*Institut Català de Paleontologia Miquel Crusafont, Universitat Autònoma de Barcelona, Edifici ICTAICP, Carrer de les Columnes s/n, Campus de la UAB, 08193 Cerdanyola del Vallès, Barcelona, Spain*

Diplocynodon is a genus of basal alligatoroid comprising nine species, which spanned the late Palaeocene to middle Miocene of Europe. Despite recent revisions of most *Diplocynodon* species, one of the earliest named and most complete, *Diplocynodon hantoniensis*, has not been re-described for over 150 years. This species is known from the remains of numerous individuals from the Priabonian (late Eocene) Headon Hill Formation, which crops out at Hordle (Hordwell) Cliff in Hampshire, United Kingdom. Here we re-describe and diagnose *Diplocynodon hantoniensis*, providing the first detailed description of postcranial anatomy in *Diplocynodon*, and indeed any basal alligatoroid. *Diplocynodon hantoniensis* is diagnosed by four autapomorphies, including retention of the ectopterygoid–pterygoid flexure through ontogeny and a unique anterior process of the ectopterygoid adjacent to the posteriormost maxillary alveoli. A critical review of previously referred remains from elsewhere in Europe and the USA restricts *Diplocynodon hantoniensis* to the late Eocene of the UK. Through comparisons with extant crocodylians, the well-preserved postcranial skeleton enables the interpretation of numerous muscle attachments in the forelimbs and hindlimbs, providing a potentially rich source of character data for future phylogenetic analyses. Based on a comparison of humeral morphology between a large sample of crocodylian species, we outline two new morphological characters in the humerus. We include *D. hantoniensis* in a phylogenetic analysis, including all putative *Diplocynodon* species (103 taxa scored for 187 characters). We use four different character-weighting schemes: equal weighting, implied weighting (*k* value = 8) and extended implied weighting with *k*-values of 4 and 8. In general, these weighted analyses produce congruent results with the equal-weights analysis, and increase the resolution within *Diplocynodon*. We recover a monophyletic *Diplocynodon* in three of the four analyses. However, the fourth analysis, with the strongest downweighting of homoplastic characters and missing data (extended implied weighting with *k* = 4), recovers the Palaeocene *Diplocynodon remensis* outside *Diplocynodon*. Our comprehensive revision of one of the most completely known *Diplocynodon* species facilitates comparisons in the genus, as well as between other basal alligatoroids, and forms the basis for comparing postcranial anatomy in other fossil crocodylians.

KEYWORDS: Crocodyliformes – Crocodylomorpha – *Diplocynodon* – Eocene – implied weights – phylogenetic analysis – postcrania.

*Corresponding author. E-mail: jonathan.rio12@imperial.ac.uk

INTRODUCTION

Alligatoroids such as *Deinosuchus* and *Leidyosuchus* first appear in the fossil record in Campanian (latest Cretaceous) deposits in North America (Brochu, 1999). After diverging into alligatorines and caimanines approximately 66 Mya (Brochu, 1999; Roos *et al.*, 2007; and possibly earlier: see Bona *et al.*, 2018), alligatoroids dispersed in the Palaeocene, with caimanines present in South America (e.g. Brochu, 2011), alligatorines living alongside basal alligatoroids in North America (e.g. Brochu, 1997) and basal alligatoroids in both Asia (Wang *et al.*, 2016) and Europe (Martin *et al.*, 2014; Puértolas-Pascual *et al.*, 2016).

Diplocynodon is a genus of basal alligatoroid (Brochu, 1999) whose fossil record extends from the late Palaeocene to the middle Miocene of western Europe (Martin, 2010; Martin & Gross, 2011; Delfino & Smith, 2012; Martin *et al.*, 2014; Díaz Aráez *et al.*, 2017). Nine species are currently considered valid, comprising: (1) *Diplocynodon remensis* Martin *et al.*, 2014 from the late Palaeocene of France, (2) the middle Eocene species *D. darwini* Ludwig, 1877 (Hastings & Hellmund, 2015) and *D.* (*Baryphracta*) *deponiae* Frey *et al.*, 1987 (Delfino & Smith, 2012) from Germany and *D. tormis* Buscalioni *et al.*, 1992 from Spain (3) *D. elavericus* Martin, 2010 and *D. hantoniensis* (Wood, 1846) from the late Eocene of France and the UK, respectively, (4) *D.* (*Hispanochampsa*) *muelleri* Kälin, 1936 from the early Oligocene of Spain (Piras & Buscalioni, 2006), (5) the type species *D. ratelii* Pomel, 1847 from the early Miocene of France (Vaillant, 1872) and Spain (Díaz Aráez *et al.*, 2017) and possibly from the early Oligocene of France (Brinkmann & Rauhe, 1998) and Italy (Kotsakis *et al.*, 2004) too and (6) *D. ungeri* Prangner, 1845 from the middle Miocene of Austria (Martin & Gross, 2011) and France (Ginsburg & Bulot, 1997). Whereas remains of nearly all of these species of *Diplocynodon* have been described or revised recently, one of the earliest named, *Diplocynodon hantoniensis*, has not been revised for over 150 years.

The Headon Hill Formation is a late Eocene (Priabonian) freshwater unit in the Hampshire Basin that crops out in southern England and the Isle of Wight (Edwards & Daley, 1997; Daley, 1999). One mainland locality, Hordle (=Hordwell) Cliff, near the town of Lymington (Hampshire) has yielded abundant fossil remains from several beds of the lowermost unit of the Headon Hill Formation: the Totland Bay Member (formerly the 'Lower Headon Beds'; Edwards & Daley, 1997). These remains were first reported in a series of papers by Wood (1844, 1846), Owen (1848), the Marchioness of Hastings (1848, 1853) and Wright (1851). In addition to numerous invertebrate and plant fossils (e.g. Wood, 1846; Hastings, 1853; Chandler, 1961), a diversity of vertebrates has also

been recovered from the beds at Hordle Cliff (Benton & Spencer 1995), including mammals (e.g. Owen, 1848; Cray, 1973; Hooker, 2014), turtles (e.g. Seeley, 1876; Hooley, 1905), frogs (Holman & Harrison 2003) and squamates (e.g. Hoffstetter, 1942; Holman *et al.*, 2006).

The first report of crocodylian remains from the beds at Hordle Cliff was presented by Edward Charlesworth on behalf of Searles Wood in the *Annals and Magazine of Natural History* in 1844. This short account reported the discovery of: 'A great portion of the head of an alligator, having nearly all the upper range of teeth (42 in number) remaining, along with the humerus, dermal scutæ and other parts of the skeleton' and that 'Mr. Wood proposes to call the Hordwell alligator *A. Hantoniensis*' (Wood, 1844: p. 351). A second account of Hordle Cliff was published by Wood (1846: p. 6), in which he reported, under the genus *Alligator*, that: 'A considerable portion of the skeleton of a crocodile, resembling the New World type, for which I propose the specific name Hantoniensis'. Wood (1846: pls 1, 6, 7) also figured some cranial remains, a femur and a cervical vertebra, under the name '*Alligator Hantoniensis*'. Because the 1844 publication lacks an accession number or figures to identify the material, Wood (1846) is the accepted authority for the name *Alligator hantoniensis*.

Both the Marchioness of Hastings and Owen presented new crocodylian remains from Hordle Cliff at the Seventeenth Meeting of the British Association for the Advancement of Science held at Oxford in June 1847, which were published as reports the following year (Hastings, 1848; Owen, 1848). According to these reports, Lady Hastings exhibited two crocodylian skulls from Hordle Cliff, that Owen (1848: p. 66) argued more closely resembled modern crocodiles than alligators or gavials, based on 'the festooned contour of the alveolar border of the upper jaw' and that 'the inferior canines rest in grooves or notches upon the outer margin of the upper jaw when the mouth is closed, and their entire crowns are exposed'. Consequently, 'Owen proposed to call the extinct species from Hordle *Crocodilus Hastingsiae*, in honour of the accomplished lady by whom the singularly perfect examples of the species had been recovered and restored' (Owen, 1848: p. 66). This report also noted that Mantell, who was in the audience, mentioned the presence of 'a fossil species of *Alligator* (*Alligator Hantoniensis*) described by Mr. Searles Wood, from a specimen of the lower jaw and teeth found in the freshwater beds at Hordwell Cliff', but that Owen 'had not seen this specimen' (Owen, 1848: p. 66). The year associated with the first appearance of '*Crocodilus Hastingsiae*' in the literature is, therefore, 1848 (see also: Gramann, 1958), not 1847 as is often reported in the literature (e.g. Woodward, 1885).

Owen (1850) subsequently described and figured this material as *Crocodilus Hastingsiae*. He also commented

upon a suite of similarities with the type specimen of *Alligator hantoniensis*, noting that the skulls of these two taxa were almost indistinguishable. However, the one notable difference pertained to the nature of the occlusion of the jaws. Whereas the fourth dentary tooth in the skulls of *Crocodilus hastingsiae* occludes into a notch (i.e. it remains visible with the jaws closed), that of *Alligator hantoniensis* occludes into a pit (i.e. it is obscured with the jaws closed). Although Owen (1850) suggested that this difference might merely reflect individual variation, he was also wary that this was a feature consistently used to distinguish modern crocodiles from alligators. As such, he maintained that *Crocodilus hastingsiae* represents a crocodile, rather than an alligator, and tentatively retained *Alligator hantoniensis* as a distinct taxon. The crocodylian-bearing bed was subsequently informally named the 'Crocodile Bed' by Wright (1851) and this fine white sandstone unit is one of the most fossiliferous layers at Hordle Cliff (Wright, 1851).

Pomel (1853: p. 124) referred *Alligator hantoniensis* to *Diplocynodon* on the basis of shared features with the French species *Diplocynodon ratelii*, which he had named several years earlier (Pomel, 1847). However, this new combination, *Diplocynodon hantoniensis*, seems to have gone unnoticed for the next three decades. Meyer (1857: p. 538) also noticed close affinities between the French and UK remains, but did not make any taxonomic referral. Subsequently, Huxley (1859) described the dermal armour of the Hordle Cliff crocodylian. He contended that only one crocodylian was present at this locality and that this taxon should be referred to as *Crocodilus hastingsiae*. Woodward (1885) also only recognized one taxon and argued that the differences in occlusion were likely individual variation. Although Woodward (1885: p. 509) commented that the Hordle Cliff crocodylian 'combines the characters both of Crocodiles and Alligators to a remarkable extent; and it also possesses some features that would quite entitle it to rank as a distinct genus', he also made no mention of Pomel's (1853) referral to *Diplocynodon*, continuing to refer to the material as *Crocodilus hastingsiae*. Finally, following Pomel (1853), Lydekker (1887) argued that this material should be referred to *Diplocynodon hantoniensis* (see also: Lydekker, 1888). The latter assignment has since been followed in the literature and was supported in later phylogenetic analyses (e.g. Buscalioni *et al.*, 1992; Brochu, 1999), with the differences in occlusal morphology likely to reflect ontogenetic variation (Brochu, 1999).

Here, we provide the first revision of *Diplocynodon hantoniensis* since Owen (1850), presenting a comprehensive description of all cranial and postcranial remains from Hordle Cliff accessioned in NHMUK and CAMSM. We provide a new diagnosis for the species and incorporate our anatomical observations into a recent phylogenetic analysis. We also briefly comment on referrals to *Diplocynodon hantoniensis* from approximately contemporaneous deposits in Switzerland (Pictet *et al.*, 1857), Germany (Gramann, 1958), France (Vignaud *et al.*, 1996) and the USA (Weems, 1999). Finally, we outline several anatomical features of the usually neglected postcranial skeleton, including numerous muscle scars that could form the basis for future phylogenetic characters.

INSTITUTIONAL ABBREVIATIONS

AMNH, American Museum of Natural History, New York, USA; CAMSM, Sedgwick Museum, Cambridge, United Kingdom; FMNH, Field Museum of Natural History, Chicago, USA; HLMD, Hessisches Landesmuseum, Darmstadt, Germany; IRSNB, Institut Royal des Sciences Naturelles de Belgique, Brussels, Belgium; MACN, Museo Argentino de Ciencias Nauturales 'Bernardino Rivadavia', Buenos Aires, Argentina; MNHN, Muséum national d'Histoire Naturelle, Paris, France; NHMUK, Natural History Museum, London, United Kingdom; QM, the Queensland Museum, Brisbane, Australia; SMF, Senckenberg Naturmuseum, Frankfurt, Germany.

SYSTEMATIC PALAEONTOLOGY
EUSUCHIA HUXLEY, 1875
CROCODYLIA GMELIN, 1789
ALLIGATOROIDEA GRAY, 1844
DIPLOCYNODON POMEL, 1847
DIPLOCYNODON HANTONIENSIS WOOD, 1846

Alligator hantoniensis Wood, 1846
Crocodilus hastingsiae Owen, 1848
Crocodilus hastingsiae Owen, 1850
Diplocynodon hantoniensis Pomel, 1853
Crocodilus hastingsiae Huxley, 1859
Crocodilus hastingsiae Woodward, 1885
Diplocynodon hantoniensis Lydekker, 1887
Diplocynodon hantoniensis Buscalioni et al., 1992
Diplocynodon hantoniensis Brochu, 1999

Holotype: NHMUK OR 25166 (holotype of '*Alligator hantoniensis*'), anterior portion of a skull (Fig. 1). Type locality: Hordwell Cliff, near Lymington, Hampshire, United Kingdom. Type horizon: Totland Bay Member, Headon Hill Formation; Priabonian (late Eocene) (Edwards & Daley 1997; Daley, 1999).

Synonym: *Crocodilus hastingsiae* Owen, 1848. *Crocodilus hastingsiae* (Owen, 1850; Huxley, 1859; Woodward, 1885).
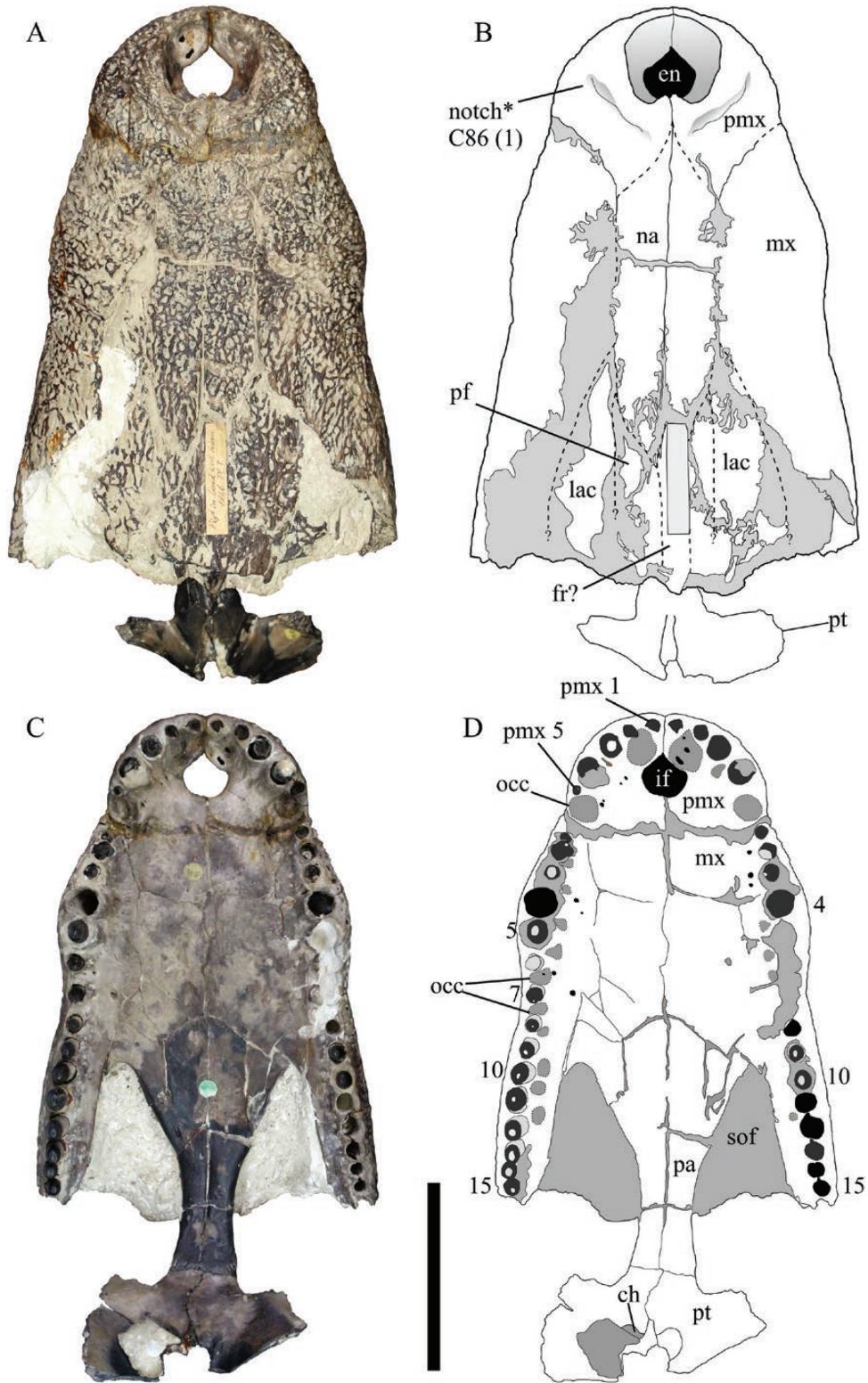
Figure 1. The skull of *Diplocynodon hantoniensis*, holotype of '*Alligator hantoniensis*' (NHMUK OR 25166) in dorsal (A, B) and ventral (C, D) views. Abbreviations: en, external naris; ch, choana; fr, frontal; if, incisive foramen; lac, lacrimal; mx, maxilla; na, nasal; occ, occlusal pit; pa, palatine; pmx, premaxilla; pmx 1, premaxillary tooth 1; pt, pterygoid; sof, sub-orbital fenestra. Scale bar = 10 cm.

Holotype: NHMUK OR 30393, from the same locality and horizon.

Referred material (NHMUK): Skulls (R 1041, R 1042, OR 25167, OR 25170.a, OR 29694, OR 30287 partim, OR 30392, OR 30414 partim); rostrum fragment (OR 30381 partim); premaxillae (OR 30289 partim, OR 30369, OR 30370, OR 30414 partim); maxilla (R 5010 partim, OR 25168, OR 25169, OR 25170, OR 30289 partim); nasal (OR 30289 partim); jugals [OR 25188 (with partial quadratojugal), OR 25219, OR 30289 partim]; quadrates (OR 25187, OR 25193. OR 30372, OR 30382, OR 30414 partim); pterygoid [OR 30251 (with fragmentary ectopterygoids and palatine)]; ectopterygoids [OR 25216 (with pterygoid fragment), OR 25217]; basioccipital (OR 36812); lower jaws [R 1043, R 1045 partim, R 5267 partim, OR 25178, OR 30274, OR 30381 partim, OR 30394, OR 30396 (two rami in connection), OR 30397]; dentaries (R 1044, R 5010 partim, R 5121, R 5212, R 5216, R 5217, OR 30318 partim, OR 30321, OR 30287 partim, OR 30289 partim, OR 30338, OR 30365, OR 30378, OR 30383); angulars (R 5217 partim, OR 30285, OR 30289 partim, OR 30307, OR 30308, OR 30318 partim, OR 30414 partim); articulars [OR 25192, OR 30282, OR 30283, OR 30284, OR 30388 partim, OR 30289 partim, OR 30363, OR 30363.a, OR 30388 partim (joined with 30289), OR 30414 partim]; surangular (OR 30414 partim); tooth-bearing bone (OR 25260); isolated teeth (R 1043, R 5009, R.6323, R 6852, OR 25165, OR 25598, OR 30317 partim); proatlas (OR 30289 partim); odontoid process (OR 25186); axes (two unnumbered specimens); vertebrae (R 1041, R 1045 partim, R 1046, R 1047, R 1048, R 1049, R 1050, R 1051, R 1052, R.1068 partim, R 5213, R 5267 partim, OR 25175, OR 25177, OR 25176, OR 25179, OR 25180, OR 25181, OR 25182, OR 25195, OR 25199, OR 25201, OR 25207, OR 25208, OR 25209, OR 25210, OR 25213, OR 25214, OR 25215, OR 25222, OR 25223, OR 25224, OR 30289 partim, OR 30402 partim, plus unnumbered specimens); ribs (R.1068 partim, OR 25191, OR 25248, OR 30402 partim, OR 30414 partim); osteoderms (R 1043, R 1045 partim, R 1068 partim, R 5214, R 5267 partim, OR 25174, OR 30318 partim, OR 30366, OR 30367, OR 30368, OR 30388 partim, OR 30414 partim, plus one unnumbered specimen); scapulae (OR 30247 partim, OR 30414 partim); coracoids (OR 25245, OR 30359); humeri (OR 25237, OR 30206, OR 30206.a, OR 30219, OR 30247 partim); radii (OR 25244 partim, OR 30401); ulnae (OR 25239, OR 30236, OR 30237, OR 30247 partim, OR 30389); radiale (R.1054); ilia (OR 25252, OR 25253, OR 30362, OR 30414 partim); ischia (OR 30354 partim); femora (R 5215, R 5267 partim, OR 25231, OR 25232, OR 25238, OR 25244 partim, OR 30210, OR 30211, OR 30213, OR 30214, OR 30222, OR 30223, OR 30228, OR 30247 partim, OR 30399, OR 30414 partim); tibiae (R 5267 partim, OR 25236, OR 30215, OR 30216, OR 30217, OR 30242, partim, OR 30414 partim); fibulae (OR 30233, OR 30234, OR 30235, OR 30241); metapodials (R 1053 partim, R 5267 partim, OR 25244 partim, OR 25254, OR 30240, OR 30242 partim, OR 30243, OR 30246, OR 30247 partim, OR 30336); phalanges (R 1053 partim, R.1054 partim, R 5267 partim, OR 25243). CAMSM: skulls (TN 907 partim, TN 917, TN 918 partim); lower jaws (TN 904; TN 907 partim); dentaries (C31041, C31042, C31043, plus 8 unnumbered specimens); angulars (C31044, 31045); cervical vertebrae (C31026–40); dorsal vertebrae (C31012–25); caudal vertebrae (C30999–31011); osteoderms (C31046–95; C31352–87).

Revised diagnosis: Diplocynodon hantoniensis can be diagnosed by the following unique combination of characters (autapomorphies marked by an asterisk): (1) premaxillary surface posterolateral to naris with a deep notch; (2) short anterior ectopterygoid process, which forms the medial wall of the posteriormost maxillary alveolus, before veering medially to the suborbital fenestra*; (3) ectopterygoid–pterygoid flexure retained throughout ontogeny*; (4) surangular–angular suture meets the articular dorsal to its ventral tip in the mandibular adductor chamber*; (5) broad preorbital ridge on the lacrimal; (6) prominent laminae and sulci either side of the choana.

Description: skull

General proportions, preservation and ornamentation: Several remains represent portions of the skull, including three nearly complete skulls: NHMUK OR 30392, NHMUK OR 30393 (Figs 2–4) and CAMSM TN 907. All three of these skulls are large: NHMUK OR 30392 is 375 mm long from the anterior tip of the premaxillae to the posterior margin of the skull table (measured along the midline on the skull surface), with NHMUK OR 30393 and CAMSM TN 907 comparable in size (Table 1). The preserved portion of NHMUK OR 25166 also indicates a similarly sized individual. At the other end of the spectrum, NHMUK OR 25170.a is a partial juvenile skull that is about 60 mm long from the anterior tip of the maxillae (the premaxillae are not preserved) to the posterior edge of the skull table.

Preservation varies significantly from specimen to specimen, with different degrees of completeness, but deformation is generally minor. For example, the nasals of NHMUK OR 30393 are slightly lowered in respect to the maxillae. Some partial skulls, including NHMUK R 1042, OR 25170a and OR 29694, are still partly embedded in matrix, whereas others have been internally reinforced with plaster or a cement-like material, including NHMUK OR 30392. The surfaces of the two best-preserved skulls have been partly covered by plaster in order to provide the impression of completeness.

The overall appearance of the skull is that of a generalized crocodylian, with the rostrum (the region anterior to the orbits) representing about 65% of the
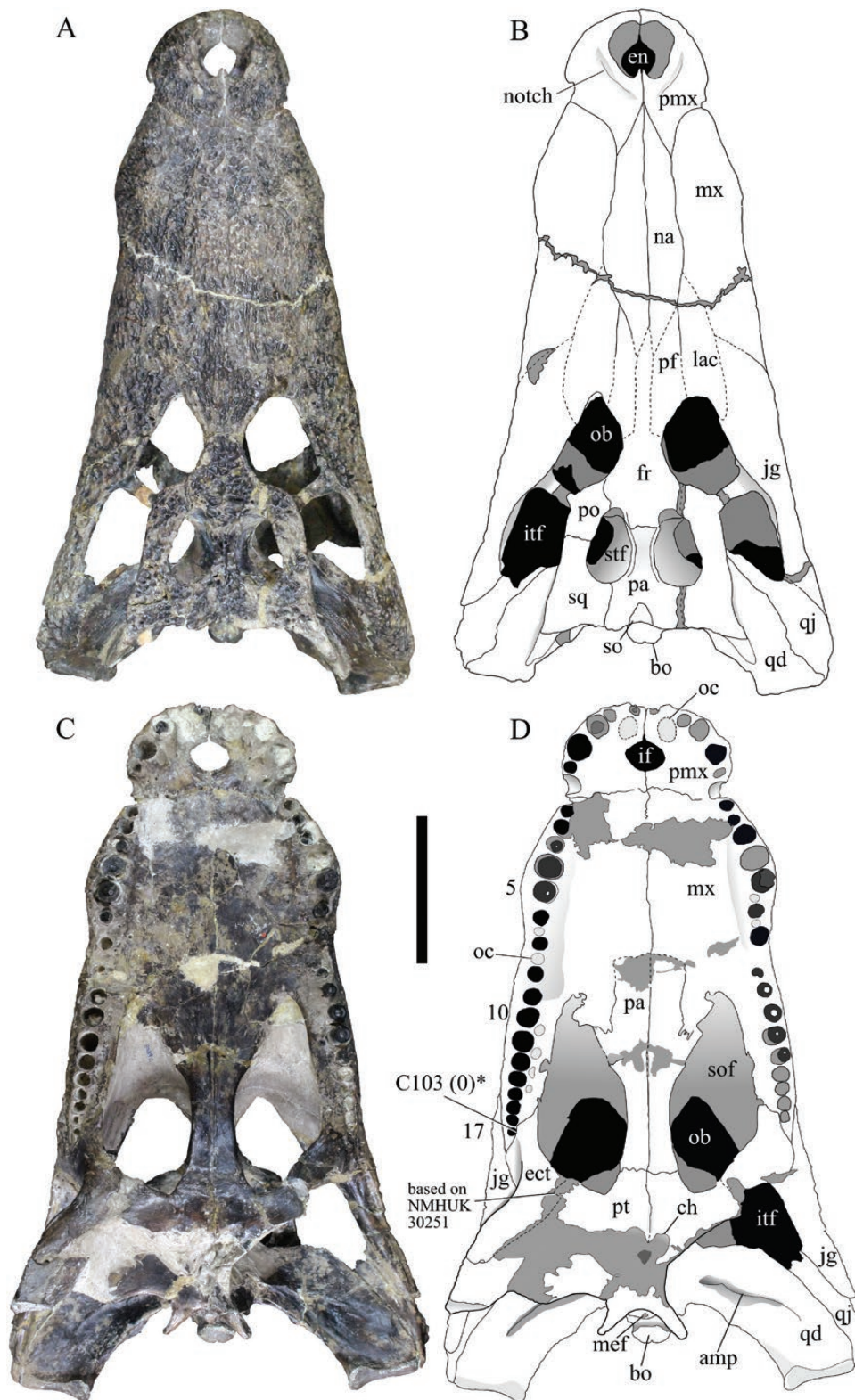
Figure 2. The skull of *Diplocynodon hantoniensis* (NHMUK OR 30392) in dorsal (A, B) and (C, D) ventral view. Abbreviations: amp, scar for musculus adductor mandibulae posterior; bo, basioccipital; ch, choana; en, external naris; fr, frontal; itf, infratemporal fenestra; jg, jugal; lac, lacrimal; mef, median eustacian foramen; mx, maxilla; na, nasal; ob, orbit; oc, occlusal pit; pmx, premaxilla; pf, prefrontal; po, postorbital; qd, quadrate; qj, quadratojugal; so, supraoccipital; sq, squamosal; stf, supratemporal fenestra. Scale bar = 10 cm.
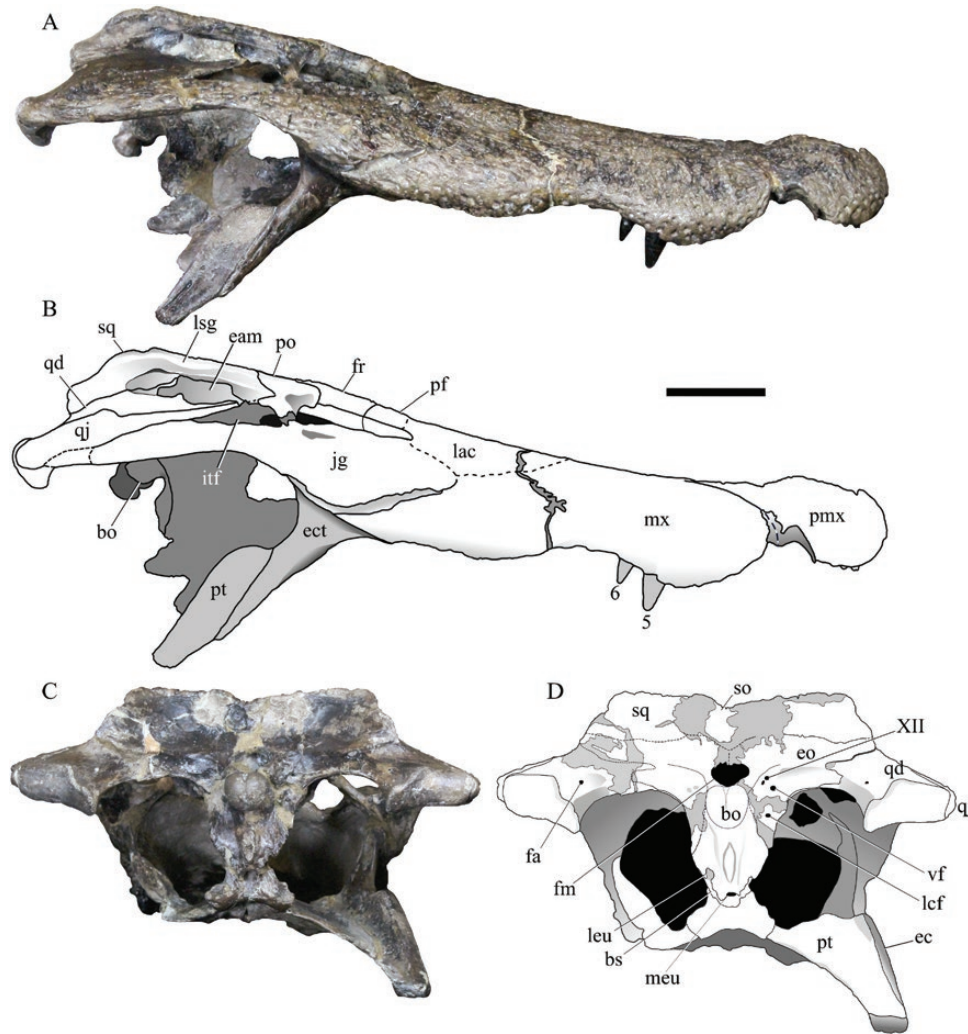
Figure 3. The skull of *Diplocynodon hantoniensis* (NHMUK OR 30392) in lateral (A, B) and occipital (C, D) views. Abbreviations: 5, 6, maxillary tooth numbers; bo, basioccipital; bs, basisphenoid; eam, external auditory meatus; ect, ectopterygoid; eo, exoccipitals; fm, foramen magnum; fr, frontal; itf, infratemporal fenestra; jg, jugal; lac, lacrimal; leu, lateral eustachian foramen lsg, lateral squamosal groove; meu, median eustachian foramen; mx, maxilla; pf, prefrontal; pmx, premaxilla; po, postorbital; pt, pterygoid; qd, quadrate; qj, quadratojugal; so, supraoccipital; sq, squamosal; vf, vagus foramen; XII, foramen for cranial nerve 12. Scale bar = 5cm.

entire length of the skull. There is no medial dorsal boss on the rostrum. Canthi rostrali are clearly absent, but preorbital ridges are prominent in adult individuals (see description of the lacrimal). In posterior view, the skull table is approximately planar, except for a modest depression in mature specimens (e.g. NHMUK OR 30392 and 30393) (Fig. 3D), at the dorsal exposure of the supraoccipital. The lateral sides of the skull table are convex in juvenile specimens (NHMUK OR 25167 and OR 25170.a), and the paroccipital processes have short squamosal rami (Figs 5, 6). However, the lateral sides are straight or slightly concave in adult specimens (NHMUK OR 30392 and 30393), in which the squamosal rami are long.

Cranial fenestrae and openings: The dorsally facing naris is entirely hosted within the premaxillae (Figs 1, 2). It is approximately circular and has a rounded, convex anterior rim, nearly straight lateral rims (especially in NHMUK OR 25166) and a concave posterior rim (as a result of an anterior projection of the medial edge of each premaxilla). The rim of the external naris is flush with the dorsal surface of the surrounding premaxillae, which is posterolaterally marked by a depression that is nearly as developed as the one that characterizes *Alligator* (Figs 1B, 2B). Whereas the lateral walls of the naris are nearly vertical, the anterior walls are very shallowly inclined posteroventrally.
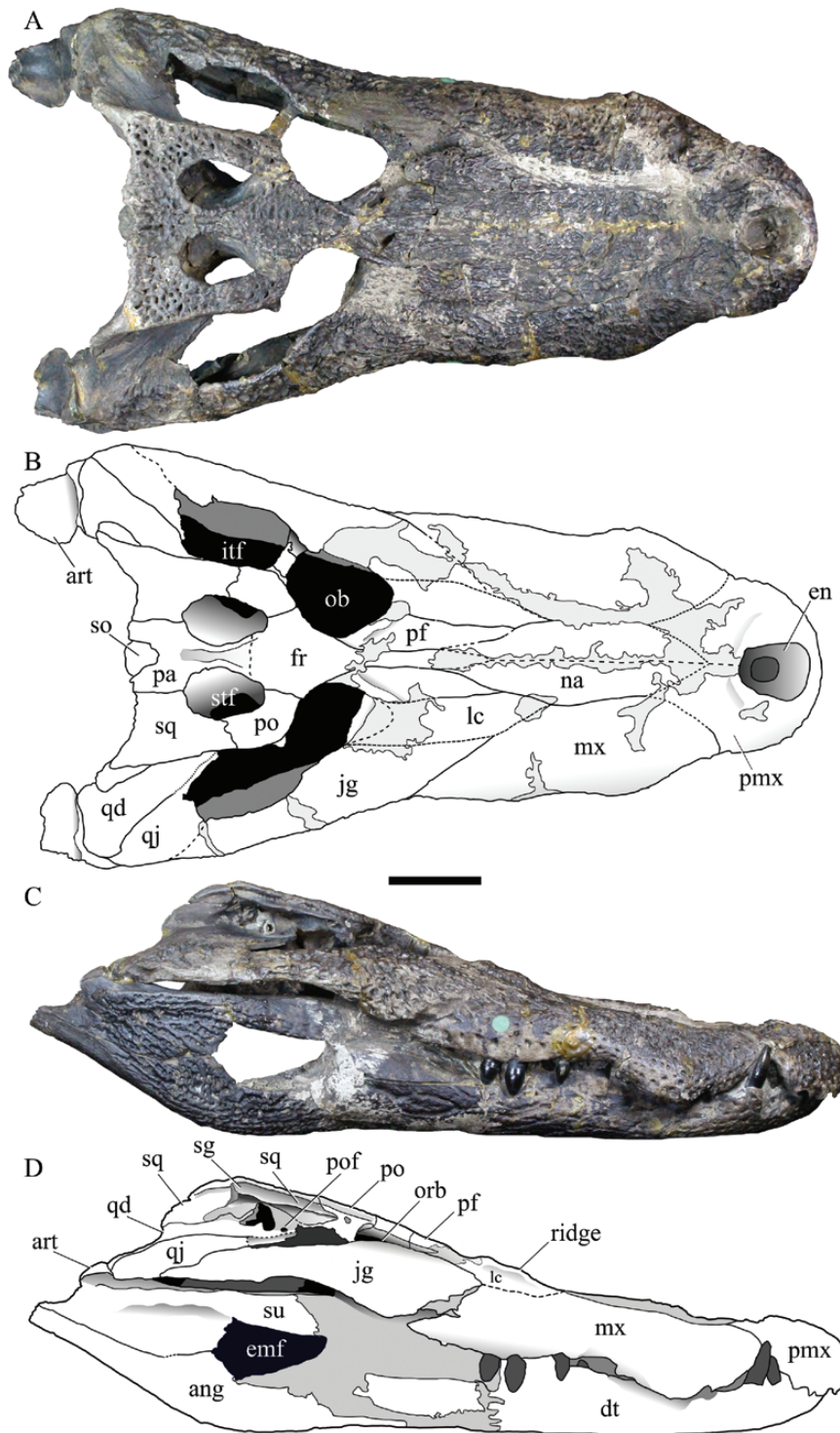
Figure 4. Articulated skull and mandibles of *Diplocynodon hantoniensis* (NHMUK OR 30393) in dorsal (A, B) and lateral (C, D) view. Abbreviations: art, articular; dt, dentary; emf, external mandibular fenestra; en, external naris; fr, frontal; itf, infratemporal fenestra; jg, jugal; lac, lacrimal; mx, maxilla; na, nasal; ob, orbit; pmx, premaxilla; pf, prefrontal; pof, preotic foramen; po, postorbital; qd, quadrate; qj, quadratojugal; so, supraoccipital; sq, squamosal; stf, supratemporal fenestra; su, surangular. Scale bar = 5 cm.

Table 1. Skull measurements of *Diplocynodon hantoniensis* (mm)

Feature	NHMUK OR 30393	NHMUK OR 25166	NHMUK OR 30392	CAMSM TN 907
Dorsal skull length	375	NA	375	344
Narial length	37	40	33	41
Narial width	29	40	35	42
Snout length along medial axis	255	240	240	213
Rostrum width at notch/pit for fourth dentary tooth	97	102	84	82
Orbit length	60	NA	59	58
Interorbital width	25	NA	23	25
Supratemporal fenestra length	46	NA	44	41
Supratemporal fenestra width	25	NA	26	28
Skull table anterior width	86	NA	79	77
Maximum skull width across quadrates	227	NA	220	215

The dorsal margin of each orbit is composed of the frontal, the posterior margin by the postorbital, the posterolateral and lateral margins by the jugal, and the anterior margin is formed by the lacrimal and prefrontal. The orbits are deeply concave medially, but straight or slightly convex laterally, and are truncated by the postorbital bars posteriorly. The orbital rim is flush with the jugal surface (a hint of a crest is present in NHMUK OR 30392), but raised into a crest along the prefrontal edge. In the juvenile partial skull NHMUK OR 25170a, the posterolateral edge of the prefrontal is extremely high and forms a vertical laminar ridge delimiting the anteromedial surface of the orbit (Fig. 5). It is not clear if palpebral bones were originally absent or are simply not preserved in any available specimen.

The supratemporal fenestrae are oval-shaped, with their long axes oriented anteroposteriorly. They are much smaller than either the orbits or infratemporal fenestrae in adult specimens, but comparatively large in the juvenile individual NHMUK OR 25170.a, which has a very broad supratemporal fossa. The medial rim of each supratemporal fenestra is slightly raised into a ridge in the largest specimens, with a depressed interfenestral bar (Figs 3B, 4B). However, in smaller specimens (e.g. NHMUK OR 25167 and 25170a) the rim of the supratemporal fenestra is nearly flush with the parietal surface (Figs 5, 6). Whereas the posterior and medial fenestral margins are curved, the anterolateral margins are straight and the fenestrae taper in width anteriorly to form an acute corner (Fig. 2B). The rim of each supratemporal fenestra does not significantly overhang the supratemporal fossa. A shallow fossa occurs at the anterior corner of the supratemporal fenestra. The medial parietal wall of the supratemporal fenestra is imperforate.

The infratemporal fenestrae are triangular in shape and are approximately as long as the orbits, although their surface area is smaller overall than that of the orbits. The most completely preserved infratemporal fenestra is the right opening of NHMUK OR 30392, which is missing only a very small portion of the quadratojugal, close to the postorbital (Fig. 3B). The jugal forms the ventral margin and anterior angle of the infratemporal fenestra, and the dorsal angle appears to be formed by the quadratojugal (CAMSM TN 918). From the juvenile specimen NHMUK OR 25167 (Fig. 6), it is clear that the quadratojugal formed the entire posterior corner of the infratemporal fenestra.

The external auditory meatus is clearly visible in NHMUK OR 30392 and 30393 (Figs 3B, 4D) and has a cloverleaf shape. Whereas the dorsal margin of the external auditory meatus is composed of the squamosal, the quadrate forms the bowed posterior rim, as well as the ventral and anterior margins. The quadrate–squamosal suture extends dorsally along the posterior margin of this opening. The quadrate forms a narrow ridge on the floor of the external auditory meatus, extending medially into the ear canal. A large preotic foramen pierces the quadrate anterior to the external auditory meatus (Fig. 4D).

The elliptical foramen magnum, delimited by the exoccipitals and the basioccipital, is equal in width to the occipital condyle (Fig. 3D). Post-temporal fenestrae are rather small: they are delimited by the parietal and squamosal dorsally, and by the supraoccipital and exoccipital ventrally. The lateral carotid foramen opens lateral to the basisphenoid, and the small lateral Eustachian canals open dorsally to the large, medial canal.

The suborbital fenestrae are fully visible in NHMUK OR 30392 (Fig. 2D) and CAMSM TN 907. Anteriorly, they reach the level of the ninth maxillary alveolus,
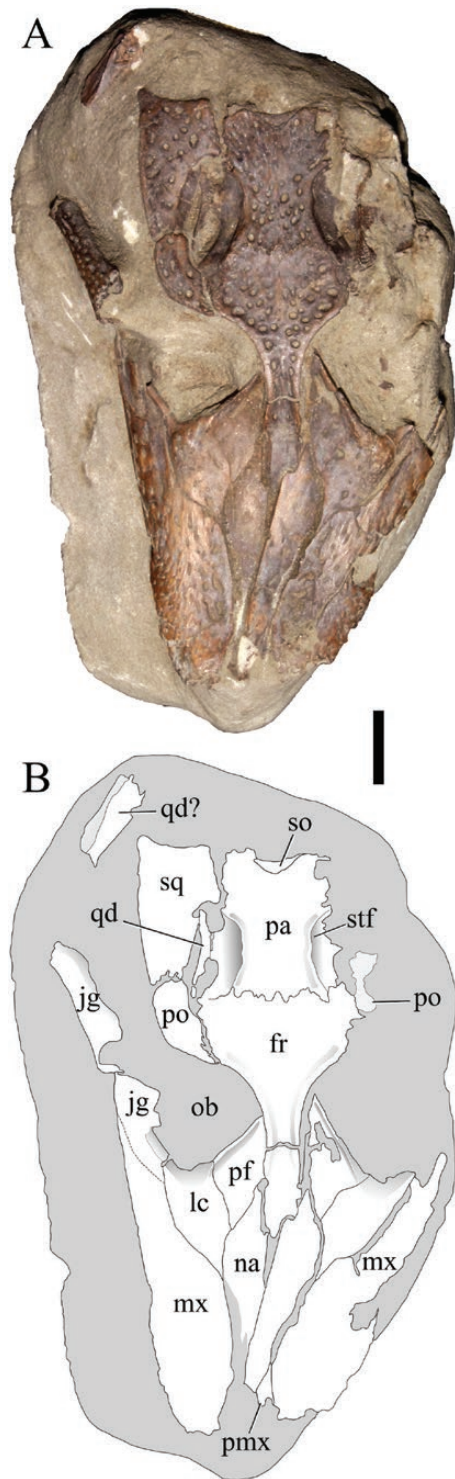
Figure 5. Juvenile skull of *Diplocynodon hantoniensis* (NHMUK OR 25170a) in dorsal view. Abbreviations: fr, frontal; jg, jugal; lac, lacrimal; mx, maxilla; na, nasal; ob, orbit; pmx, premaxilla; pf, prefrontal; po, postorbital; qd, quadrate; so, supraoccipital; sq, squamosal; stf, supratemporal fenestra. Scale bar = 1 cm.

but reach the tenth alveolus in NHMUK OR 25166 (Fig. 1D). The lateral edge of the suborbital fenestra is straight, not bowed medially at the ectopterygoid–maxilla suture. Each suborbital fenestra has a posterior notch (best observed on the right opening of NHMUK OR 30392). The posterior corner of the suborbital fenestra is formed by the pterygoid, with the pterygoid–ectopterygoid suture situated on the posterolateral margin of the fenestra. Anteriorly, the suborbital fenestra tapers to an acute tip. The anterolateral margin of the fenestra is longer than the posterolateral margin.

The incisive foramen is relatively large and is located far from the tooth row, with the anterior rim corresponding to the third alveolus, and the posterior margin corresponding to the fourth or fifth alveolus. Whereas this foramen is circular in NHMUK OR 30392 and CAMSM TN 907, it is teardrop-shaped in NHMUK OR 25166, with an acute anterior margin, resulting from the intrusion of the occlusal pits for the first dentary teeth.

The internal choana is best preserved in CAMSM TN 907 and the juvenile specimen NHMUK OR 25167 (Fig. 6D). The posteroventrally oriented choana is heart-shaped and situated entirely within the posterior region of the pterygoids, with its posterior rim close to the posterior edge of the pterygoids. The anterior rim of the choana is flush with the pterygoid surface, whereas the lateral rim develops a large lamina that separates the choana from a slightly depressed area. In addition, the midline of the anterior margin of the choana is interrupted by a posteriorly directed process of the pterygoid. This is observed in all specimens where preserved. In NHMUK OR 30392, this process extends far posteriorly into the choana, although it does not fully bisect it. The posterior rim of the choana, preserved in NHMUK OR 25167 and CAMSM TN 907, is smooth, lacking the sharp notch that characterizes *Caiman*, but there is a small concavity on the posterior edge. Although slightly incomplete in its median sector, these specimens show the presence of a sagittal bony septum recessed within the choana.

Premaxilla: The premaxillae completely encircle the external naris. They are characterized by five alveoli, even in adult specimens. Palatal laminae are flat, with no obvious ornamentation, except for a slightly rugose texture leading up to the alveolar necks (e.g. NHMUK OR 25166). Numerous small foramina pierce the premaxillary palate, adjacent to the alveoli. The dorsal process of the premaxilla is relatively short and wide, posteriorly reaching the level of the second or third maxillary alveolus. The premaxilla–maxilla suture is slightly irregular, rather than straight. One large reception pit for the first dentary tooth occurs lingually, in between the first and second premaxillary alveoli.
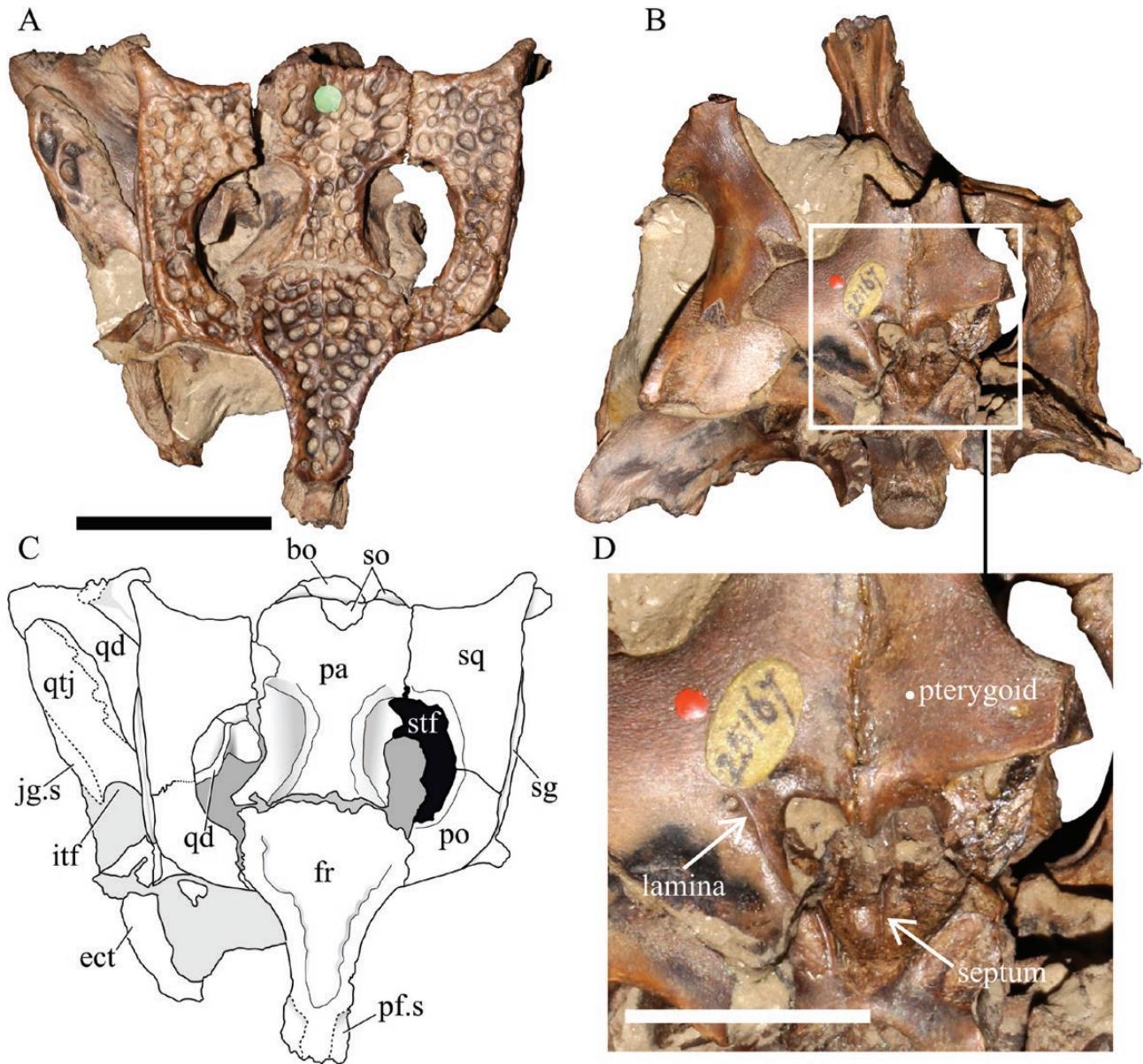
Figure 6. Juvenile skull of *Diplocynodon hantoniensis* (NHMUK OR 25167) in dorsal view (A, C). B, ventral view; D, enlargement of the choana in B. Abbreviations: bo, basioccipital; ect, ectopterygoid; fr, frontal; itf, infratemporal fenestra; jg.s, jugal suture; pa, parietal; po, postorbital; qd, quadrate; qtj, quadratojugal; sg, squamosal groove; so, supraoccipital; sq, squamosal; stf, supratemporal fenestra. Scale bar = 5 cm in A, B and C, but 3 cm in D.

Posteriorly, the premaxillae are separated along their midline by the anterior process of the nasal.

Maxilla: The well-preserved maxillary tooth rows of NHMUK OR 30392 host 17 alveoli on each side (Fig. 2C, D). In ventral view, the tooth row has a slight lateral concavity at the level of the sixth and seventh alveoli, but it is nearly straight posteriorly. The fourth and fifth alveoli are about the same size. They are not fully confluent in any of the three best-preserved skulls and are separated by a thin (but complete) bony septum. Confluent alveoli, in which the septum is not complete, having a V-shaped fenestration, is observed in one small, isolated maxilla NHMUK OR 25168–9. In dorsal view, at the level of the fifth maxillary alveolus, and slightly medially inset, there are two protuberances. On the ventral surface of the skull, the maxilla terminates a significant distance anterior to the postorbital bar, forming a short edentulous process that is as long as the distance between the last two maxillary alveoli (Fig. 2D). The penultimate alveolus

is slightly less than twice the diameter of the last alveolus. The medial walls of the last two maxillary alveoli are formed by the ectopterygoid.

Nasal: An acute process of the nasal protrudes anteriorly between the premaxillae, but does not reach the external naris. In NHMUK OR 30392 (Fig. 2), this nasal process terminates about 20 mm posterior to the external naris. The nasals broaden posteriorly along the maxilla–nasal suture, reaching a maximum width at their midlength. Whereas the nasal–prefrontal suture is concave, the nasal–lacrimal suture is linear.

Lacrimal: The lacrimal forms the anterolateral rim of the orbit. It is longer than the prefrontal (Fig. 7A). NHMUK OR 30381 preserves the right lacrimal duct, which is large and opens immediately lateral to the lacrimal–prefrontal suture. The lacrimal and the nasal appear to be in broad contact, lacking any posterior process from the maxilla (Fig. 7A), although the poor demarcation of sutures makes this morphology difficult to establish conclusively in the four largest skulls. Preorbital ridges are present in all three of the adult skulls preserving the lacrimals: they are more prominently developed in NHMUK OR 30393 and CAMSM TN 907 than in NHMUK OR 30392. A low

ridge is present in the smaller specimen NHMUK OR 30381 and a clear boss is present in the juvenile skull NHMUK OR 25170.a, immediately anterior to the anterior orbital corner (Fig. 5A).

Jugal: The jugal forms the ventral margin of the orbit and extends posteriorly past the level of the infratemporal fenestra (Fig. 4D). The lateral and ventral margins of the jugal are heavily ornamented with pits, whereas the medial side is smooth. A very large medial jugal foramen is visible in the isolated juvenile jugal NHMUK 20219, the juvenile partial skull NHMUK R 1041 and in NHMUK OR 30393. Three of the four isolated jugals catalogued as NHMUK OR 30289 have large medial foramina, but the fourth one shows a foramen of moderate size. Two medial jugal foramina are visible in the isolated jugal arch NHMUK OR 25188 (Fig. 7B) and in the left jugal of NHMUK OR 30392, although there is only one foramen on the right jugal. The ectopterygoid is sutured onto the anteromedial side of the jugal, ventral to the postorbital bar. The ventral portion of the postorbital bar that is formed by the jugal is inset from the dorsal edge of the jugal, with a moderately developed sulcus. At the level of the postorbital bar there is a small step
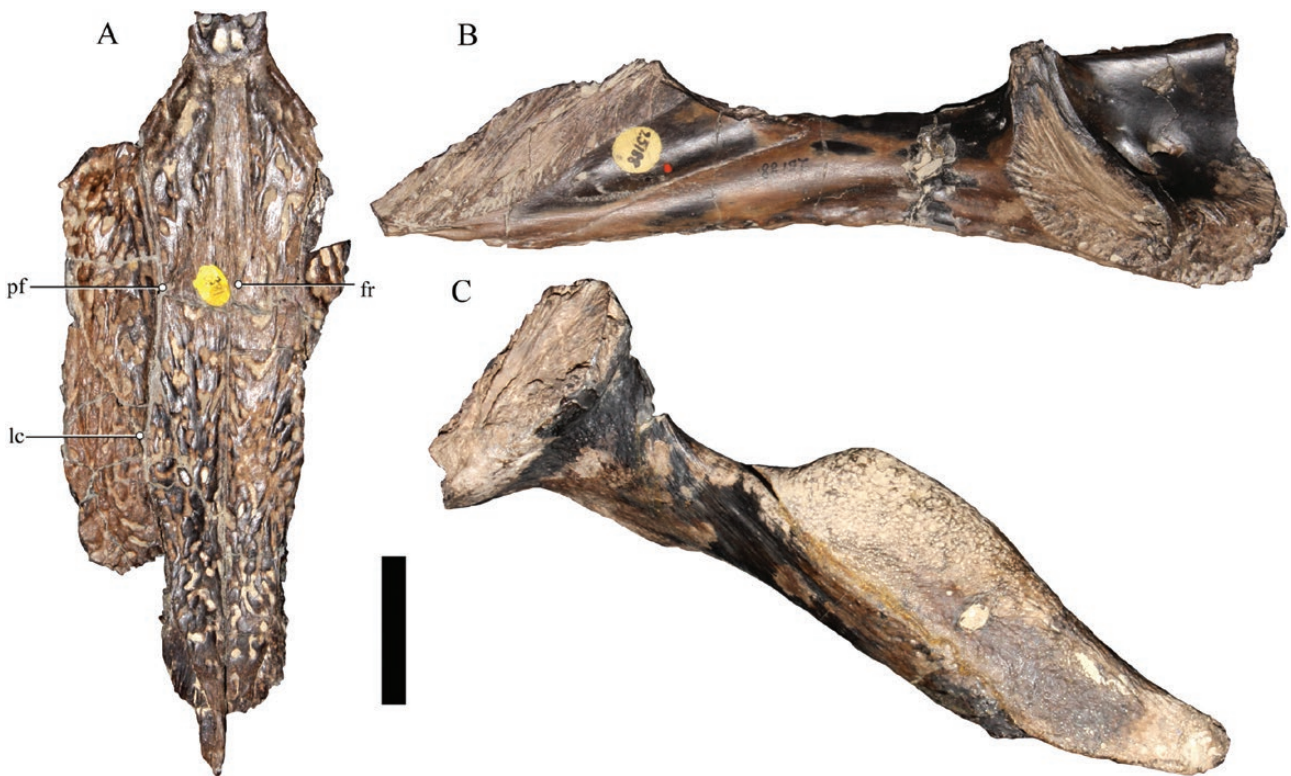

Figure 7. Selected skull details of *Diplocynodon hantoniensis*. A, NHMUK OR 30381, fragment of the rostrum showing the anterior extent of the prefrontal, frontal and lacrimal; B, NHMUK OR 25188, isolated left jugal in medial view; C, NHMUK OR 30251 isolated pterygoids and ectopterygoids in left lateral view. Abbreviations: fr, frontal; lc, lacrimal; pf. prefrontal. Scale bar = 4cm.

in the dorsal outline of the jugal, reminiscent of the condition in *Alligator* and *Caiman*, and differing from the straight dorsal outline of *Crocodylus*. Posteriorly, the jugal terminates in an acute process that is sutured ventrolaterally to the quadratojugal. This process extends slightly further posteriorly than the level of the basioccipital tubera.

Prefrontal: The prefrontals are separated from one another along the midline by the frontal process and by the posterior tip of the nasals (Fig. 4B). Around the orbit, the prefrontal surface is raised into a ridge (Figs 4, 5). The prefrontal pillars are poorly preserved and/or partially obscured in all specimens, limiting anatomical observations. Ventrally, they form a suture with the dorsolateral margin of the palatines, forming two walls.

Frontal: There is no distinct step at the base of the frontal process in two of the largest skulls, NHMUK OR 30392 and NHMUK OR 30393, and is very weakly developed in CAMSM TN 907. However, a slight step is present in both the juvenile skull NHMUK OR 25167 (Fig. 6) and the much larger, though not fully grown, individual represented by NHMUK OR 30381 (Fig. 7A). A very steep slope is visible in the very small individual represented by NHMUK OR 25170.a (Fig. 5). The step in both NHMUK OR 25167 and 30381 is highlighted by the ornamentation of the frontal: it is pitted posterior to the step (similar to that of the skull table), but smooth along the frontal process. The dorsal surface of the frontal is gently concave and its dorsolateral (orbital) margin is slightly upturned. The anterior process of the frontal extends beyond the orbital margin, to the level of the anterior tip of the prefrontal and the midlength of the lacrimal. It is difficult to discern the anterior extent of the frontal relative to the jugal in NHMUK OR 30392 and 30393 as a result of poorly defined sutures, as well as the plaster that covers the dorsal surface. However, based on NHMUK R 1042 and OR 29694, the anterodorsal tip of the jugal lies just posterior to the anterior extent of the frontal process. In the juvenile specimen NHMUK OR 25170.a, the anterior extent of the frontal and jugal appear to be approximately equal; however, the frontal process is not well preserved in this specimen. On the skull table, the linear frontoparietal suture enters so deeply into the supratemporal fenestrae that the parietal and postorbital are not in contact.

Often in crocodylians, the anterior frontal process bisects the nasals for a short distance. The morphology in this area is extremely difficult to discern in the largest specimens of *Diplocynodon hantoniensis* (i.e. NHMUK OR 30392, 30393 and 25166). In NHMUK OR 30381 (Fig. 7A) (and possibly also NHMUK OR 29694), the frontal appears to invade the nasals anteriorly via two separate processes, between which the nares project posteriorly. However, in the juvenile

NHMUK OR 25170.a, the usual condition is observed. In NHMUK OR 30381 and 29694, the elements may have been pulled apart at their sutures and filled with matrix. Consequently, this unusual morphology might merely be an artefact of preservation.

Postorbital: The postorbital bar is incomplete in most specimens and often reconstructed with plaster. However, it appears strongly inclined laterally and inset from the lateral surface of the skull based on NHMUK OR 30392 and CAMSM TN 918. The bar is slender and circular in cross-section, with a short and low process. A deep fossa excavates the lateral surface of the dorsal portion of the postorbital bar, pierced by a large foramen. The postorbital is in contact with a thin dorsal projection from the quadratojugal, but not with the quadrate (see NHMUK OR 30392, CAMSM TN 918) (Fig. 3B).

Squamosal: The squamosals form the posterolateral corners of the cranial table and the posterolateral margins of the supratemporal fenestrae. Their dorsal surfaces are flat in both juvenile (NHMUK OR 25167 and 25170.a) and fully grown individuals (NHMUK OR 30392, 30393, CAMSM TN 907). A prominent squamosal groove is delimited by subparallel rims. A linear series of foramina pierce the groove, as well as the dorsal margin of the groove. Dorsal to the external auditory meatus, there is a slight ventral deflection along the ventral margin of the squamosal. The squamosal–quadrate suture is visible on the right side of NHMUK OR 30393 (Fig. 4D), extending along the posterior margin of the external auditory meatus. In lateral view, the posterodorsal edge of the squamosal is curved gently ventrally. The squamosal rami do not reach the tip of the paroccipital processes.

Parietal: The parietal forms the medial margin of the supratemporal fossa and fenestra, a large portion of the post-temporal fossa and the roof of the braincase. Posterior to the supratemporal fenestra, the dorsal surface of the parietal is concave and the interfenestral bar has a sagittal sulcus (Fig. 4). The medial wall of the supratemporal fossa is steeply inclined, facing laterally and slightly dorsally, and the parietal rim of the supratemporal fenestra only slightly overhangs the supratemporal fossa. On the medial wall of the supratemporal fenestra, the laterosphenoid–parietal suture is horizontal. The post-temporal fossa is prominent, forming a shelf that is principally composed of the parietal, anterior to the post-temporal fenestra. Laterally, the parietal approaches, but does not contact, the squamosal on the posterior wall of the supratemporal fenestra. The parietal–quadrate suture undulates strongly.

Quadrate: The quadrate condyle is characterized by a small, ventrally deflected medial hemicondyle, and by a dorsal notch (open medially) that hosts the foramen aëreum (Fig. 3D). The latter opening is relatively small

and placed on the dorsal surface of the quadrate, far from the mediodorsal edge. Whereas the articular surface of the medial hemicondyle faces posteriorly and ventrolaterally, the lateral hemicondyle faces posteroventrally. On the midline of the ventral surface of the quadrate ramus, there is a well-developed attachment scar for M. adductor mandibulae posterior (Holliday *et al.*, 2013) [scar 'B' of Iorndansky (1973)] (Fig. 2D). This scar develops into a large sharp lamina, projecting approximately 10 mm from the ventral surface of the quadrate in NHMUK OR 30392 and NHMUK OR 30393. The scar continues ventrally along the posterolateral braincase wall, although it becomes less pronounced.

Quadratojugal: The quadratojugal is well preserved on the right side of NHMUK OR 30392 and CAMSM TN 918, in which it is represented by a small step situated far from the posterior corner of the infratemporal fenestra, immediately dorsal to the midpoint of the posterior fenestral margin (Fig. 2B). As can be observed on NHMUK OR 25188 (Fig. 7B), a moderately developed process extends along the medial surface of the lower temporal bar. The quadratojugal has a long, apically very thin process that reaches the dorsal corner of the infratemporal fenestra. Posteriorly, the quadratojugal extends to the level of the quadratic condyles, forming the lateral margin of the lateral hemicondyle. The ventral suture with the jugal is approximately parallel with the quadrate–quadratojugal suture.

Supraoccipital: The supraoccipital is well exposed on the posterior surface of the skull and delimits the ventromedial rim of the post-temporal fenestra. The dorsal exposure of the supraoccipital is clearly visible in the juvenile specimen NHMUK OR 25170.a (Fig. 5), in which it forms a broad and dorsoventrally short triangle. This triangle becomes taller in mature specimens, in which the sutures delimiting the supraoccipital are not easily discernible. The posterior surface of the supraoccipital is excavated by two circular sulci that are separated by a vertical, sagittal crest. Two processes project posteriorly from the supraoccipital, immediately ventral to the slit-like post-temporal fenestrae, and are most clearly observable in NHMUK OR 30393 and NHMUK OR 25167 (Fig. 6). These processes are not large enough to exceed the level of the posterior margin of the cranial table in the adult specimen NHMUK OR 30392, but they are clearly visible in dorsal view of the juvenile specimen NHMUK OR 25167.

Exoccipital: The exoccipitals have a smooth paroccipital surface devoid of any boss. They extend considerably lateral to the posterior opening of the cranioquadrate passage, but do not reach the basioccipital tubera ventrally (Fig. 3D). Lateral to the post-temporal fenestra, the surface of the exoccipital is strongly concave. Overall, the occipital surface formed by the

exoccipitals faces posterodorsally. The paroccipital process extends posterolaterally, sitting above the posterior quadrate rami. The ventral margin of the paroccipital process above the cranioquadrate canal is marked by a ventrally directed lamina. This lamina terminates immediately medial to the cranioquadrate canal, continuing towards the foramen magnum as a faint horizontal ridge. Neurovascular foramina pierce the exoccipitals and are well preserved in NHMUK OR 30392, 30393 and 25166. Four foramina are present on the right exoccipital of NHMUK OR 30392 (Fig. 3D). Two foramina occur close together at the level of the foramen magnum for the hypoglossal (XII) nerve. Slightly ventral and lateral to these foramina is the vagus (X) foramen. Further ventrally, close to the lateral margin the descending process of the exoccipital, approximately at the dorsoventral midpoint of the occipital condyle, is the much larger lateral carotid foramen. This foramen sits within a fossa and appears to be orientated posteroventrally and slightly laterally.

Basisphenoid and basioccipital: The basisphenoid forms the anterior margin of the median eustachian foramen and extends ventrally on to the posterior pterygoid processes. Ventral to the basioccipital, the basisphenoid is anteroposteriorly very thin, but dorsoventrally tall. The median eustachian foramen opens between the basioccipital plate and the basisphenoid. The lateral eustachian foramina are poorly preserved; however, in NHMUK OR 30392, the left foramen is visible, albeit filled with matrix (Fig. 3D). It occurs roughly in line with the median eustachian foramen, but slightly posterior to it. The external surface of the basioccipital faces posteriorly, ventral to the spherical occipital condyle. A small vertical, sagittal crest extends along the basioccipital plate.

Braincase and orbitotemporal region: One unnumbered juvenile specimen in the CAMSM preserves some of the braincase anatomy. The epipterygoid appears to be absent in this specimen. There is little to no exposure of the prootic on the external braincase wall ventral to the foramen ovale. The anterior margins of the laterosphenoid capitate processes are oriented obliquely relative to the midline. The well-formed lateral laterosphenoid bridge is anteroposteriorly thick, fully enclosing the ophthalmic foramen medially. The lateral surface of the laterosphenoid bridge is excavated by a broad groove for the maxillary ramus of cranial nerve V, and there is no development of a caudal laterosphenoid bridge dorsal to the foramen ovale. The supraorbital foramen, which usually pierces the laterosphenoid–quadrate suture at this level, cannot be discerned. The pterygoid is broken away ventrally, but it is unlikely that any ascending process of the pterygoid contributed to the laterosphenoid bridge sensu *Alligator*. Although missing, the suture scar for

the pterygoid can be traced on the quadrate, and this was most likely linear from the large, posterior, semilunate basisphenoid exposure to the foramen ovale. Only the posteriormost portion of the basisphenoid rostrum is preserved, which lacks a large lateral fossa, and is poorly exposed on the lateral braincase wall anterior to the foramen ovale. The foramina for the palatine ramus of cranial nerve VII are not preserved. *Palatine:* The palatines flare anteriorly, developing a lateral process projecting into the suborbital fenestra. The palatine–maxilla suture enters the suborbital fenestra at its anteromedial margin. The anterior tip of the palatine, truncated and with a slightly convex edge, reaches the level of the seventh interalveolar space (i.e. anterior to the suborbital fenestra), without tapering. The palatines do not significantly flare posteriorly, and thus do not form a palatine shelf, such as the one seen in *Alligator*; instead, the lateral margins of the palatines are roughly parallel posteriorly. The palatine–pterygoid suture is well preserved in NHMUK OR 25166, 30392 (Figs 1, 2) and CAMSM TN 907; in all specimens it is situated far anterior to the posterior corner of the suborbital fenestra, but varies in shape from being straight to prominently 'W' shaped.

Ectopterygoid: The relationship between the ectopterygoid and the maxilla was evaluated on the basis of NHMUK OR 30392, the only specimen preserving the posterior region of the maxillary tooth row. The anterior process of the ectopterygoid is pointed, reaching the level of the anterior margin of

the 15th maxillary alveolus (Fig. 2D). The ectopterygoid forms the medial wall of the last maxillary alveolus only. Anterior to this alveolus, the maxilla is so prominently developed medially that the ectopterygoid does not about the maxillary tooth row. As commented upon by Brochu (1997), this condition is closer to other alligatoroids than to the plesiomorphic crocodylian condition. The posteroventral process is approximately twice the length of the anterior process. This posteroventral process does not reach the tip of the pterygoid at maturity; instead it terminates beyond midlength of the pterygoid wing. The ectopterygoid–pterygoid flexure is clearly visible in the juvenile skull NHMUK OR 25167, as well as the pterygoids and associated ectopterygoids (NHMUK OR 30251) (Fig. 8A) of a fully-grown individual that might belong with NHMUK OR 30393. Based on NHMUK OR 30251, the ventrolateral surface of the ectopterygoid, near the margin of the suborbital fenestra, is pierced by two foramina on the right side and three on the left. The ectopterygoid has a blunt posterior process on the medial surface of the jugal arch (Fig. 7B), and sends an ascending branch along the medial surface of the postorbital bar. Immediately anterior to the sutural surface for the jugal, on the anterior branch of the left ectopterygoid, there is a large foramen.

Pterygoid: The pterygoid forms the posterior margin of the suborbital fenestra. The pterygoid–ectopterygoid suture, visible in lateral view, intersects the posterolateral/posterior edge of the suborbital fenestra. The pterygoid wings are large and robust.
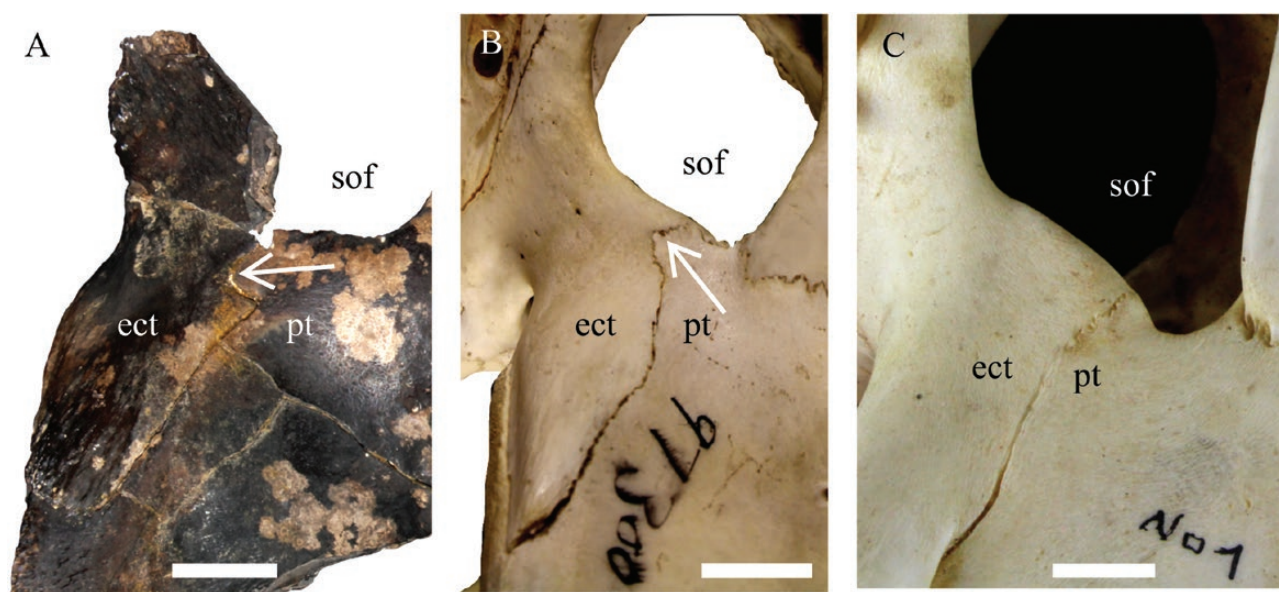

Figure 8. Comparisons of the ectopterygoid–pterygoid suture in *Diplocynodon hantoniensis* and other crocodylians: A, *D. hantoniensis* (NHMUK OR 30251); B, *Caiman yacare* (AMNH 97300); C, *Crocodylus acutus* (FMNH 69884). White arrows indicate the position of the ectopterygoid–pterygoid flexure. Scale bars = 2 cm in all specimens.

Their lateral margins are thickened and expanded dorsoventrally, with a rugose texture. A distinct sulcus runs parallel and dorsal to the suture with the ectopterygoid along the lateral surface of the pterygoid (Fig. 7C). Two foramina are present within the fossa on the left side of NHMUK OR 30251: a large posterior foramen, filled with matrix, and a much smaller anterior foramen. An equivalent small anterior foramen is also present on the right side. Anteriorly, the pterygoid is sutured to the palatine. Dorsally, they form the dorsolateral walls of the nasopharyngeal passage. The two halves of the pterygoids rise dorsomedially, meeting at the midline to surround the airways, forming a dorsoventrally tall and transversely very thin wall, immediately below the level of the frontal. The posterior pterygoid processes project posterodorsally and slightly laterally. They are dorsoventrally tall and posteriorly prominent, and developed ventrally to the median eustachian foramen. The choanae open centrally within the pterygoids. In posterior view, the pterygoid wings extend posteroventrally at around 30° from the horizontal. The dorsal surface of each wing is strongly concave. This concavity results from the large rugose 'buttress' that defines the lateral edge of each pterygoid wing, the dorsomedially directed lamina that encloses the nasopharyngeal duct, as well as the posteromedial process. This concavity flattens out posteriorly towards where the pterygoid wing forms an acute process.

Mandible

Preservation: As with the crania, some lower jaws are completely isolated [NHMUK OR 25188 (Fig. 9), NHMUK OR 30394 (Fig. 10), NHMUK OR 30397, NHMUK OR 30396, CAMSM TN 904], whereas others are preserved on a slab along with vertebrae, e.g. NHMUK R 1045. NHMUK OR 30396 is a fused pair of mandibles braced with a metal rod. Only one pair of mandibles is associated with a cranium – NHMUK OR 30393, but very few mandibular features can be discerned from this specimen. Across these specimens, nearly all elements of the mandible are preserved, with the exception of the coronoid. A list of mandibular measurements is presented in Table 2.

Mandibular fenestrae and major openings: The external mandibular fenestra is moderately large and oval-shaped, but the foramen intermandibularis caudalis is barely visible in lateral view. The presence of the foramen intermandibularis medius cannot be determined due to the absence of the coronoid in all specimens. The dentary–surangular suture intersects this fenestra slightly anterior to the posterodorsal angle of the opening (very close to the angle in NHMUK OR 25178) (Fig. 9C, D), whereas the

dentary–angular suture reaches about the midlength of the ventral rim of the fenestra. The angular–surangular suture intersects the fenestra ventral to the posterodorsal angle.

Dentary: The best-preserved dentaries (i.e. NHMUK OR 30396, 30397) each host 20 alveoli. The dentaries are gently curved between the fourth and 11th alveoli. There is some variation in the posterior extent of the dentary symphysis: it extends to the middle of the fourth alveolus in NHMUK OR 25178 and 30394 (Figs 9A, 10A), to the posterior rim of the fourth alveolus in NHMUK OR 30397 and to the middle of the fifth alveolus in NHMUK OR 30396 and R 1043. In lateral view, the dorsal edge of the dentary gently undulates: the concavities correspond to the second, seventh and 14th alveoli, whereas the convexities correspond to the first alveolus, the third interalveolar space, and the 12th alveolus. The jaw is also slightly festooned in dorsal view, with a main lateral convexity corresponding to the confluent third and fourth alveoli. Posteriorly, between the fourth and tenth alveoli, the jaw is slightly concave laterally. The third and fourth alveoli are the largest, with the latter slightly the larger of the two, and are confluent with one another. Posteriorly, alveoli five to nine are smaller and approximately equal in anteroposterior length. The next largest dentary alveolus is the 12th. The seventh interalveolar space is at least a little larger than the surrounding ones in all specimens (for very clear examples, see NHMUK OR 30287 and 30321). The Meckelian groove begins at the posterior end of the dentary symphysis, at approximately mid-height. In NHMUK OR 30397, a foramen perforates the dentary along the Meckelian groove, at the level of the ninth dentary alveolus.

Splenial: The splenials are well preserved in at least NHMUK OR 25178, 30394 and 30396. They are not involved in the symphysis of the lower jaw and their anterior tip is located ventral to the Meckelian groove (Fig. 9E, F). Given the lack of foramina in this region, the mandibular ramus of cranial nerve V can be inferred to have left the Meckelian groove at the anterior end of the splenial. There is a foramen at mid-height of the splenial, at the level of the 16th dentary alveolus in NHMUK OR 30394 (Fig. 10F) and possibly in NHMUK OR 25178 too. In NHMUK OR 30396, the splenial does not form the dorsomedial wall of the posteriormost dentary alveoli; however, in NHMUK OR 25178, the splenial approaches the medial wall of the final three alveoli, and formed the wall at least in the last two. The anterodorsal margin of the foramen intermandibularis caudalis is open in all specimens where preserved, indicating that the splenial formed the anterior margin of this foramen.

Angular: The angular of NHMUK OR 30394 (Fig. 10) is well preserved. Towards its anterior end, the angular extends dorsally to the foramen intermandibularis
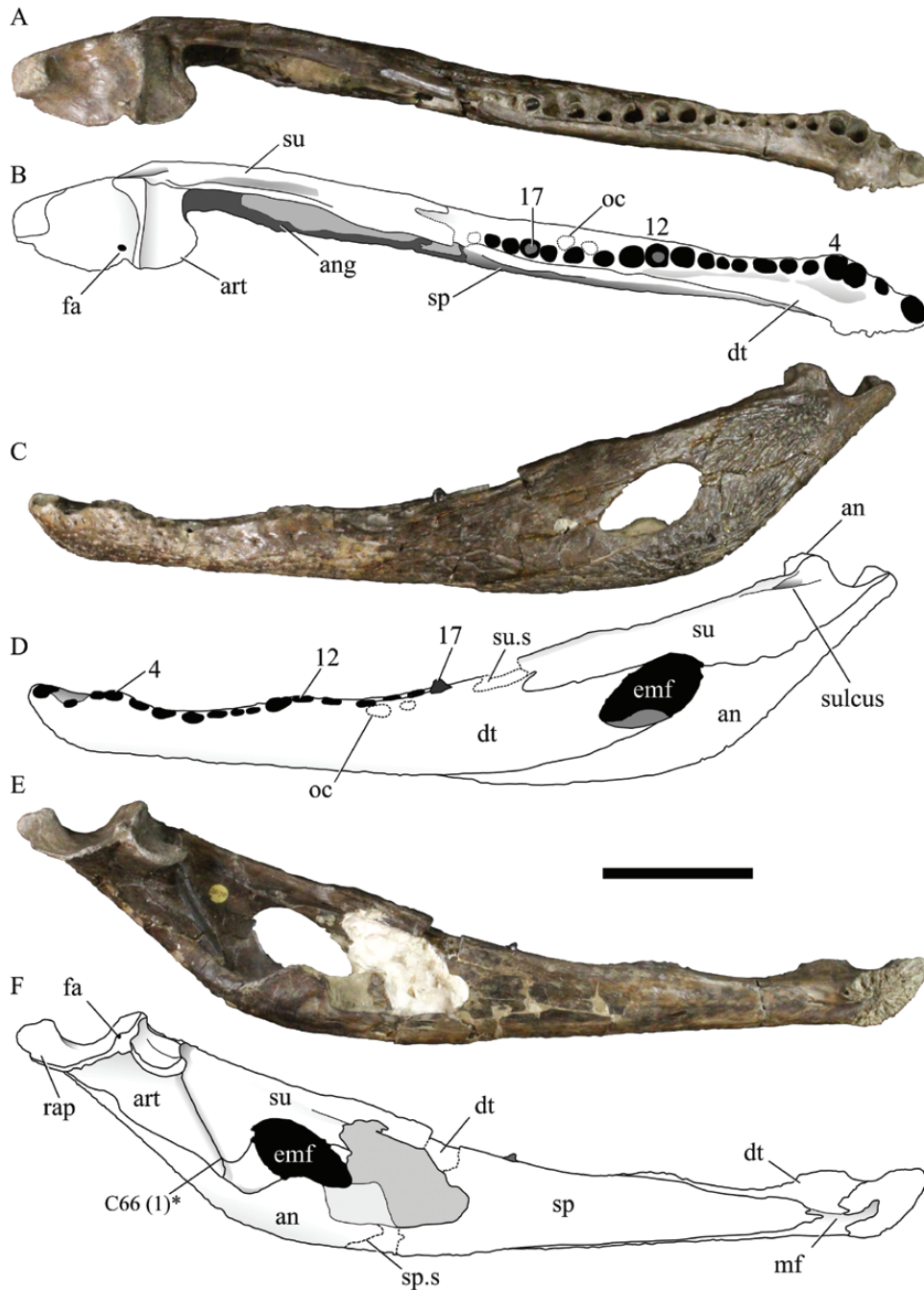
Figure 9. Left mandibular ramus of *Diplocynodon hantoniensis* (NHMUK OR 25188) in dorsal (A, B); lateral (C, D); and medial (E, F) views. Abbreviations: 4, 12, 17, alveolus positions in the dentary; an, angular; art, articular; dt, dentary; emf, external mandibular fenestra; fa, foramen aerum; fo, foramen; mf, Meckelian fossa; oc, occlusal pit; sp, splenial; sp.s, suture scar for the splenial; su, surangular. Scale bar = 10 cm.

caudalis, with a tip that is rather rounded and dorsoventrally tall (Fig. 10F). The lateral surface of the angular is strongly ornamented with pits and furrows (Figs 9C, 10C). However, they do not continue onto the ventral surface, nor do they extend onto the lateral surface of the retroarticular process. A longitudinal ridge occurs on the ventral margin of the angular, extending onto the lateral surface, and defines the boundary between the anterior ornamented surface of the angular from the posteriorly smooth surface, beneath the retroarticular process (Fig. 11A). This ridge is very prominent in NHMUK OR 30396,
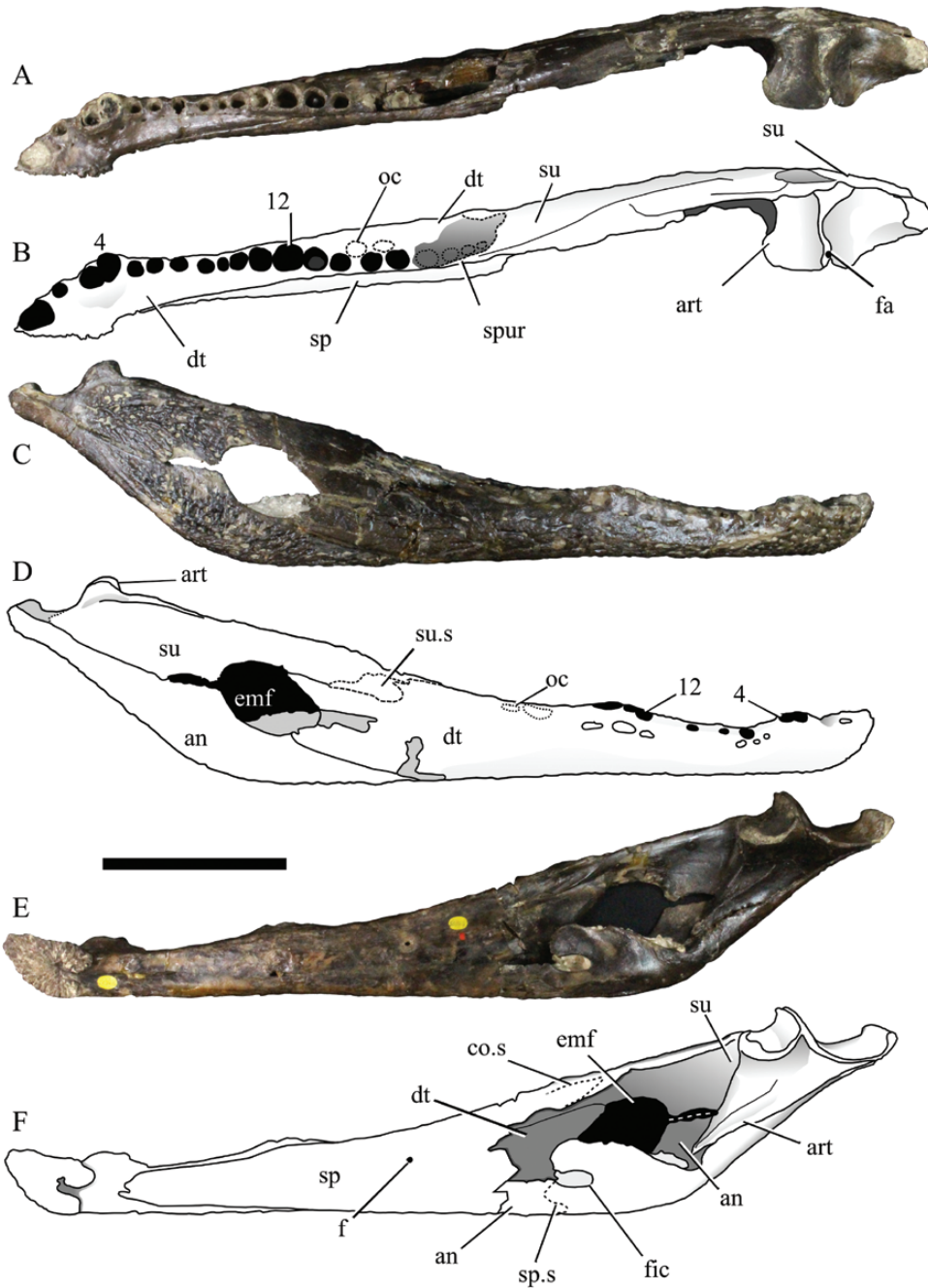
Figure 10. Right mandibular ramus of *Diplocynodon hantoniensis* (NHMUK OR 30394) in dorsal (A, B); lateral (C, D); and medial (E, F) views. Abbreviations: 4, 12, alveolus positions in the dentary; an, angular; art, articular; co.s, suture scar for coronoid; dt, dentary; emf, external mandibular fenestra; fa, foramen aerum; fic, foramen intermandibularis caudalis; fo, foramen; mf, Meckelian fossa; oc, occlusal pit; sp, splenial; sp.s, suture scar for the splenial; su, surangular. Scale bar = 10 cm.

NHMUK OR 30397 and CAMSM TN 904 but less well-developed in NHMUK OR 30394 and 25178. This feature probably marks the anterior limit of the insertion of M. pterygoideus ventralis, which inserts in a similar position in living caimans (Bona & Desojo, 2011), imparting the same ridge (Fig. 11B). This differs markedly to the condition in all *Crocodylus* (Fig 11C) and *Alligator* species, which lack a sharp ridge and in which the ventral margin of the angular is very exposed in lateral view. There is a large longitudinal sulcus along the ventromedial surface of the angular. This sulcus begins posterior to the foramen intermandibularis

Table 2. Mandibular measurements of *Diplocynodon hantoniensis* (mm)

Feature	NHMUK OR 30394	NHMUK OR 25188
Mandible length	480	469
Tooth row length	265	259
External mandibular fenestra length	62	60
External mandibular fenestra height	29	32
Width across glenoid fossa	42	42
Retroarticular process length	61	62
Mandible height at fourth tooth	39	37
Symphysis length	54	52

Figure 11. Comparison of the posterior ramus of the mandible in lateral view in A, *Diplocynodon hantoniensis* CAMSM TN 904; B, *Caiman latirostris* Daudin, 1801 MACN V 1420; and C, *Crocodylus siamensis* Schneider, 1801 NHMUK 1921.4.1.168. Black arrow indicates the boundary between the ornamented and unornamented surface. Scale bar = 5 cm.

caudalis, and terminates approximately at its anterior margin. A series of large foramina occur posterior to this sulcus in all specimens except for NHMUK OR 30397, which is poorly preserved in this region. Whereas there are two foramina in NHMUK OR 30394, there are three in NHMUK OR 25178 and NHMUK OR 30396. The anterior extent of the angular is difficult to fully discern; however, it appears to reach the level of the 17th alveolus based on the articulated mandible NHMUK OR 30396 and the isolated left ramus NHMUK OR 25178. Posteriorly, the angular extends to the posterior end of the retroarticular process, along the ventrolateral margin, terminating in an acute process.

Surangular: The anterior processes of the surangular are best preserved in in NHMUK OR 30381 (Fig. 12) and NHMUK OR 30396. They are subequal in length, with the dorsal process extending slightly further anteriorly than the ventral one. This morphology is confirmed by NHMUK OR 25178 (Fig. 9D), in which the dorsal process, despite being slightly incomplete anteriorly, is so thick and robust at its preserved anterior end that it had to be longer than the completely preserved ventral process. NHMUK OR 30394 preserves a broken ventral process of the
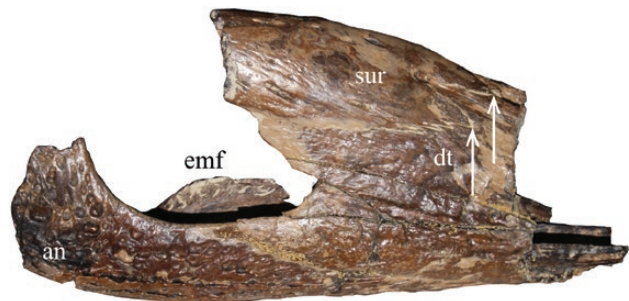

Figure 12. Posterior ramus of the right mandible of *Diplocynodon hantoniensis* (NHMUK OR 30381), lateral view. Arrows indicate the anterior extent of the dorsal and ventral surangular processes. Abbreviations: an, angular; dt, dentary; emf, external mandibular fenestra; sur, surangular. Scale bar = 4 cm.

surangular (whose development is implied by the scar it left on the accompanying dentary) and a very long, tapering, laminar dorsal process (Fig. 10D). The surangular spur between the dentary and splenial is not completely preserved in any one specimen. In NHMUK OR 30394, the spur is mostly preserved and visible sutured to the medial surface of the splenial (Fig. 10B). The posteriormost alveoli are not preserved in this specimen, but the process most likely reached at least the 17th interalveolar space. This can be confirmed in NHMUK OR 25178 and CAMSM TN 904. In both specimens, the surangular spur is not completely preserved. However, the scar for the spur on the splenial is adjacent to the last three alveoli.

Just above the external mandibular fenestra and up to the glenoid fossa, the dorsal edge of the surangular is flat and gently laterally sloping area (Fig. 9A, B). Posterior to this smooth area, the surangular approaches the dorsal tip of the lateral wall of the glenoid fossa, though does not completely cover it in lateral view. A very prominent sulcus occurs on the dorsolateral margin of the surangular, at the level of the glenoid fossa (Fig. 9D). Posteriorly, the tip of the surangular does not reach the posterior tip of the retroarticular process in either of the mandibular rami of NHMUK OR 30396, but it is much more posteriorly developed in NHMUK OR 25178 (Fig. 9D). The surangular–angular suture intersects the articular close, but dorsal to the ventral tip (Fig. 9F).

The surangular–articular suture is very straight in the posterior wall of the adductor chamber, lacking laminae and not recessed in a sulcus. A lingual foramen for the articular artery, infilled with matrix, can be discerned in all specimens. In NHMUK OR 30396 and CAMSM TN 904, the lingual foramen is situated on the surangular–articular suture, whereas it is located solely on the articular in remaining specimens (i.e. NHMUK OR 25178, 30394 and 30397). Posteriorly, the surangular–articular suture is situated on the lateral edge of the glenoid fossa, and is not bowed within the fossa. It also extends onto the dorsolateral surface of the transverse ridge that separates the retroarticular process from the glenoid fossa. At its posteriormost extent, the suture forms the sharp lateral margin of the retroarticular process.

Articular: The retroarticular process is short and oriented posterodorsally. The foramen aëreum is large and clearly inset from the margin of the retroarticular process. A sharp, vertical lamina occurs for a short distance posterior to the foramen aëreum. On the medial surface, there is a prominent, wedge-shaped sulcus, dorsally defined by a ridge. This runs approximately parallel to the articular–angular suture, and is perpendicular to the anteromedial corner of the articular. This ridge was probably associated with the attachment of M. pterygoideus dorsalis, which is known to attach to the medial surface of the articular in living crocodylians, e.g. *Alligator mississippiensis* (Holliday *et al.*, 2013). The medial edge of the retroarticular process is sharp, and overhangs the medial surface of the articular as a shelf, as does the medial edge of the hemifossa. At the level of the transverse ridge, there is a large medial notch dividing the retroarticular process from the glenoid fossa.

Pattern of occlusion: There are five alveoli in each premaxilla, 17 in each maxilla and 20 in each dentary. All of the alveoli are approximately circular in cross-section. None of the juvenile specimens preserve the premaxilla, meaning that it is not possible to directly assess the changes through ontogeny of the relationships between the fourth dentary tooth and the region corresponding to the premaxillo-maxillary suture. However, the four fully grown specimens show significant variation, suggesting that ontogenetically the primitive condition was the one with the tooth hosted in a pit, and that in some cases the outer wall of the pit could be progressively eroded, giving origin to a notch. In particular, NHMUK OR 25166 has a deep pit on the premaxilla between the last alveolus and the suture with the maxilla (Fig. 1C, D). NHMUK OR 30392, 30393 and CAMSM TN 907 all clearly show a notch corresponding to the premaxillo-maxillary suture (Figs 2D, 3B). Such variability is also shown in isolated premaxillae NHMUK OR 30369 and 30370, with a pit in the former and a lateral notch in the latter. The left premaxilla of NHMUK OR 25166 (the type of *Diplocynodon hantoniensis*) shows a very deep and large occlusal pit located lingual to the tooth row, close to the suture with the maxilla; a second pit, much smaller but as deep, is placed lingual to the first maxillary alveolus. The preservation on the right side of the same skull hinders the detection of the latter pit, but the one on the premaxilla is placed more in line with the alveoli than the corresponding pit on the left premaxilla.

The disposition of the occlusal pits on the maxillae indicates that the dentary teeth occluded lingual to the maxillary teeth, except for those occluding in line after the sixth and seventh maxillary teeth. This is clearly shown in the maxillae of NHMUK OR 25166 (Fig. 1D), 25168–9 and 30392 (Fig. 2D), and is confirmed by the dentaries of NHMUK R1043, 25178, 30394 and 30397, all of which have occlusal pits labial to interalveolar spaces 14 and 15 (Figs 9B, 10B).

In the premaxilla, the third and fourth alveoli are the largest, with the latter slightly larger. The fifth alveolus is the smallest, and the first and second alveoli are equally intermediate in size. Two large occlusal pits (one on each side) occur within the premaxillary palate, between the first and second premaxillary alveoli, and are separated posteromedially from the incisive foramen by a thin straight wall. Only the left

occlusal pit is visible in NHMUK OR 30392, as the right is infilled with matrix. In NHMUK OR 25166, the walls of the pit are very thin and worn.

In the maxilla, alveoli four and five are the largest, and subequal in size, corresponding to the first lateral and ventral convexity of the maxilla. Alveoli six to eight are smaller and subequal in size. Alveolus size increases posteriorly from alveolus eight, reaching a second maximum at position ten and 11, which are subequal. Posteriorly from alveolus 11, the alveoli gradually decrease in size and remain circular.

In the dentary, the first alveolus is largest and the second alveolus is considerably smaller. Alveoli three and four are subequal and confluent; they are larger than alveolus two, and slightly smaller than alveolus one. Alveoli five to ten are smaller than alveoli three and four. Alveoli 11 and 12 are larger than the preceding six alveoli. In some specimens, alveolus 13 is as large as 11 and 12, e.g. NHMUK OR 30396. Posteriorly from alveolus 13, the alveoli are subequal and smaller.

Dentition

NHMUK OR 25166 preserves a nearly continuous series of premaxillary and maxillary teeth in place. All premaxillary and anterior maxillary teeth are conical and lingually curved, with smooth carinae, and commonly preserve faint longitudinal striations (Fig. 13A, B). Carinae occur on the medial and lateral edges of the anteriormost premaxillary teeth, but on the anterior and posterior edges of all other premaxillary and maxillary teeth (Fig. 13D).

Posteriorly, the maxillary teeth become shorter, more globular and less lingually curved, though never becoming blunt as they retain modest carinae and pointed tips (Fig. 13C). A small constriction separates the tooth crown from the root, as in *D. remensis* (Martin *et al.*, 2014) (Fig. 13E, F).

Fewer dentary teeth are preserved in place (e.g. NHMUK OR 30396). However, the same pattern is observed, with anteriorly very conical teeth, with smooth carinae, becoming shorter and more globular posteriorly.

Axial column

Cervical, dorsal, lumbar, sacral and caudal vertebrae are all preserved, as are postaxial ribs from these regions (excluding gastralia). Most vertebrae in the NHM collections are isolated, except for a continuous series of cervical to sacral vertebrae (NHMUK OR 30402), which have been manually assembled. It is unknown whether these associated vertebrae belong to one or multiple individuals. However, the preservation of the vertebrae is similar, and there is serial variation in size and morphology, indicating that they might belong to one individual. We use this specimen as a basis for a description of the axial column. *Diplocynodon hantoniensis* appears to have had nine cervical, 15 dorsal and two sacral vertebrae, as in extant crocodylians (Hoffstetter & Gasc, 1969). The number of caudal vertebrae cannot be determined. None of the associated cervical to sacral vertebrae of NHMUK OR 30402 show any hint of neurocentral suture, suggesting that they belong to an adult individual. All of the vertebral centra are fully procoelous, with the exception of the first sacral centrum that is concave anteriorly and flat to slightly convex posteriorly and the second sacral centrum that is nearly flat anteriorly and slightly concave posteriorly.

Atlas–axis complex: The boomerang-shaped proatlas NHMUK OR 30289 is incomplete (Fig. 14G–I): the right posteroventral tip is missing and the long anterior process is partially damaged. When compared to the dorsal crest, the ventral tubercle is rather short in lateral view. The height of the dorsal keel cannot be fully determined because it is partly damaged. No atlantal intercentrum is preserved.

The odontoid process and the axis are preserved in connection only in NHMUK R 1045 (a block hosting a fragmentary lower jaw, several cervical vertebrae, ribs and osteoderms), but the large odontoid process NHMUK OR 25186 (Fig. 14E, F) fits well in size, shape and colour with an unnumbered axis (Fig. 14A). The anterior surface of the axial centrum is flat for reception of the odontoid process, whereas the posterior end forms a condyle. Two deep grooves, pierced by foramina, excavate the lateral surface of the centrum, delimiting a prominent ridge (Fig. 14A). The ventral surface of the centrum is defined by a sharp midline keel. The unforked axial hypapophysis does not approach the anterior end of the centrum. In lateral view, the neurocentral suture is clearly visible. The neural canal is taller than wide. Whereas the circular prezygapophyses are very small, postzygapophyses are much larger and oval-shaped. In axial view, both sets of zygapophyses are inclined at an angle of approximately 45° to the horizontal. The axial neural arch bears an anteroventrally facing, sub-rounded facet directly ventral to the prezygapophyses, which contacts the odontoid process. The lateral margins of the neural arches are sculpted with fossae and ridges, and there is no trace of a diapophysis on their lateral surfaces. The axial neural spine is tall, with a consistent thickness along its length. Its dorsal margin is near-horizontal (although the anterior sector of the neural spine is broken off in NHMUK R 1045), and does not develop any posterior crest. The posteriormost tip of the axial neural spine extends beyond the posterior margins of the condyle and postzygapophyses. A fossa excavates the lateral surface of the axial neural spine at midlength.
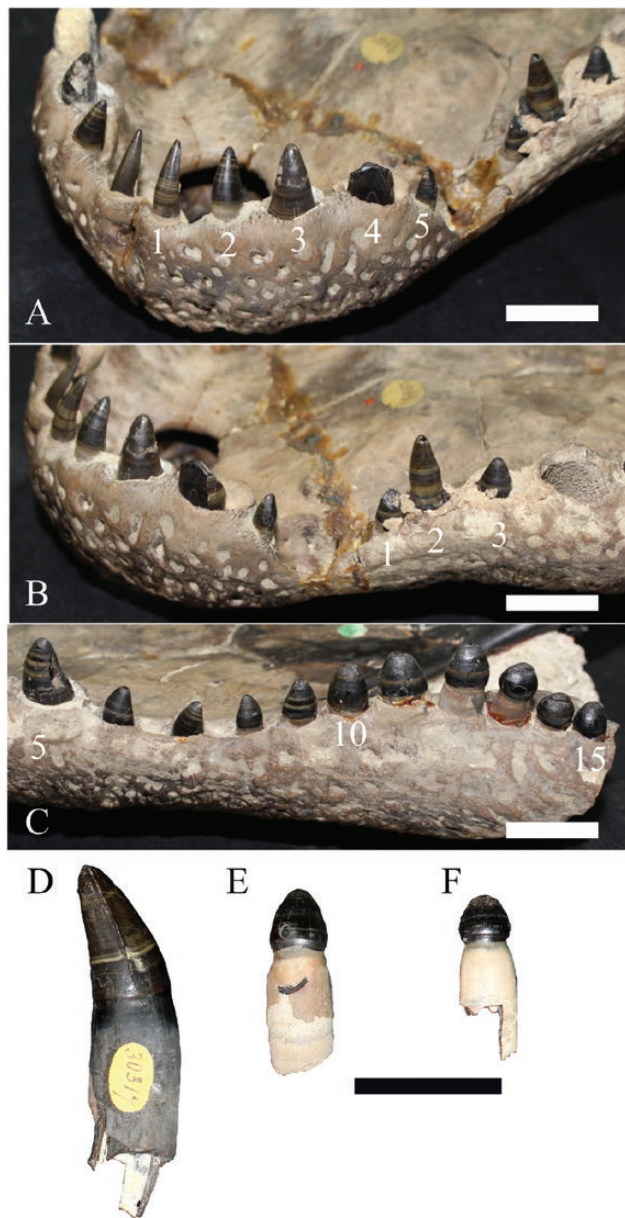
Figure 13. The dentition of *Diplocynodon hantoniensis*. A–C, NHMUK OR 25166 in anteroventral view (A), anterolateral view, showing the premaxilla–maxilla transition (B) and lateral view showing the posterior maxillary dentition (C). D, NHMUK OR 30317, isolated tooth from the anterior region of the dentition in mesial view; E–F, unregistered isolated teeth from the posterior region of the dentition in labial view. All scale bars = 2 cm.

Cervical vertebrae: The ventral surfaces of the cervical centra lack deep pits (these are also absent from the first dorsal vertebra, Dv1). Posterior to the hypapophyses, the ventral margin of the centrum is very sharp in most cervical vertebrae, except in cervical vertebrae (Cv) 4 and 5, in which the ventral

margin is flat and wide. Assuming that the sequence of the associated series of vertebrae NHMUK OR 30402 is correct, the posteriormost hypapophysis is represented by a small elongated knob on the 12th vertebra posterior to the atlas.

The hypapophyses are not preserved in Cv3–5 of NHMUK OR 30402 (Fig. 15), but a raised, broken surface indicates that they were still present. Relatively short hypapophyses are consistently positioned towards the anterior margin of the centrum, and are closely flanked either side by parapophyses. In Cv7, 8 and Dv3, 4 of NHMUK OR 30402, hypapophyses are swept slightly anteriorly. This can also be observed in several well-preserved isolated cervical vertebrae (NHMUK R 1046, NHMUK OR 25177 and NHMUK OR 25210). However, Cv9 and Dv1 of NHMUK OR 30402, although slightly worn, have hypapophyses that are directed almost directly ventrally.

The parapophyses in the first postaxial cervical vertebra (Cv3) are poorly preserved, but are situated very close to the hypapophyses. Moving posteriorly through the cervical vertebrae, the parapophyses remain approximately at the same level on the centrum. Parapophyses are preserved and articulated with cervical ribs in Cv4–7. Here, the parapophyseal articular facets are elliptical, with the long axis oriented anteroposteriorly. The parapophyseal facets are directed ventrolaterally, slightly more laterally than the diapophyses. In the tenth postaxial vertebra (Dv3), the parapophyses move dorsally to the base of the transverse process. In between the parapophyses and diapophyses, the lateral surface of the centrum has a prominent sulcus in Cv3–7. A lateral fossa is still present in Cv8 to Dv2, although it is much shallower and located posterior to the parapophysis on the lateral surface of the centrum. Diapophyses have small circular facets on Cv3, which are directed ventrally and slightly laterally. In subsequent cervical vertebrae, the diapophyseal facets become more elliptical, with the long axis oriented anteroposteriorly, although they still project ventrolaterally. The width across the prezygapophyses is smaller than that of the postzygapophyses in Cv3–4. Further along the cervical series, the zygapophyseal widths are subequal. The prezygapophyseal facets are elliptical, inclined approximately at 45° to the horizontal in axial view. The size of the prezygapophyseal facets increases posteriorly from Cv3 to Cv5 as vertebral size increases. The anteriormost cervical vertebrae have anterolaterally orientated prezygapophyses, but these become more laterally elongated in subsequent cervical vertebrae. The postzygapophyses have the same inclination as the prezygapophyses, with elliptical facets. Cervical neural spines are positioned at the posterior end of the neural arch. The dorsally incomplete neural spine of Cv3 is anteroposteriorly
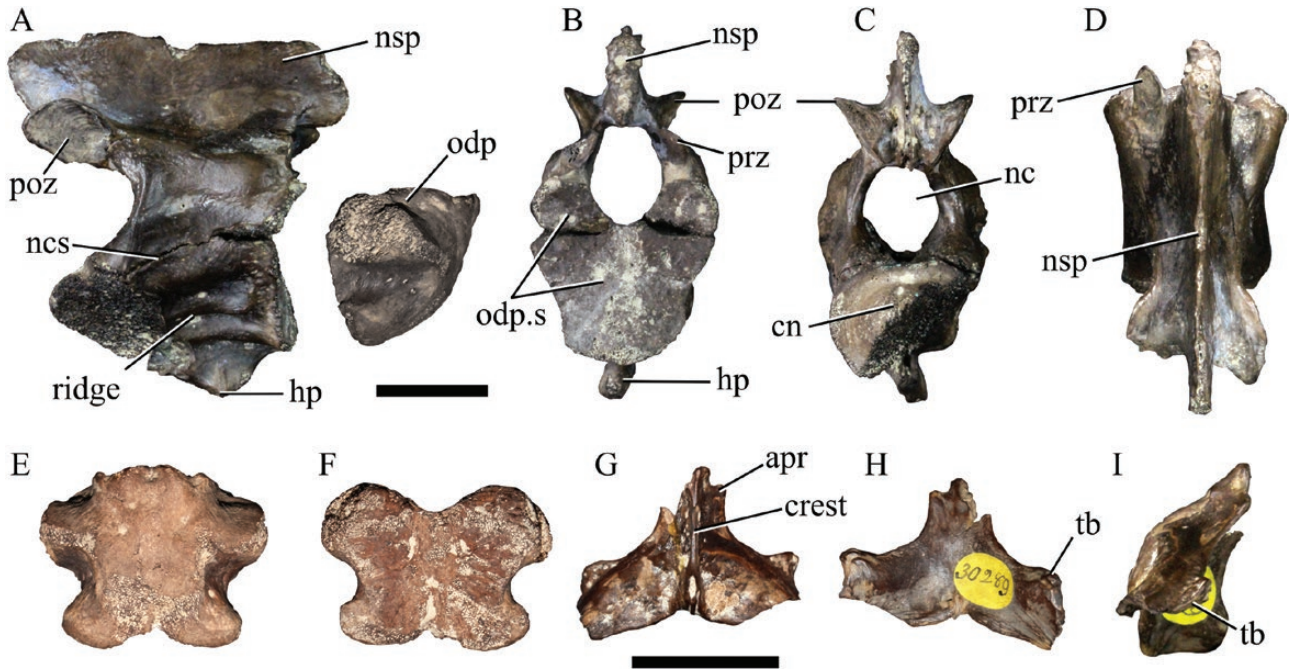
Figure 14. Atlas–axis complex of *Diplocynodon hantoniensis*. A–D, axis in lateral (A), anterior (B), posterior (C) and dorsal (D) views. E–F, unregistered odontoid process in anterior (E) and posterior (F) views. G–H, proatlas NHMUK OR 30289 in dorsal (G), ventral (H) and ventrolateral (I) views. Abbreviations: apr, anterior process; cn, condyle; hp, hypapophysis; nc, neural canal; ncs, neurocentral suture; nsp, neural spine; odp, odontoid process; odp.s, sutural surface for the odontoid process; poz, postzygapophysis; prz, prezygapophysis; tb, ventral tubercle. All scale bars = 3 cm.

long, greater than half the anteroposterior length of the non-condylar centrum. An isolated, but better preserved, Cv3 (NHMUK R 1046) preserves the same shape, but the neural spine is anteriorly hooked at its dorsal tip (Fig. 15A). Cv4 has a similarly wide neural spine, but the neural spines become anteroposteriorly shorter in Cv5–7. In Cv4, the neural spine is oriented primarily dorsally, with a slight anterior deflection. In lateral view, it has a concave anterior margin. The neural spines of Cv5–6 have a similar orientation, but lack the concave anterior margin. The neural spines become anteroposteriorly longer in Cv8 and Cv9.

Dorsal vertebrae: The lateral and ventral surfaces of the dorsal vertebral centra are featureless, lacking the lateral fossa seen in cervical vertebrae, as well as a hypapophysis after Dv3 (Fig. 16). Dorsal vertebrae have prominent transverse processes and their zygapophyses are more shallowly inclined than those of the cervical vertebrae (Fig. 17). The width across the prezygapophyses is consistently greater than that across the postzygapophyses, but the long axes of both are laterally directed. Neural spines are anteroposteriorly long, with an inclined dorsal edge (i.e. higher at the anterior end and sloping posteriorly) and laterally flared dorsal tips (Fig. 17). Neural spine height decreases across the first four dorsal vertebrae, stabilizing at a consistent height from Dv4.

Sacral vertebrae: The tuberculum and capitulum of the sacral vertebrae (Fig. 18) are approximately equally well-developed, such that it is not possible to see the latter in dorsal view (e.g. NHMUK OR 25179). This is also the case in three anterior sacral vertebrae accessioned under NHMUK R 1050. However, the tuberculum is slightly shorter than the capitulum (meaning that the latter is visible) in a fourth anterior sacral vertebra, bearing the same collection number, and in NHMUK OR 30402 (Fig. 18D).

Caudal vertebrae: Relatively few caudal vertebrae are preserved and they are disarticulated (NHMUK R 1052 and several unnumbered specimens) (Fig. 19). The vertebral centrum is very elongated, with tuberosities on the ventral surface, immediately anterior to the posterior condyle, for articulation with chevrons (which are not preserved). A longitudinal sulcus occurs on the ventral surface of the centrum, defined on each side by a ridge. Where preserved, the anteroposteriorly narrow neural spine is directed vertically and positioned towards the level of the midlength of the centrum. Transverse processes are short and the width across the prezygapophyses is significantly greater than the postzygapophyseal width.

Osteoderms: Osteoderms are preserved both as isolated elements and embedded in blocks of matrix along with other skeletal elements (Fig. 20). The rectangular
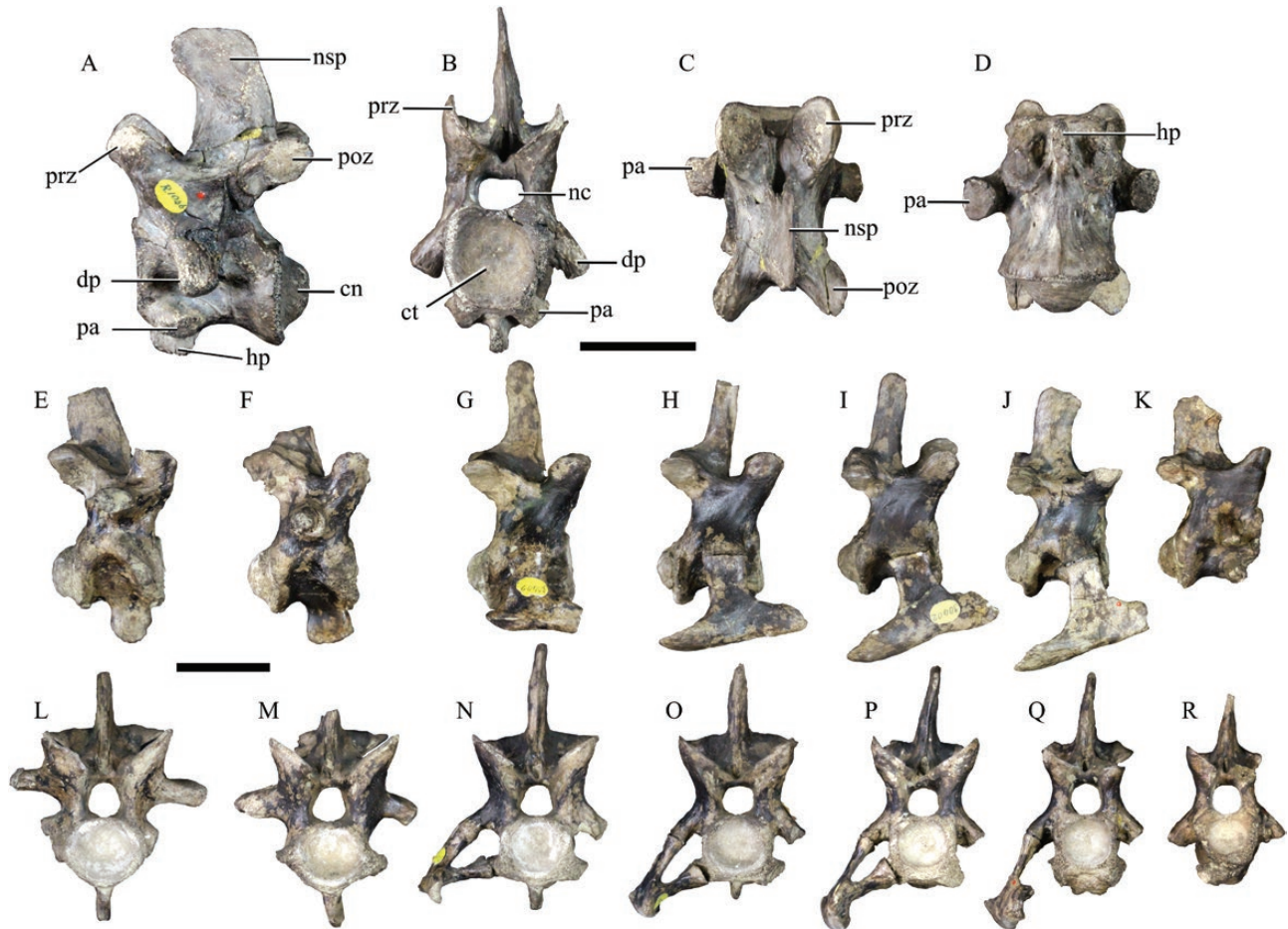
Figure 15. Cervical vertebrae of *Diplocynodon hantoniensis*. A–D, cervical vertebra 3, NHMUK R 1046 in left lateral (A), anterior (B), dorsal (C) and ventral (D) views. E–K, NHMUK OR 30402, cervical vertebra 9 (E), 8 (F), 7 (G), 6 (H), 5 (I), 4 (J) and 3 (K) in right lateral view. Abbreviations: cn, condyle; ct, cotyle; dp, diapophyses; hp, hypapophysis; nc, neural canal; nsp, neural spine; pa, parapophysis; poz, postzygapophysis; prz, prezygapophysis. All scale bars = 3 cm.

dorsal osteoderms are characterized by a smooth and narrow anterior strip, followed by a broad and pitted area that hosts a medial keel (Fig. 20A). In most of the dorsal osteoderms, the anterior margin is straight, but at least three specimens (NHMUK R 5267 partim, R 5214 partim and 46434) show an undulating anterior profile that can be defined as an anterior process (*sensu* Norell & Clark, 1990; Brochu, 1997) (Fig. 20C). The ventral osteoderms are represented by two units that are sutured together: the anterior one is anteroposteriorly narrow, with a smooth anterior half and a pitted posterior one (Fig. 20D); the posterior unit is entirely pitted and devoid of any keel (Fig. 20E, F).

Appendicular skeleton

Appendicular remains comprise most of the pectoral and pelvic girdles, as well as the proximal (upper) elements of the limbs. The limb bones are represented by robust elements, exemplified by large-sized remains, including a humerus (NHMUK OR 30206), an ulna (NHMUK OR 30236), femora (NHMUK OR 25244, 30210, 30211, 30213, 30399), tibiae (NHMUK OR 25236, 30215, 30216, 30217) and fibulae (NHMUK OR 30333, 30335). Although no associated limb bones are available, it seems likely that the forelimb was shorter than the hindlimb, as all the preserved femora are longer than the largest preserved humerus (NHMUK OR 30206). The relative anatomical orientations (i.e. medial, lateral, dorsal, ventral, etc.) reflect the sprawling posture of the forelimb, following Meers (2003: fig 1), whereas those for the hindlimb are based on Klinkhamer *et al.* (2017: fig 2).

Scapula: The horizontal articular surface for the coracoid is poorly preserved in all scapulae, but is teardrop-shaped, with a narrow anterior tip and a much larger posterior area, close to the glenoid surface. The fact that the largest scapula (NHMUK
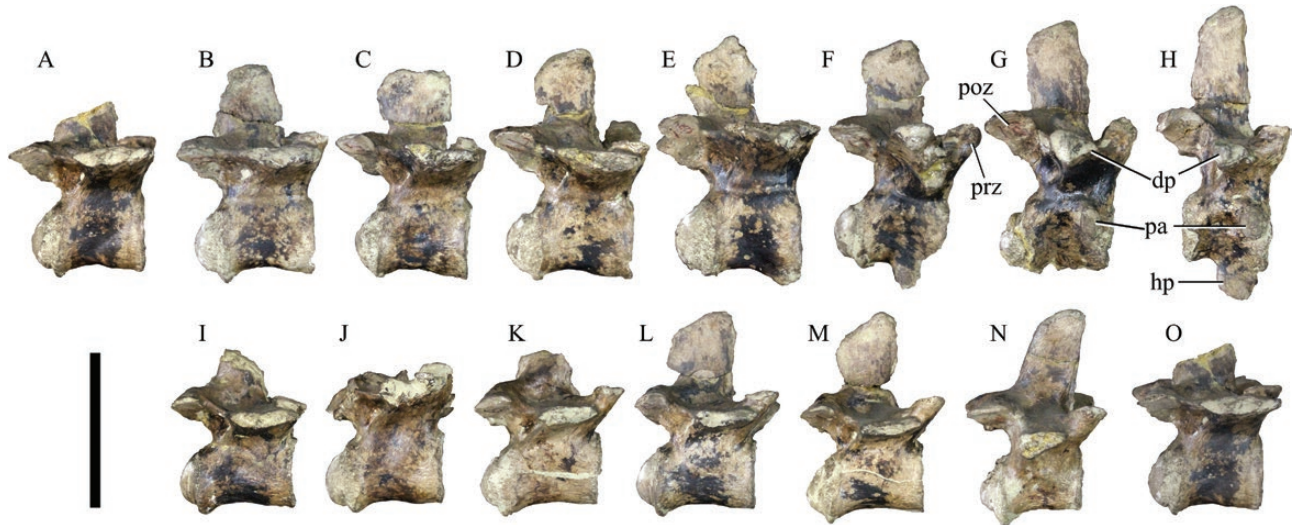
Figure 16. Dorsal vertebrae of *Diplocynodon hantoniensis* (NHMUK OR 30402). A–O, dorsal vertebrae 15–1, respectively, in right lateral view. Abbreviations: dp, diapophysis; hp, hypapophysis; pa, parapophysis; poz, postzygapophysis; prz, prezygapophyis. Scale bar = 5 cm.

OR 30247) is large, but not fused to the coracoid, implies that their fusion must have occurred very late in ontogeny. The glenoid surface of the scapula faces posterolaterally (Fig. 21A). It is large and ovoid, with a rounded dorsal margin and a modest constriction at its anterior margin. This constriction is related to a prominent fossa anterior to the glenoid surface that is pierced by a small foramen (see NHMUK OR 30247 and 30414) (Fig. 21E, F). In all specimens, regardless of size, the deltoid crest is thin.

The posterior edge of the scapular blade is straight to slightly convex and the anterior edge is concave. There is a large constriction between the ventral corpus of the scapula and the distal blade, which flares. In dorsal view, the blade is sharp and straight. The lateral surface of the scapula blade is smooth and slightly convex proximally, becoming flatter distally. Attachment sites for several muscles can be recognized on the lateral surface of the largest scapula NHMUK OR 30247 (Fig. 21F). Two distinct, broad depressions extend over the greater part of the blade. The anterior of these two depressions is the larger origin site for M. deltoideus scapularis. A low ridge separates this scar from a posterior depression, which is inferred to be the smaller origin site of M. teres major (Meers, 2003). Anterior to the attachment for M. deltoideus scapularis is a depression that occupies the anteriormost edge of the scapula and adjacent to the deltoid crest. This is the origin of M. deltoideus clavicularis. The posteriormost edge of the scapula blade also has a depression, which is inferred to be the area of insertion of M. serratus ventralis thoracis dorsally, and the site of origin for M. scapulohumeralis

caudalis ventrally (Fig. 21F). The medial surface of the blade is less sculpted than the lateral surface, with one broad depression situated slightly posterior to the blade at midlength: this likely marks the origin of M. subscapularis. Dorsal to the glenoid surface, on the glenoid buttress, is a large tubercle. This scar is prominent even in the smallest scapulae (e.g. NHMUK OR 30414) and is the attachment site for M. triceps longus lateralis (Meers, 2003).

Coracoid: Two left coracoids are preserved (NHMUK OR 30359 and 25245), although the distal ends of both are missing (Fig. 21G). The ventral surface of the glenoid surface is circular and faces posterolaterally. A small projection of the glenoid surface overhangs the recess ventral to the glenoid surface. A large coracoid foramen is situated anterior to the glenoid surface. The coracoid blade is directed ventrally and medially. Although incomplete, it expands distally, but the shape and width of the distal end cannot be determined.

Humerus: Two right humeri (NHMUK OR 30219 and 30206) are preserved, along with a partial left humerus (NHMUK OR 30206a) (Fig. 22). The proximal extremity is poorly preserved in the largest humerus (NHMUK OR 30206). In NHMUK OR 30219, the dorsal border of the articular surface is significantly raised relative to the proximal extremity of the humeral shaft. The medial condyle of the proximal end is larger than its lateral counterpart. Although slightly eroded, the deltopectoral crests of NHMUK OR 30219 and 30206a clearly emerge abruptly from the humerus. The straight deltopectoral crest is aligned with the lateral margin of the humerus (Fig. 22D, H). The apex of the deltopectoral crest projects ventrally, perpendicular to
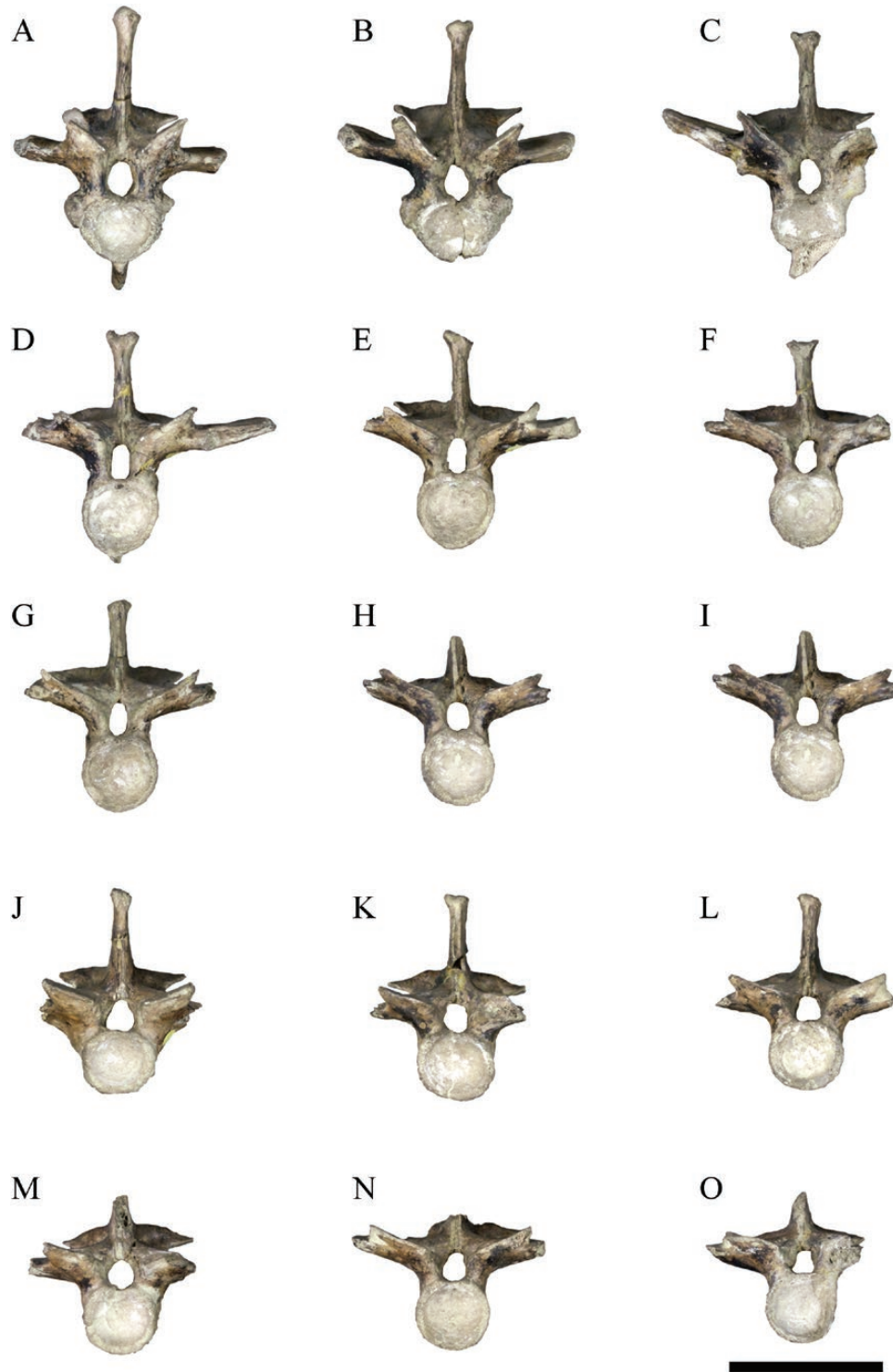
Figure 17. Dorsal vertebrae of *Diplocynodon hantoniensis* (NHMUK OR 30402). A–O, dorsal vertebrae 1–15, respectively, in anterior view. Scale bar = 5 cm.

the humeral shaft, with no medial deflection. Dorsal to the deltopectoral crest, on the lateral margin of the humeral shaft, there is a single scar for the insertion of M. teres major and M. latissimus dorsi, which is especially prominent in NHMUK OR 30206 (Fig. 22G). In lateral view, a longitudinal ridge can be
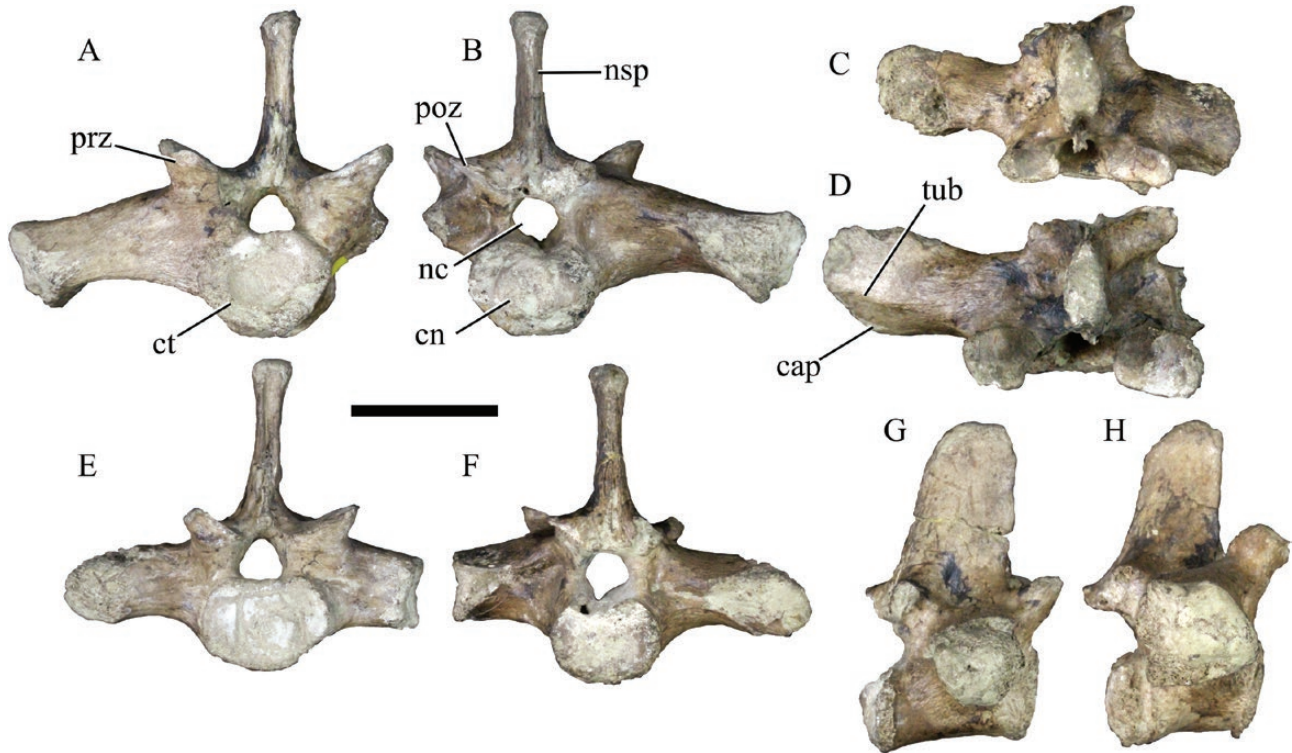
Figure 18. Sacral vertebrae of *Diplocynodon hantoniensis* (NHMUK OR 30402). The first sacral vertebra in anterior (A), posterior (B), dorsal (D), right lateral (H) views; and the second sacral vertebra in anterior (E), posterior (F), dorsal (C) and right lateral (G) views. Abbreviations: cap, capitulum; cn, condyle; cot, cotyle; nc, nueral canal; nsp, neural spine; poz, postzygapophysis; prz, prezygapophysis. Scale bar = 5 cm.
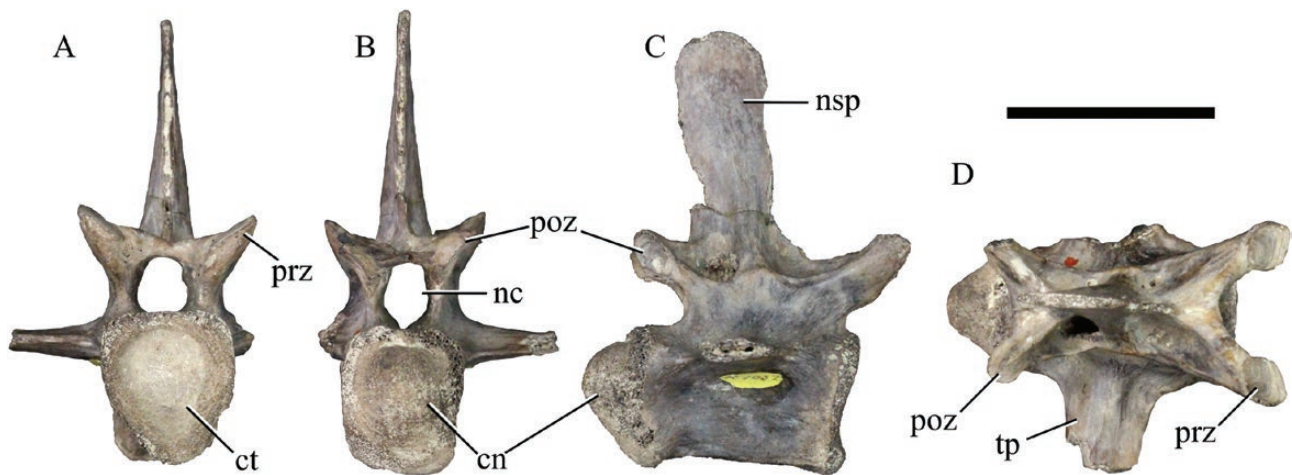

Figure 19. Caudal vertebrae of *Diplocynodon hantoniensis*. A–D, NHMUK R 1052 in anterior (A), posterior (B), right lateral (C) and dorsal (D) views. Abbreviations: cn, condyle; ct, cotyle; nc, neural canal; nsp, neural spine; poz, postzygapophysis; prz, prezygapophysis; tp, transverse process. Scale bar = 3 cm.

traced, extending from the proximal articular border, through the scar for M. latissimus dorsi, then running diagonally across the lateral side of the diaphysis (Fig. 22F). This ridge probably defines the boundary between M. humeroradialis and M. triceps brevis cranialis from the extensive dorsal origin of M. triceps brevis intermedius (Meers, 2003). Medial to the M. teres major scar, there is a broad depression on the dorsal surface of the proximal metaphysis. Based on a comparison with extant crocodylians this might be
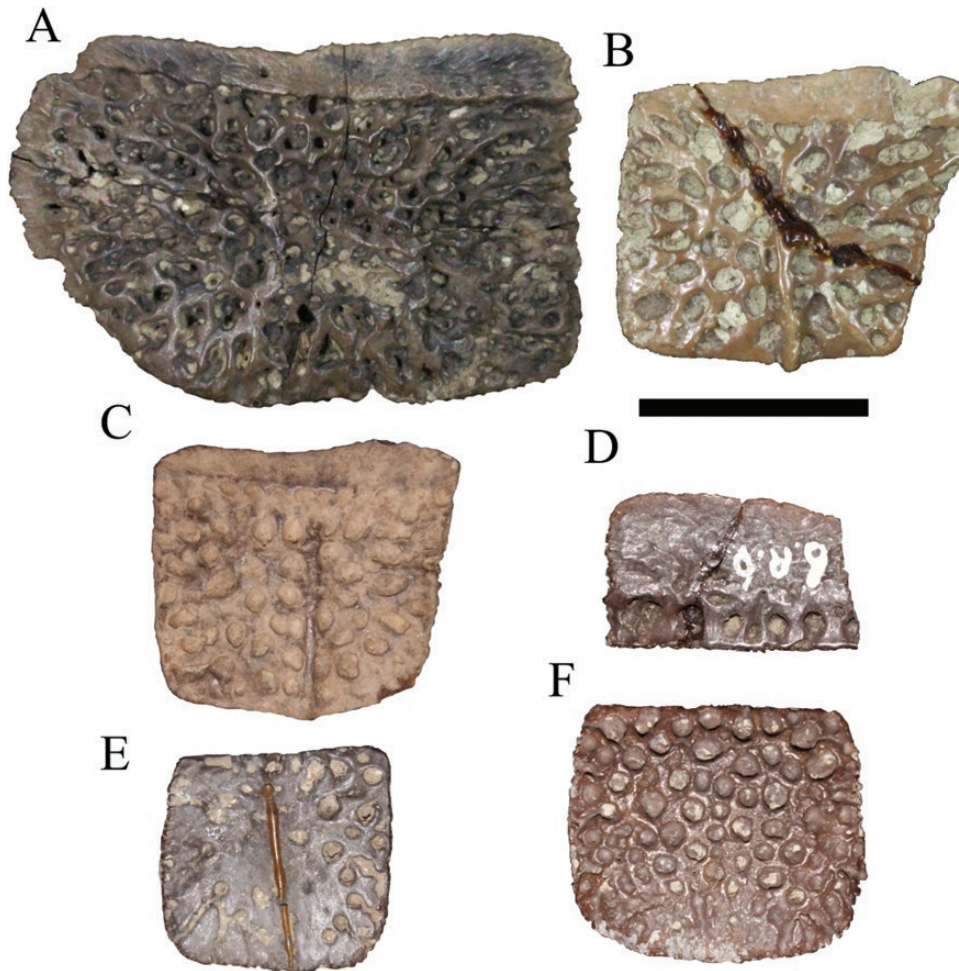
Figure 20. Osteoderms of *Diplocynodon hantoniensis*. A, unregistered dorsal midline osteoderm. Accessory osteoderms: B, NHMUK OR 46434; C, NHMUK R.5214; D, unregistered, anterior half of bipartite ventral osteoderm; E–F, unregistered posterior halves of bipartite ventral osteoderms.

the insertion of M. scapulohumeralis caudalis (Meers, 2003) (Fig. 22G).

The proximal and distal epiphyses are offset, with the former extending further dorsally and resulting in a sigmoidal outline to the humerus in medial view. The medial margin of the proximal extremity extends dorsally and medially away from the humeral shaft, forming a tuberosity that would have articulated with the glenoid surface of the scapula and coracoid. The medial edge of this tuberosity is scarred, possibly marking the origin of M. triceps brevis as in extant crocodylians (Meers, 2003; Klinkhamer *et al.*, 2017). The medial margin of the humeral shaft is strongly concave. Posteriorly, the humeral shaft widens towards the distal extremity. Scarring on the medial side of the distal metaphysis may mark the origins of M. pronator teres and M. flexor digitorum longus (Meers, 2003). The medial and lateral condyles of the distal extremity are not equidimensional. The medial

condyle is mediolaterally compressed and has an acute posterior termination, whereas the lateral condyle is wider and rounded. In distal view, the medial edge of the distal epiphysis is straight, whereas the lateral edge is diagonal. In dorsal view, the lateral margins of the distal and proximal extremities are approximately in line, and the humeral shaft has a distinct lateral bow between these extremities. The medial distal extremities are more offset, with the proximal medial margin directed more medially than the distal margin. A prominent trochlea divides the lateral and medial hemicondyles of the humerus. A broad depression occurs on the ventral surface of the distal extremity, at the midline, immediately anterior to the condyles. The border of the distal articular surface is worn.

Ulna: There are three right ulnae (NHMUK OR 30326, 30327, 30389) and one left ulna (NHMUK OR 30242). The proximal epiphysis of the ulna is much larger than the distal epiphysis (Fig. 23). There is a large, rounded
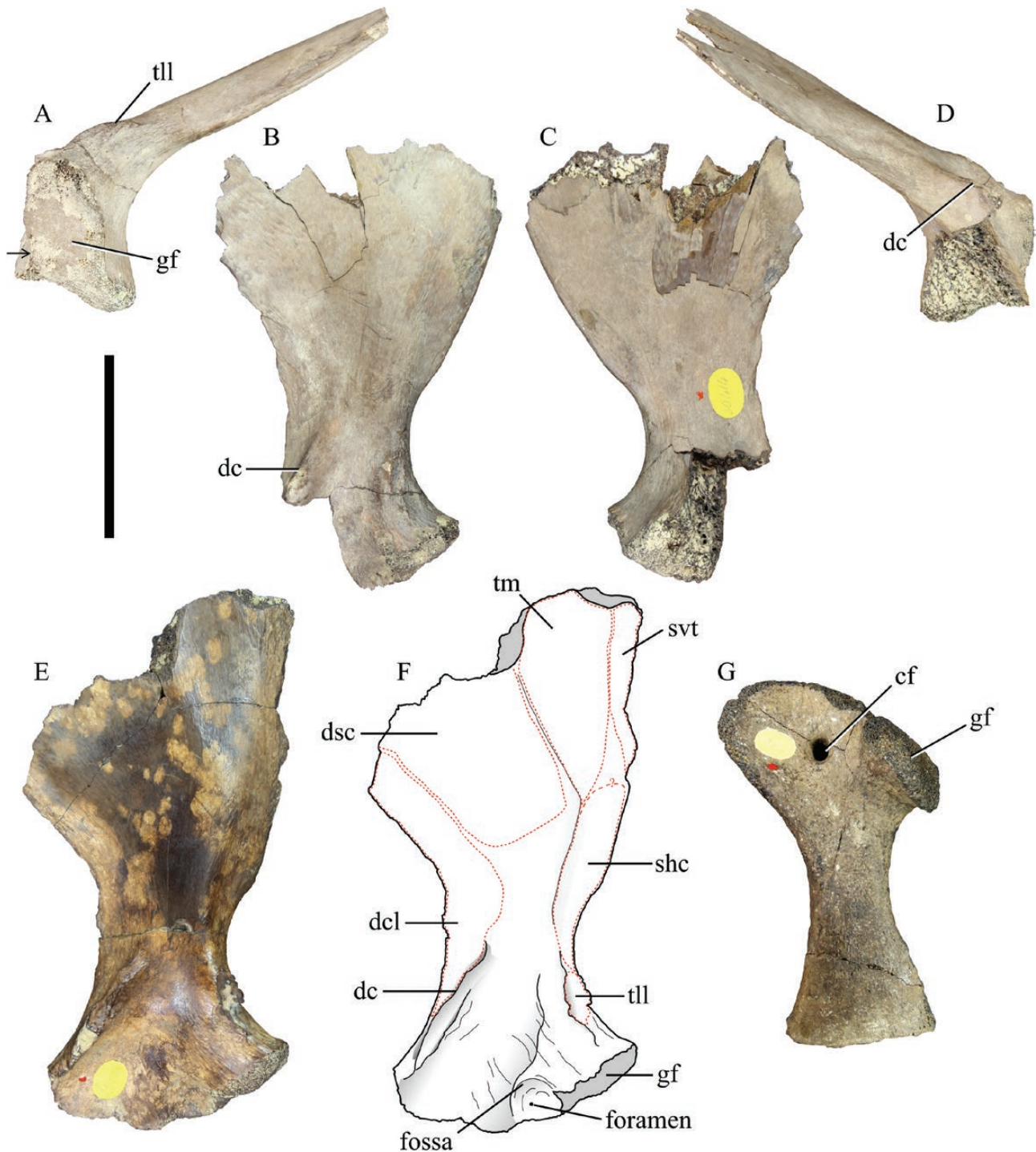
Figure 21. The pectoral girdle of *Diplocynodon hantoniensis*. A–D, left scapula (NHMUK OR 30414) in anterior (A), lateral (B), medial (C) and posterior (D) views, arrow indicates the position of a constriction in the glenoid fossa. Photograph and interpretive drawing of the left scapula (NHMUK OR 30247) in lateral view (E, F). G, left coracoid (NHMUK OR 30359) in lateral view. Abbreviations: cf, coracoid foramen; dc, deltoid crest; dcl, M. deltoideus clavicularis; dsc, M. deltoideus scapularis; gl, glenoid surface; shc, M. scapulohumeralis caudalis; svt, M. serratus ventralis thoracis; tm, M. teres major; tll, M. triceps longus lateralis. Scale bar = 4 cm.
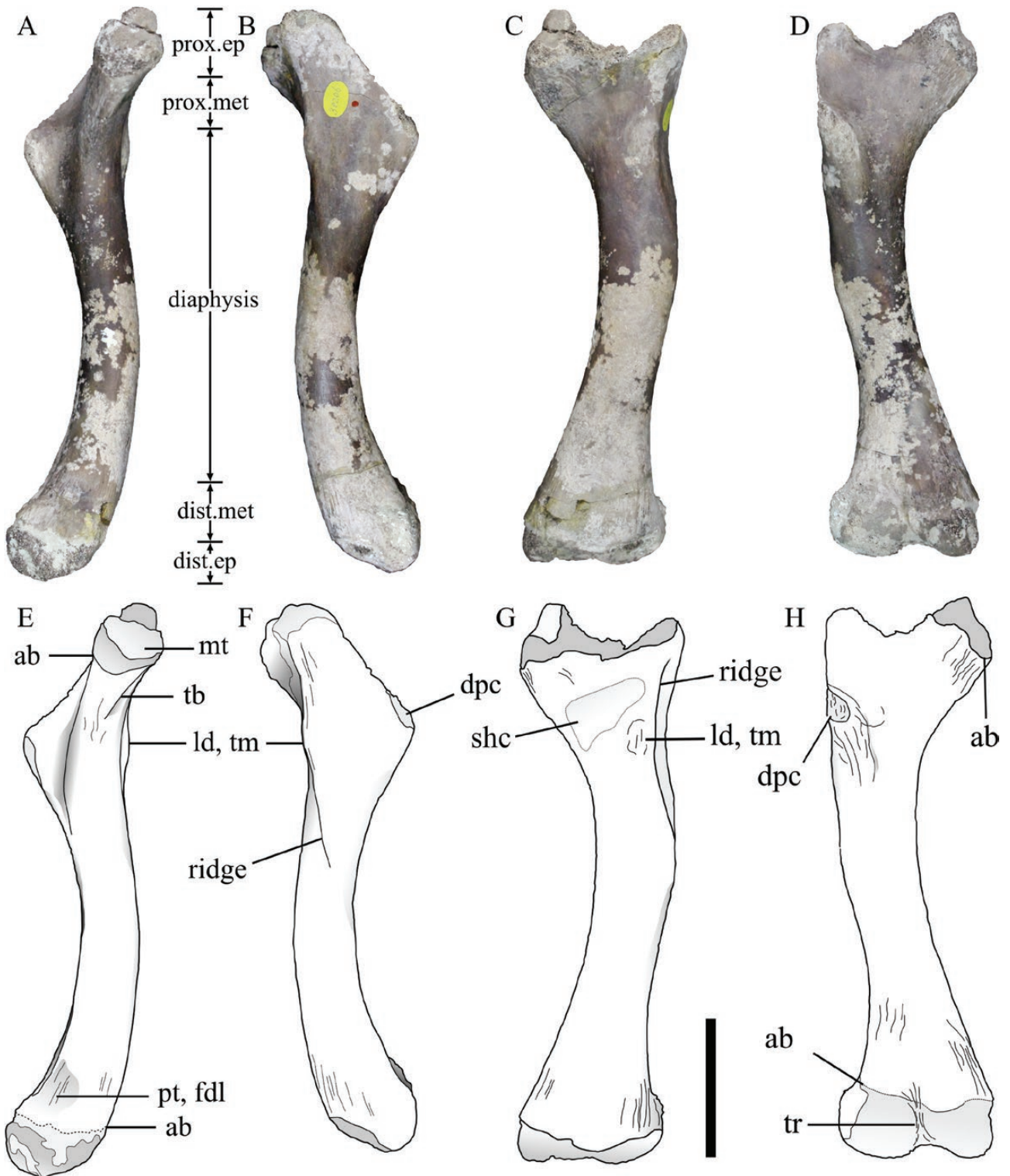
Figure 22. Humeral morphology of *Diplocynodon hantoniensis*. Right humerus (NHMUK OR 30206) in medial (A, E), lateral (B, F), dorsal (C, G) and ventral (D, H) views. Abbreviations: ab, articular border; di. diaphysis; dist.ep, distal epiphysis; dist.met, distal metaphysis; dpc, deltopectoral crest; fdl, M. flexor digitorum longus; ld, M. latissimus dorsi; mt, medial tuberosity; prox.ep, proximal epiphysis; prox.met, proximal metaphysis; pt, M. pronator teres; shc, M. scapulohumeralis caudalis; tb, M. triceps brevis; tm, M. teres major; tr, trochlea. Scale bar = 4 cm.
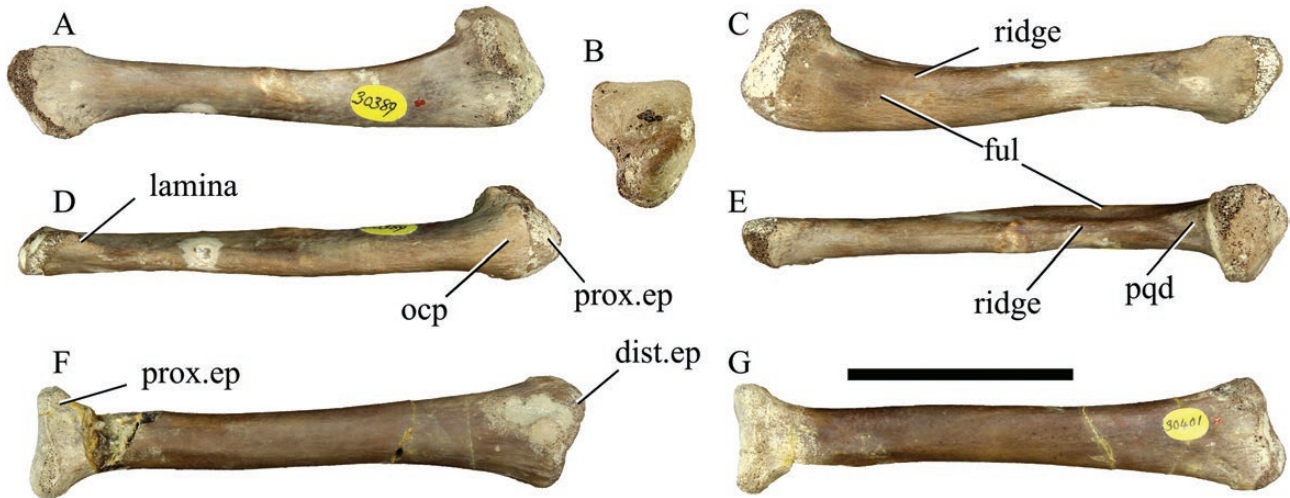
Figure 23. The ulna and radius of *Diplocynodon hantoniensis*. A–E, right ulna (NHMUK OR 30389) in medial (A), proximal (B), lateral (C), ventral (D) and dorsal (E) views. F–G, right radius (NHMUK OR 30401) in dorsal (F) and ventral (G) views. Abbreviations: dist.ep, distal epiphysis; ful, M. flexor ulnaris; ocp, olecranon process; pqd, M. pronator quadratus; prox.ep, proximal epiphysis. Scale bar = 4 cm.

olecranon process (Fig. 23D). The proximal articular surface has a subquadrangular shape (Fig. 23B), with its straight dorsal and lateral margins perpendicular to one another. The dorsal half of the medial margin of the proximal articular surface is parallel to the lateral margin, whereas the ventral half has a prominent notch. This notch might mark the posterior extent of the attachment of M. pronator quadratus on the medial surface (Meers, 2003).

The diaphysis is mediolaterally compressed across its entire length, with a modest medial bowing. It is narrowest anterior to the midlength of the shaft. In lateral view, the ventral edge of the ulna is convex and the dorsal margin is concave. On the dorsolateral surface of the diaphysis, immediately anterior to the proximal epiphysis, is a circular scar (Fig. 23E). A very prominent, straight ridge runs parallel to the long axis of the ulna along the dorsal surface (best seen in NHMUK OR 30242 and 30389). A very small sulcus extends longitudinally along the lateral surface of the diaphysis, and probably marks the insertion of M. flexor ulnaris (Meers, 2003) (Fig. 23C, E). On the dorsal surface at the distal end, posterior to the epiphysis, is a modestly developed ridge that extends posteriorly, slightly onto the medial surface. The distal epiphysis is strongly compressed mediolaterally. Its articular surface is elliptical, facing anteromedially and slightly ventrally. In anterior view, its lateral margin is crescentic, and the medial margin has a small notch around the dorsoventral midpoint. There is also a prominent ventromedial projection on the articular surface, from which a small lamina extends onto the diaphysis (see NHMUK OR 30389).

Radius: The proximal epiphysis of the radius is quadrangular, with perpendicular ventral, medial and lateral margins, and a rounded dorsal margin. This proximal articular surface is bevelled, such that the dorsolateral margin projects further dorsally than the dorsomedial margin. The mediolateral widths of the proximal and distal epiphyses are subequal. Whereas the diaphysis widens abruptly towards the proximal epiphysis, there is a much more gradual increase in mediolateral width towards the distal epiphysis. Proximally, the diaphysis has a rounded cross-section, becoming dorsoventrally compressed distally. The diaphysis is straight and sculptured with ridges that mark muscle attachment sites. On the ventromedial side, there is a longitudinal ridge, which terminates above the midlength of the diaphysis. In proximal view, the distal epiphysis has a semi-circular outline, with a flat ventral margin and rounded dorsal margin. The medial half of the distal epiphysis projects further anteriorly than the lateral half.

Ilium: Four right (NHMUK OR 30362, 25252a, 25253, 30414a) and two left (NHMUK OR 25252b, 30414b) ilia are preserved (Fig. 24). The anterior process of the ilium is not well-developed and the dorsal margin is rounded, with a smooth border and with a very deep posterior tip. The postacetabular process is approximately equivalent to the height of the acetabulum. On the posterior margin of the postacetabular process, the attachment site for M. ilioischio caudalis is situated dorsomedially (Fig. 24A). The acetabulum occupies approximately half of the lateral surface of the ilium. The supracetabular crest is narrow, with a rugose texture, ornamented with a series of small parallel
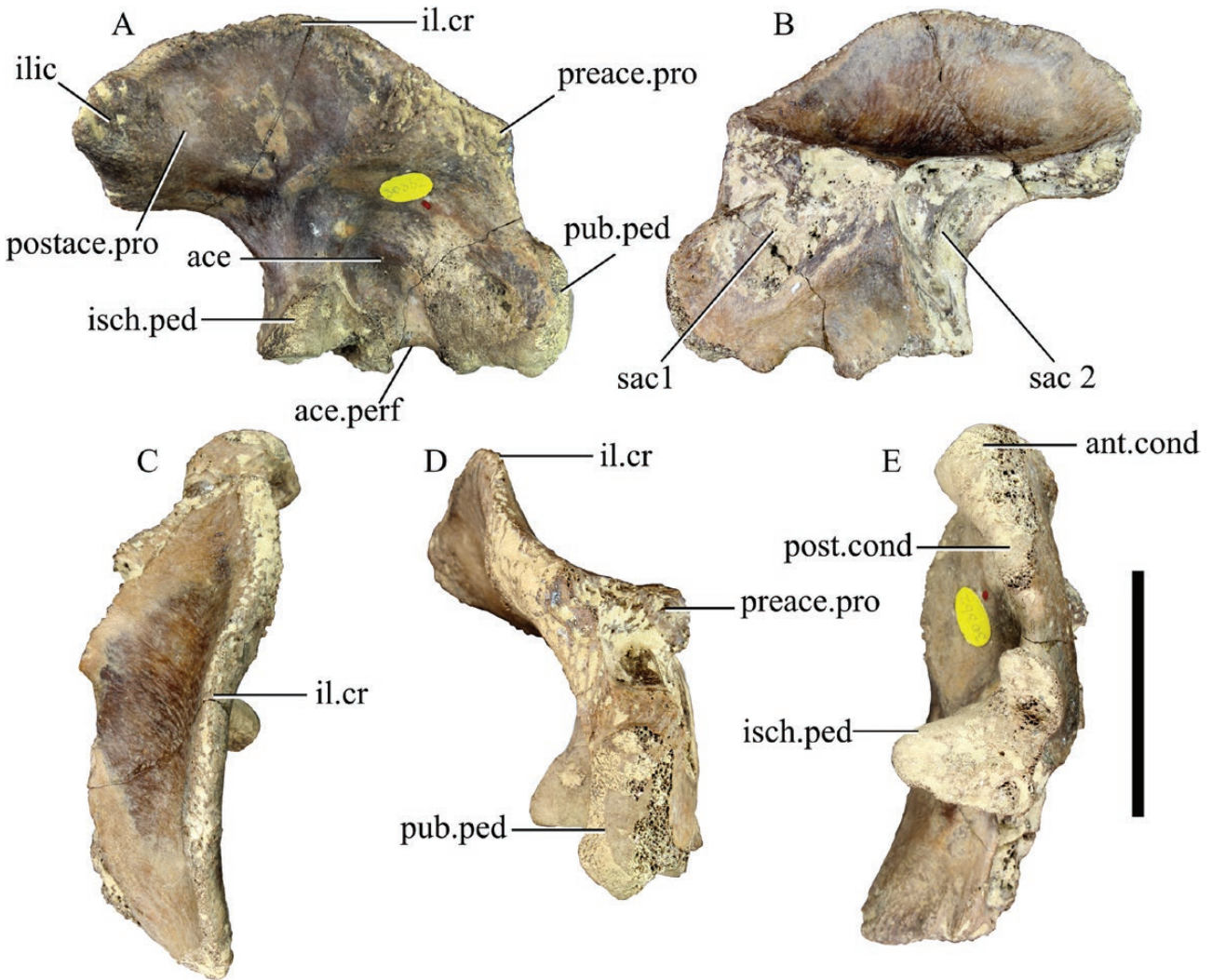
Figure 24. Right ilium (NHMUK OR 30362) of *Diplocynodon hantoniensis* in lateral (A), medial (B), dorsal (C), anterior (D) and ventral (E) views. Abbreviations: ace, acetabulum; ace.perf, acetabular perforation; ant.cond, anterior condyle; ilic, M. ilioischio caudalis; il.cr, iliac crest; isch.ped, ischial peduncle of the ilium; post.cond, posterior condyle; postace.pro, postacetabular process; prace.pro, preacetabular process; pub.ped, pubic peduncle. Scale bar = 4 cm.

vertical ridges. The inclination of the iliac crest relative to the sagittal plane varies anteroposteriorly: it rises to a subvertical orientation anteriorly, whereas the inclination of the crest becomes shallower (at approximately 45° to the sagittal plane) towards the posterior end of the postacetabular process (Fig. 24D). In dorsal view, the iliac crest is not linear, but curves laterally (Fig. 24C).

The articular surface of the pubic peduncle faces ventrally. The condyles of the pubic peduncle are asymmetric, with a large anterior condyle and small posterior condyle (Fig. 24E). Between the pubic peduncle and the preacetabular process, the anterior edge of the ilium is concave. The ischial peduncle forms the posterior wall of the acetabulum. It projects further

laterally than the pubic peduncle, but they reach the same level ventrally. Although worn in all specimens, the ventral surface of the ischial peduncle appears to be horizontal and triangular. The iliac margin of the acetabular perforation is well defined. Its dorsal margin is broadly curved, and the acetabulum is deeply concave, especially around its ventral margin.

Attachment sites for the transverse processes of the sacral vertebrae are centrally positioned on the medial surface of the ilium (Fig. 24B). The attachment for the posterior transverse process extends posteriorly along the ventral margin of the postacetabular process, leading slightly on to its ventromedial side. As such, the postacetabular process would not have extended much further than

the posterior sacral vertebra. The attachment site for the anterior sacral vertebrae is sub-triangular and adjacent to the posterior scar. An anteroposteriorly thin, vertical strut (or 'bridge') of bone separates these two attachment sites.

Ischium: Two partial ischia are preserved (both NHMUK OR 30354) (Fig. 25): a left ischiu and a smaller right element. In both specimens, the tip of the distal blade is broken off and the posterior peduncle is worn. Although worn, the posterior peduncle is larger than the anterior peduncle. The posterior peduncle would have articulated with the ilium to enclose the posterior and ventral margins of the acetabulum. A laterally directed articular surface is preserved on the posterior peduncle of the right ischium, for articulation with the proximal head of the femur. The head of the anterior peduncle is anteroposteriorly compressed, and its articular surface is flat and orientated ventromedially. This peduncle encloses the anterior margin of the acetabulum, which probably had a dorsoventrally elongated elliptical outline. The large, rounded ventral margin of the acetabular perforation is formed by the peduncle bridge of the ischium. The peduncle bridge is mediolaterally constricted at the level of the acetabular perforation. Towards the head of the anterior peduncle, the margins of the bridge flare outwards.

A prominent scar occurs ventral to the peduncle bridge, on the anterolateral surface of the ischium. This probably marks the attachment site for one of the flexor tibialis internus group muscles, as in *C. porosus* (Klinkhamer *et al.*, 2017). In the larger left ischium, this scar is significantly bigger and more rugose, extending further onto the anterior margin of the ischial blade. A prominent ridge is also associated with this scar, extending along the long axis of the ischial blade. A series of muscle attachment scars occur on the posterior margin of the ischium, ventrolateral to the posterior peduncle. The dorsalmost scar probably marks the attachment of M. pubo-ischio-tibialis, whereas the more ventral scars are for the remaining flexor tibialis internus muscles (Klinkhamer *et al.*, 2017). Again, this scar is much more prominent and rugose in the larger left ischium.

The ischial blade is directed medially and slightly posteriorly. Whereas the anterior edge of the blade is sharp, the posterior margin is more rounded. Although incomplete in both ischia, the distal blade expands towards its distal end: this expansion occurs along an anteromedial-to-posterolateral axis. However, we cannot determine whether the distal end of the blade reached a greater width than the proximal head.

Femur: There are several well-preserved femora. Among the more complete are two right (NHMUK OR 30211, 25244) and three left (NHMUK OR 30210, 30399 and R.5215) elements. Although it is not possible to determine which elements belong
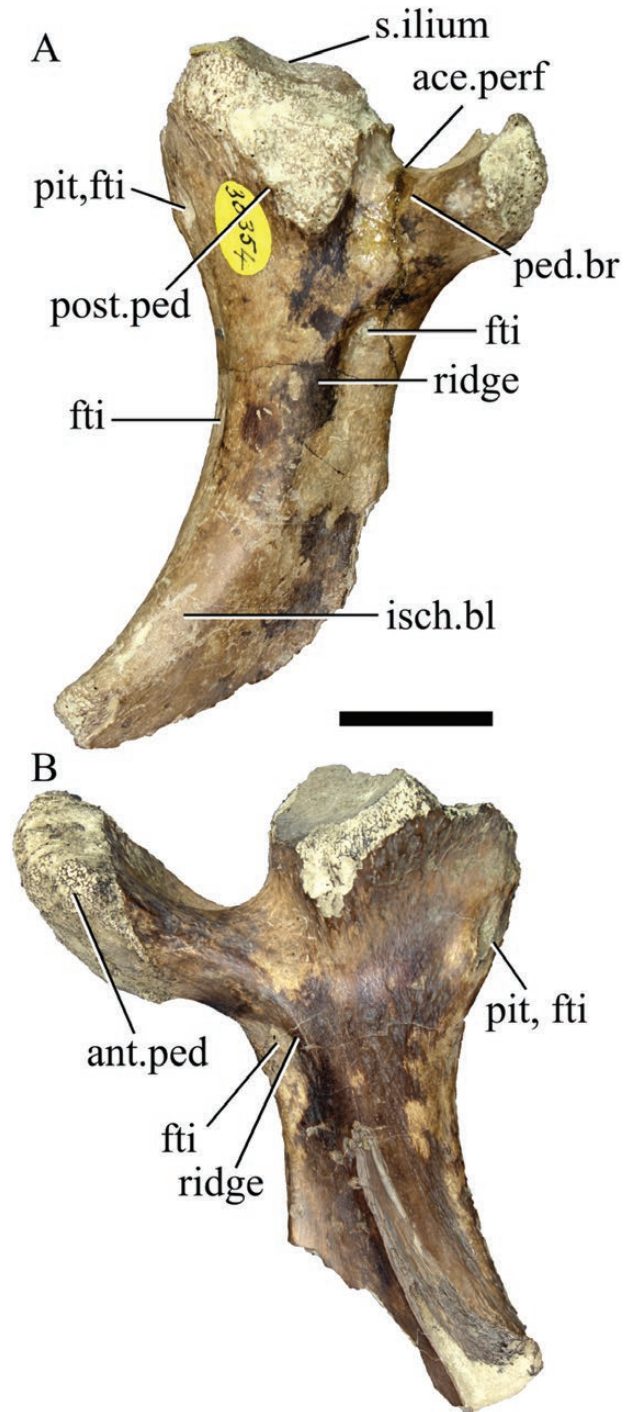
Figure 25. Ischia of *Diplocynodon hantoniensis* (NHMUK OR 30354). A, right ischium in lateral view; B, left ischium in lateral view. Abbreviations: ace.perf, acetabular perforation; ant.ped, anterior peduncle; fti, M. flexor tibialis internus; isch.bl, ischial blade; ped.br, peduncle bridge; pit, M. puboischio tibialis. Scale bar = 2 cm.

to which individuals, all femora are longer than the preserved humeri. The proximal epiphysis of the femur is mediolaterally compressed (Fig. 26). The

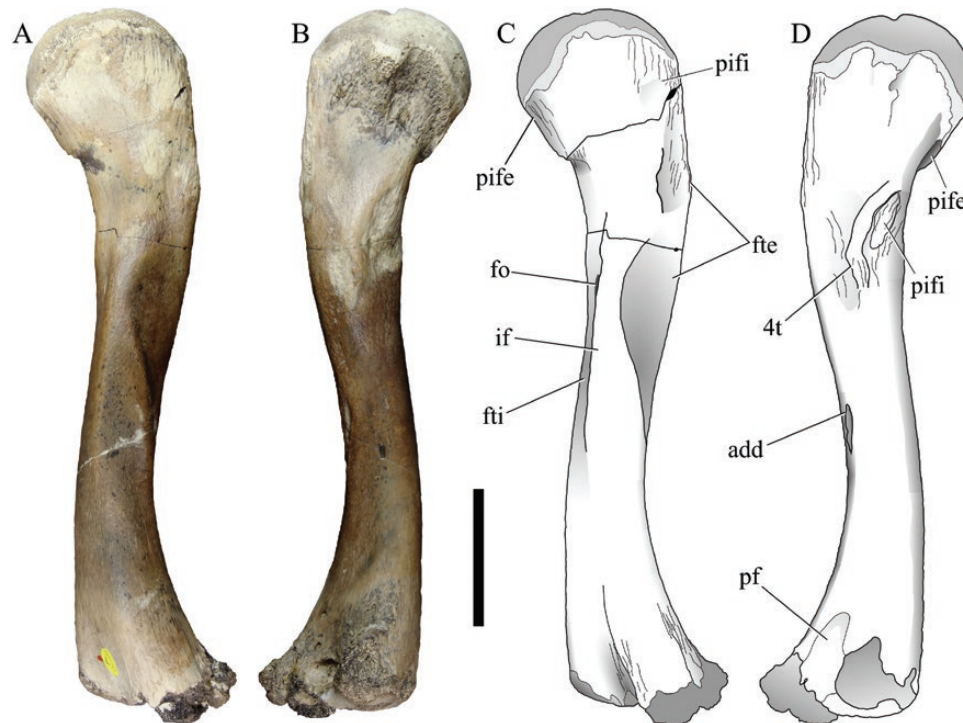**Figure 26.** Photographs and line drawings of the left femur of *Diplocynodon hantoniensis* (NHMUK OR 30210) in dorsal (A, C) and ventral (B, D) views. Abbreviations: 4t, fourth trochanter; add, M. adductor; fo, foramen; fte, M. femorotibialis externus; fti, M. femorotibialis internus; if, M. iliofemoralis; pf, popliteal fossa; pife, M. pubo-ischio-femoralis externus; pifi, M. pubo-ischio-femoralis internus. Scale bar = 5 cm.

dorsal surface of the proximal metaphysis is broadly concave. Scarring towards the posterior end of the proximo-dorsal metaphysis is regarded as evidence for the tendinous insertion of M. pubo-ischio-femoralis internus (Fig. 26C).

On the ventral surface of the proximal metaphysis, two broad fossae occur either side of a discrete knob that projects from the proximal head (Fig. 26B, D). On the proximo-anterior edge of the femur there is a prominent notch covered in striations, which extend towards the articular border of the proximal epiphysis. This is interpreted as the site for the tendinous insertion of M. pubo-ischio-femoralis externus, as in *C. porosus* (Klinkhamer *et al.*, 2017) (Fig. 26C).

In dorsal view, the femur is strongly sigmoidal in outline. This results from curvature along the diaphysis, and torsion between the proximal and distal epiphyses. The dorsal surface of the diaphysis is characterised by a centrally positioned, raised surface, which is defined by two longitudinal ridges (Fig. 26A, C) The posteriormost of these ridges intersects the posterior margin of the diaphysis at the femoral midlength, converging with the anteriormost ridge centrally on the femoral shaft. A fossa, pierced by a foramen, occurs anterior to the raised flat ridge. These ridges correspond with the insertions of three

muscles in living crocodylians: (1) M. iliofemoralis; (2) M. femorotibialis internus; and (3) M. femorotibialis externus. M. iliofemoralis has a fleshy insertion along the distal third of the dorsolateral surface of the femur in living crocodylians (Tumarkin-Deratzian *et al.*, 2007; Klinkhamer *et al.*, 2017), and it probably formed the raised flat surface that is so prominent in *D. hantoniensis*. M. femorotibialis internus and M. femorotibialis externus surround M. iliofemoralis anteriorly and posteriorly, respectively.

The ventral side of the femur is dominated by scarring associated with muscle attachments around the fourth trochanter (Fig. 26D). The fourth trochanter comprises a short, longitudinal ridge. Immediately anterior to the fourth trochanter ridge is a depression that corresponds to the area of insertion for M. pubo-ischio-femoralis internus (Klinkhamer *et al.*, 2017). The prominent ridge that defines the fourth trochanter, as well as a large scarred depression following on from the ridge, are interpreted as the sites for tendinous insertions of M. caudofemoralis longus and M. caudofemoralis brevis.

Distally, there is a depression on the ventromedial edge of the diaphysis, which is interpreted as the area of insertion for M. adductor, as in *C. porosus* (Klinkhamer *et al.*, 2017). The distal epiphysis is poorly

preserved in the largest femora, but well preserved in NHMUK R 5215. A very prominent constriction occurs at the midpoint of the distal epiphysis, dividing the lateral and medial condyles. The lateral half of the distal articular surface is dorsoventrally taller than the medial half. The ventral margin of the lateral half is very acute, extending further ventrally than the medial half.

Tibia: Several tibiae are preserved, with two right (NHMUK OR 30215, 30217) and two left (NHMUK OR 30216 and 25236) elements amongst the best preserved. The proximal epiphysis is broader than the distal epiphysis, facing dorsally and slightly posteriorly Fig. 27A–D). A large sulcus occurs towards the medial edge of the facet, for the tibial condyle of the femur. The posterior margin of the proximal articular facet forms an overhanging triangular lip. The proximal metaphysis of the tibia is circumscribed by a striated surface indicating the attachment of numerous muscles, but it is not possible to distinguish between them in detail. The proximo-medial edge is particularly scarred and in *C. porosus* this area corresponds with multiple tendinous insertions, including: M. flexor tibialis internus, M. pubo-ischio-tibialis, M. ambiens and M. iliotibialis (Klinkhamer *et al.*, 2017). A pale, discoloured tuberosity occurs on the proximal anterior surface, and probably marks the origin of M. tibialis-anterior. This tuberosity leads onto a longitudinal ridge where M. tibialis anterior attaches in *C. porosus* (Klinkhamer *et al.*, 2017).

Whereas the medial edge of the tibial diaphysis is concave, the lateral edge is slightly convex. On the posterior surface of the diaphysis, there is a prominent longitudinal ridge (Fig. 27C). This ridge begins proximally, on the centre of the diaphysis, and moves to the medial edge distally. A second ridge occurs in NHMUK OR 30215, at a slight angle to the first ridge, merging with its distal end. These ridges probably correspond to the sites of insertion of M. interosseous cruris, as in living crocodylians (Klinkhamer *et al.*, 2017).

The distal epiphysis is anteroposteriorly compressed, with a notch on the posterior side, producing an arcuate articular facet for the astragalus (Fig. 27C). This facet faces posteroventrally. The medial portion of the facet projects slightly further distally than the lateral counterpart.

Fibula: Two right [NHMUK OR 30233 (Fig. 27E–H), 30235] and two broken and fragmentary left (NHMUK OR 30241, 30234) fibulae are preserved. The proximal end is mediolaterally compressed, with a dorsomedially orientated, elliptical, articular facet. The proximal epiphysis is strongly expanded posteriorly for the long, external lateral ligament (Fig. 27L). It has a notch at its midpoint, which results in a dorsally concave outline in medial and lateral

views. The proximomedial surface of the fibula has a triangular crest, which has a rough, striated texture. This texture extends proximally until the border of the articular surface. This surface probably marks the tendinous insertion of M. interosseous cruris and another tendinous attachment for M. fibularis longus (Fig. 27H).

The trochanter for the insertion of M. iliofibularis occurs on the proximolateral surface of the fibula, near the anterior edge, as in extant crocodylians (Fig. 27G). Above the iliofibularis trochanter, on the proximolateral metaphysis, there is more scarring, although less prominent than on the medial side. In extant crocodylians, this is the location of origin for M. extensor digitorum longus and M. fibularis brevis. The distal half of the lateral fibular surface has a centrally positioned, longitudinal ridge, which likely marks the origin of M. extensor digitorum brevis (Klinkhamer *et al.*, 2017).

The distal epiphysis is compressed in a posteromedial-to-anterolateral direction. This generates a small amount of torsion between the proximal and distal epiphyses. The articular facet of the distal epiphysis faces anteroventrally for articulation with the astragalus. In distal view, the facet is sub-triangular. Its lateral edge is straight, whereas the medial edge is slightly concave, forming a distinct notch at the anteroposterior midpoint. The posterior edge of the distal metaphysis is defined by a thin ridge, possibly marking the origin of M. pronator profundus.

TAXONOMIC STATUS OF PREVIOUSLY REFERRED MATERIAL

Several specimens have been referred to *Diplocynodon hantoniensis* from Palaeogene deposits in western Europe and the USA. If correctly attributed, these remains demonstrate that this species had a much greater spatiotemporal distribution. Below we critically reassess each of these referrals.

Early Eocene of the USA

Weems (1999) referred a single tooth (USNM 496207) and a keeled dorsal osteoderm (unnumbered specimen) to *D. hantoniensis* from the early Eocene Nanjemoy Formation, which crops out in the Fisher/Sullivan site in Stafford County, Virginia. The referral was based partly on the purported presence of '*Diplocynodon stuckeri*' from the middle Eocene of Wyoming (Mook, 1960). However, this latter material has since been referred to *Borealosuchus wilsoni* Mook, 1959 (Brochu, 1997). The tooth described by Weems (1999) is conical, with carinae on the anterior and distal edges, and the osteoderm is approximately rectangular with a modest keel. The morphology of these elements
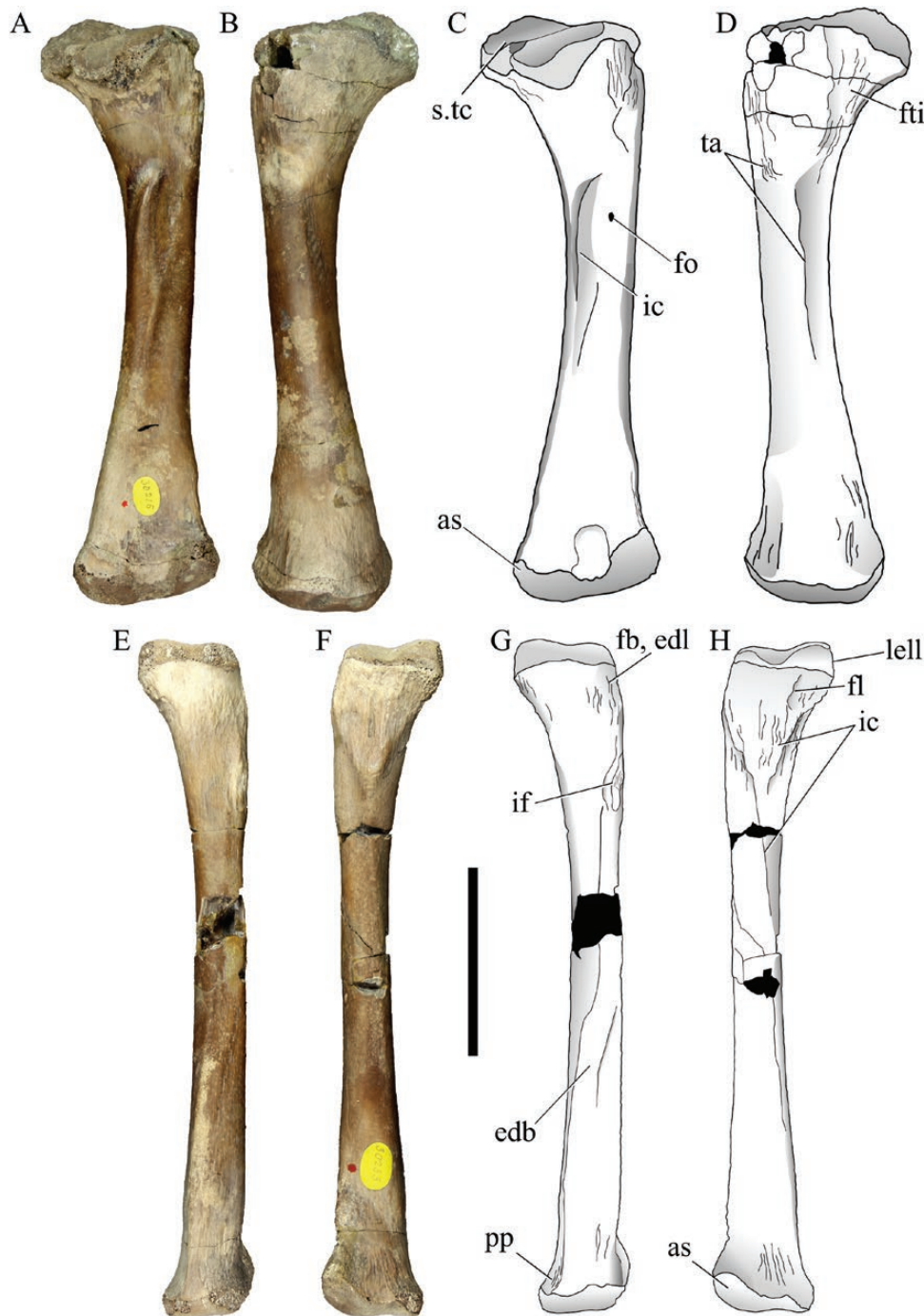
Figure 27. The tibia and fibula of *Diplocynodon hantoniensis*. A–D, right tibia (NHMUK OR 30215) in posterior (A, C) and anterior (B, D) views. E–H, right fibula (NHMUK OR 30233) in lateral (E, G) and medial (F, H) views. Abbreviations: as, astragalar articular surface; edb, M. extensor digitorum brevis; edl, M. extensor digitorum longus; fb, M. fibularis brevis; fl, M. fibularis longus; fo, foramen; fti, M. flexor tibialis internus; ic, M. interosseous cruris; if, M. iliofibularis; lell, long external lateral ligament; pp, M. pronator profundus; s.tc, surface for the tibial condyle of the femur; ta, tibialis anterior. Scale bar = 5 cm.

is insufficient for specific or even generic identification. We consider this material from Virginia to represent an indeterminate crocodylian, pending the discovery of diagnostic material from this locality.

Late Eocene of Switzerland

Pictet *et al.* (1857) described fragmentary remains of a crocodylian from the late Eocene of Mormont

(=Mauremont), in the canton of Vaud, western Switzerland. The material consists of five unnumbered cranial fragments, a fragment of the retroarticular process and two isolated teeth. Pictet *et al.* (1857) referred the material to *D.* cf. *hantoniensis* based on the presence of a large occlusal pit (for dentary tooth 1) on the ventral surface of the premaxilla (described but not figured). The shapes of both the squamosal and supratemporal fenestra were also regarded as identical to *D. hantoniensis*, along with two isolated teeth that display similar carinae. We find similarities in the material with *D. hantoniensis*, such as the long squamosal prongs and elongate supratemporal fenestra. However, none of the diagnostic features of *D. hantoniensis* recognized in this study can be identified in the Swiss material. Furthermore, large occlusal pits for the dentary teeth are not unique to *D. hantoniensis*: they occur in all other alligatoroids and crocodyloids. Carinae on the anterior and posterior edges of teeth are equally undiagnostic, being present in essentially all non-longirostrine crocodylians. We also note two potential differences: the rim of the premaxilla is very sharp in the Swiss material, unlike *D. hantoniensis*, and the size of the external naris in proportion to the surface area of the premaxilla is larger than that of *D. hantoniensis*. Given that none of the diagnostic features of *Diplocynodon* (Martin *et al.*, 2014) can be identified in the Swiss material, we regard it as Alligatoroidea indet.

Early Oligocene of Germany

Gramann (1958), and later Karl & Müller (2008), described crocodylian remains from the early Oligocene 'Melanian clay' (=Melanienton), which crops out around the Altenburg IV quarry at Borken, in Hesse, central Germany. Gramann (1958) noted the presence of an anterior dentary fragment (lacking the splenial), a lacrimal, fragments of a left and right angular, teeth, portions of two femora and numerous osteodermal and vertebral fragments, which he referred to *D. hantoniensis*. No specimen numbers were assigned to the material, but they are deposited in the Institute for Geology and Palaeontology at the University of Marburg, Germany. Additional osteoderms were later referred to *D.* cf. *hantoniensis* by Karl & Müller (2008) (PMLU HS 389-A10.02.05). Of the figured and described material, only the dentary is taxonomically informative. Three character states can be determined: (1) confluence of the 3rd and 4th dentary alveoli; (2) a gently curved dentary between alveoli 4 and 10; and (3) dentary symphysis extending to the 3rd/4th dentary alveolus. One further character, the position of the anterior splenial tip relative to the Meckelian groove, is indiscernible from figures in Gramann (1958). Confluence of the 3rd and 4th alveoli and the gently curved dentary, are features that are common to all *Diplocynodon* species. The presence of a short dentary symphysis can restrict the referral to one of four species, as it is only present in *D. ratelii*, *D. hantoniensis*, *D. muelleri* and *D. remensis*, but in *D. remensis* the splenial participates in the symphysis, unlike any other *Diplocynodon* species (Martin *et al.*, 2014). If the rostral tip of the splenial was preserved in the German specimen, this would allow us to distinguish between *D. muelleri* (where it passes dorsal to the Meckelian groove) and *D. hantoniensis* and *D. ratelii* (in which it passes ventral to the groove). No further diagnostic characters can be retrieved from the dentary and other remains are non-diagnostic. Therefore, we assign this German occurrence to *Diplocynodon* sp.

Early Oligocene of France

A relatively complete skull of an adult crocodylian was referred to *Diplocynodon* cf. *hantoniensis* by Vignaud *et al.* (1996) from early Oligocene sediments in the Razac-d'Eymet commune in Dordogne, south-western France. The specimen is unnumbered but described as part of the 'Guevel collection', which may be housed at the University of Poitiers, France. The proportions of the skull match *D. hantoniensis*, in particular the relatively wide rostrum and lack of a prominent constriction at the premaxillary–maxillary suture. Unfortunately, the figures are not detailed enough to comment on the sutural relationships of the skull. However, there are important differences based on the description, which suggest the material might not be referable to *D. hantoniensis*. Vignaud *et al.* (1996: fig. 1b) described and figured a narrow ectopterygoid that runs beside the border of the maxillary alveoli, as in *D. ratelii*. This condition contrasts with *D. hantoniensis*, which has a unique condition of the ectopterygoid (see Description). The presence of other diagnostic features of *D. hantoniensis* cannot be discerned from either the description or figures, such as the presence of ectopterygoid–pterygoid flexure, or a sulcus posterolateral to the external naris. In summary, until further descriptions of this specimen are made, it can only be referred to *Diplocynodon* sp.

PHYLOGENETIC ANALYSIS

Data matrix

Diplocynodon hantoniensis was re-scored for the data matrix of Martin *et al.* (2014), which is an expanded version of that presented in Brochu *et al.* (2012), containing all valid species of *Diplocynodon*. This resulted in 21 character score changes, as documented in the Appendix. Preliminary analyses resulted in the highly unusual recovery of the latest Cretaceous

basal eusuchian *Allodaposuchus precedens* Nopcsa, 1928 as a member of *Diplocynodon*; consequently, we added several additional allodaposuchid taxa in order to remove a potential long-branch attraction due to converging characters in the two clades. Two additional species of *Allodaposuchus* (*A. hulki* Blanco *et al.*, 2015, *A. palustris* Blanco *et al.*, 2014), as well as *Agaresuchus subjuniperus* Puértolas *et al.*, 2013 and *Arenysuchus gascabadiolorum* Puértolas *et al.*, 2011, were scored based on Blanco *et al.* (2015), and we also updated scores for *Allodaposuchus precedens* based on Martin *et al.* (2016). Eight additional characters (C180–187) from Brochu & Storrs (2012) were also added to the character list. One new character state was added to each of characters 146 and 147 following Delfino *et al.* (2008), to better characterize the unique morphology of the posterior margin of the otic aperture in allodaposuchids. Our revised dataset comprises 103 taxa scored for 187 characters. The data matrix (nexus and tnt files), and character list are provided in Supplementary Information 1–3 respectively.

Analytical protocol

In contrast to previous iterations of this data matrix, multistate characters were treated as ordered if they described meristic features, relative positions of characteristics within the skull or obvious morphoclines (following Brazeau, 2011). Characters for which none of the states could be identified as a clearly intermediate morphology between two extremes were treated as unordered. Thus, characters 17, 40, 49, 55, 63, 82, 88 and 148 were ordered. We conducted the phylogenetic analysis based on maximum parsimony with four different weighting schemes: (1) equal weighting; (2) implied weighting with a k-value of 8; (3) extended implied weighting with a k-value of 8; and (4) extended implied weighting with a k-value of 4. Implied weighting decreases the impact of variable characters, depending on their homoplastic rate during the tree search in TNT (Goloboff 1993, 2014). Because homoplastic characters might or might not bear a phylogenetic signal, or are characters that evolve faster than non-homoplastic ones, downweighting them in respect to highly phylogenetically significant ones appears to be a logical solution (Farris, 1969; Goloboff, 1993; Chippindale & Wiens, 1994; Haszprunar, 1998). Indeed, the inclusion of downweighted homoplastic characters has been shown to increase phylogenetic accuracy both in simulations and with real morphological and molecular datasets (e.g. Chippindale & Wiens, 1994; Källersjö *et al.*, 1998; Goloboff et al., 2008, 2018; Goloboff, 2014). Given that implied weighting, as implemented in the software TNT, provides the only repeatable and user-friendly methodology to date, we applied this strategy herein. However, traditional

implied weighting can be negatively influenced by missing data, especially in cases where homoplastic characters are only scored in a few operational taxonomic units (OTUs). The lack of information in these characters can lead to a misleadingly low homoplastic rate when convergent OTUs are grouped together (Goloboff, 2014; Tschopp *et al.*, 2018). In order to counteract this negative influence of missing data, Goloboff (2014) implemented extended implied weighting, which downweights homoplastic characters not only in relation to their homoplastic rate, but also based on the amount of missing data. As has been shown by Goloboff *et al.* (2018), this methodology seems to perform best, especially when using morphological datasets. Both implied and extended implied weighting use a concavity constant 'k' to define the strength of the downweighting: the lower the k-value, the stronger the downweighting function. Although there is no biological reasoning behind the choice of a specific k-value (Turner & Zandee, 1995), it is probably reasonable to exclude extreme values, and to test and compare the impact of various k-values on tree topology (Goloboff, 1995; Tschopp & Upchurch, 2019). As such, we use a number of different weighting strategies.

All analyses were performed using the New Technology search in TNT v.1.1 (Goloboff *et al.*, 2008), with all algorithms enabled, and the consensus tree stabilized five times with a factor of 75. The recovered trees from the first iteration were subjected to a second search using the 'bbreak' command, applying tree bisection and reconnection to find all most parsimonious trees (MPTs). Subsequently, a complete strict consensus tree was calculated, and synapomorphies of nodes and autapomorphies of tips in the strict consensus tree were retrieved using the menu 'Optimize > Synapomorphies > List common synapomorphies'.

RESULTS

In three of our four analyses, the genus *Diplocynodon* was recovered as monophyletic, forming the sister taxon to *D. ungeri* + *D. elavericus*, although resolution within the genus varied (Fig. 28; Table 3). The exception is the tree found under extended implied weighting with a k-value of 4, in which *D. remensis* is placed outside of *Diplocynodon* (basal to *Leidyosuchus*) and *Tsoabichi* is found deeply nested in *Diplocynodon*, forming the sister taxon to *D. ungeri*. In this topology, *D. hantoniensis* is recovered as sister taxon to *D. muelleri* + (*D. elavericus* + (*Tsoabichi* + *D. ungeri*)). Three local autapomorphies support the distinctiveness and validity of *D. hantoniensis* in all four analyses: 66-1, 86-1, 125-1. Although the number and combination
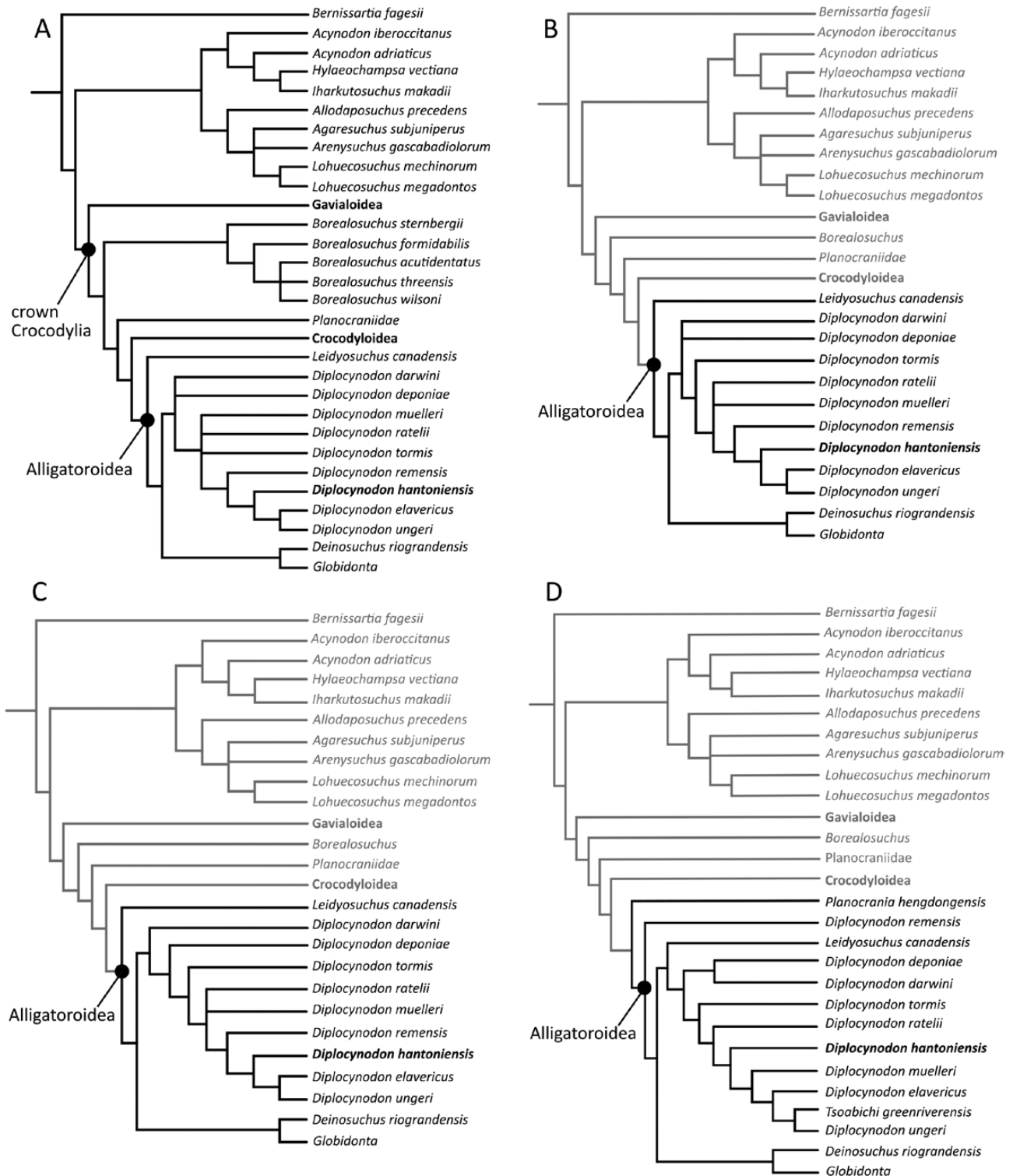
Figure 28. Results of the phylogenetic analysis. A, strict consensus of 2880 MPTs from the analysis with equal weighting; B, strict consensus of 10 MPTs from the analysis with implied weighting, $k = 8$; C, strict consensus of 5 MPTs from the analysis with extended implied weighting, $k = 8$; strict consensus of 5 MPTs from the analysis with extended implied weight, $k = 4$.

Table 3. Summary of results from the phylogenetic analyses

Analysis	Protocol	Number of MPTs	Tree length
Analysis 1	Equal weights	2880.0	756
Analysis 2	Implied weights, $k = 4$	10.0	39.6
Analysis 3	Extended implied weights, $k = 8$	5.0	37.1
Analysis 4	Extended implied weights, $k = 4$	5	54.35737

of synapomorphies found for the genus *Diplocynodon* varies between the analyses, all of them are present in *D. hantoniensis*.

Analysis 1, using equal weighting, found 2880 MPTs with a length of 756 steps (Fig. 28A). The genus *Diplocynodon* can be diagnosed by four autapomorphies: 15-0, 34-4, 149-1 and 181-1. Some trees also find the following four possible autapomorphies for *Diplocynodon*: 42-2, 69-1, 82-2, and 153-1 (see also Discussion).

Analysis 2, using implied weighting ($k = 8$), recovered 10 MPTs with a length of 39.56116 steps. *Diplocynodon* is slightly more resolved than in the strict consensus tree found under equal weighting (Fig. 28B), but the position of *D. hantoniensis* in the genus is the same. Seven autapomorphies were found for *Diplocynodon*: 15-0, 34-4, 69-1, 82-2, 149-1, 153-1 and 181-1. All of these autapomorphies were also found by at least some MPTs under equal weighting, but one synapomorphy found with equal weighting (42-2) was not recovered here; this is likely because of the better resolution at the base of *Diplocynodon* in this second analysis.

The third analysis (Fig. 28C), using extended implied weighting with a *k*-value of 8, recovered five MPTs with a length of 37.09033 steps. Resolution within *Diplocynodon* is the best of all four analyses. *D. darwini* is the most basal species, and *D. hantoniensis* remains in the same position as when using equal and implied weighting. Seven synapomorphies support *Diplocynodon* as a distinct genus: six of them were found by all MPTs (15-0, 34-4, 82-2, 149-1, 153-1 and 181-1) and one of them by some (69-1).

The fourth analysis, using extended implied weighting with a *k*-value of 4, found five MPTs with a length of 54.35737 steps. The recovered topology of the strict consensus tree is different from the other analyses (Fig. 28D), with *Diplocynodon remensis* basal to *Leidyosuchus* and *Tsoabichi* deeply nested in *Diplocynodon*, as the sister taxon to *D. ungeri*. The clade including all *Diplocynodon* species (except *D. remensis*) and *Tsoabichi* was united by the following synapomorphies, which were all found by at least one other analysis as well: 15-0, 34-4, 82-2, 149-1, 153-1 and 181-1.

In order to explore these conflicting topologies, we performed constrained searches to force the analyses to find the conflicting topology, and compared the relative length increases (following Tschopp *et al.*, 2015). The constraints forced *Tsoabichi* to be recovered in *Diplocynodon*, *D. remensis* to be positioned basal to *Leidyosuchus* in the first three analyses and *Diplocynodon* to be fully monophyletic for analysis 4. In addition, we performed tree searches for analyses 1–3 in which we forced all *Diplocynodon* species, except *D. remensis*, to form a monophyletic clade, with *Tsoabichi* as a wildcard taxon (i.e. it could be found within or outside *Diplocynodon*). Search strategies were the same as in the unconstrained analyses, although we refrained from the second iteration of tree bisection and reconnection, because the first iteration generally already found the shortest trees. Since we only compare tree length, this test should provide accurate results without this second step.

The resulting topologies of the constrained analyses 1–3 place *Tsoabichi* as the sister taxon to *D. ungeri*, as in the unconstrained analysis 4, but *D. remensis* is recovered in *Borealosuchus* instead. Relative length increases vary considerably between equal-weighting and implied-weighting approaches, averaging to 0.48% (Table 4).

The topology resulting from the constrained analysis 4 recovered *D. remensis* in the same relative position as in the unconstrained analyses 1–3, and found *D. deponiae* as the most basal member of the genus. This is contrary to the unconstrained analysis 3, which found *D. darwini* as the most basal member of the genus. However, the other unconstrained analyses found *D. deponiae* in a polytomy with *D. darwini* and a clade uniting the other species of *Diplocynodon*. Therefore, this difference probably just indicates the lack of data to resolve the relationships between these basal species. The relative length increase of the constrained analysis 4 amounts to 0.14%.

Using the single constraint for a monophyletic *Diplocynodon* that excludes *D. remensis* and with *Tsoabichi* as a wildcard taxon, analyses 1–3 all recovered *D. remensis* in *Borealosuchus*, as in the other constrained searches. None of the analyses recovered *Tsoabichi* in *Diplocynodon*. Relative length increase was less than half compared to the more constrained analyses (Table 4) and reached lower values in analyses 2 and 3 than in the constrained analysis 4.

Although generally low, relative length increases are, therefore, considerably higher when constraining analyses 1–3 to find the unexpected topology of analysis 4 than in the opposite case, but values decrease significantly if *Tsoabichi* is found outside the genus. These results indicate that a monophyletic *Diplocynodon* appears to be the most parsimonious solution, although it remains unclear if *D. remensis* should be included or not.

When comparing the Overlap Indices (Tschopp *et al.*, 2015, 2018) of the three topologies found for *Diplocynodon*, both the AOI and COI obtain higher values for a unique genus excluding *Tsoabichi*, but equal values regardless as to whether or not *D. remensis* is included (Table 5). The Overlap Indices simply quantify the anatomical overlap in a specific group among all characters (AOI) and among the comparable characters only (COI) and can thus not be regarded as a support value for the analysed group of OTUs (Tschopp *et al.*, 2018). However, the combination of less overlap with a stronger downweighting strategy, as occurred in our unconstrained analysis 4, indicates that this result might be affected by the negative impact of missing data (Tschopp *et al.*, 2018). The fact that analysis 3, which used extended implied weighting

with a weaker downweighting function than analysis 4, recovers the same monophyletic *Diplocynodon* as the analyses under implied weighting with an equal *k*-value and under equal weighting, supports this interpretation. Further investigation into the indices reveals that the group including *Tsoabichi* has two more characters with overlaps than *Diplocynodon* alone, but still lower values. These are characters 75 and 76, which are only scored in *D. darwini* within *Diplocynodon*. In total, only 24% (character 75) and 23% (character 76) of the OTUs are scored for these characters, which is much less than the average (62%). Of the eight potential synapomorphies found by the four unconstrained analyses, *Tsoabichi* could only be scored for three. In one of these three synapomorphies (82-2), *Tsoabichi* was scored differently (82-1; this reversal was recovered as a local autapomorphy of the species in *Diplocynodon* in analysis 4) and the other two are either shared (42-2) or ambiguous (149-1) synapomorphies, meaning that they both occur in species outside *Diplocynodon* as well (Tschopp *et al.*, 2015).

In summary, whereas we can probably exclude the possibility that *Tsoabichi greenriverensis* Brochu, 2010 is a species of *Diplocynodon*, we cannot currently

Table 4. Relative tree length increases using different constraints. Abbreviations: NA, not applicable

Constraint	Relative length increase				Average
	Analysis 1	Analysis 2	Analysis 3	Analysis 4	
D. remensis basal to *Leidyosuchus*, and *Tsoabichi* nested in *Diplocynodon*.	0.92%	0.29%	0.22%	NA	0.48%
D. remensis outside a monophyletic *Diplocynodon*, with *Tsoabichi* as a floating taxon.	0.40%	0.11%	0.10%	NA	0.20%
Diplocynodon monophyletic	NA	NA	NA	0.14%	0.14%

Table 5. Overlap indices for different compositions of *Diplocynodon* found in the phylogenetic analyses

	Diplocynodon monophyletic	*Diplocynodon* without *D. remensis* but including *Tsoabichi*	*Diplocynodon* without *D. remensis* and *Tsoabichi*
Group members (M)	9	9	8
Characters (C)	187	187	187
Possible anatomical overlaps per character (M-1)	8	8	7
Characters with overlap (Co)	158	160	158
Total overlaps in group (Om)	873	812	761
(Om/C)	4.67	4.34	4.07
(Om/Co)	5.53	5.08	4.82
Overlap index for all characters. AOI = (Om/C)/(M-1)	58%	54%	58%
Overlap index for comparable characters. COI = (Om/Co)/(M-1)	69%	63%	69%

be certain whether or not *Diplocynodon remensis* is a member of the genus.

DISCUSSION

PHYLOGENETIC RELATIONSHIPS OF *DIPLOCYNODON*

Our results do not alter the generic diagnosis of *Diplocynodon* presented by Martin *et al.* (2014). However, we provide a categorization of the synapomorphies resulting from our analyses into unambiguous, shared and ambiguous. Only one unambiguous synapomorphy is recovered for *Diplocynodon*, i.e. known solely in that genus: a rounded dorsal margin of the iliac blade, which is posteriorly very deep. However, this character cannot currently be scored for *D. elavericus*, *D. remensis*, *D. ungeri* or *D. tormis*. Four shared synapomorphies are identified, i.e. present in all *Diplocynodon* species (where preserved), but also in other taxa: (1) nasals excluded, at least externally, from the naris; (2) axial hypapophysis located towards the centre of the centrum; (3) one row of postoccipital osteoderms; and (4) ventral armour formed of paired ossifications. We also identify three ambiguous synapomorphies, i.e. present in some *Diplocynodon* species, but also in other taxa: (1) lingual foramen for the articular artery and alveolar nerve perforating the surangular/angular suture (absent in *D. muelleri* but present, for example, in *Alligator*); (2) frontoparietal suture linear between the supratemporal fenestrae (concavo-convex in *D. ratelii*, but linear also in *Paleosuchus*); and (3) parietal and squamosal approach each other on the posterior wall of the supratemporal fenestrae (absent in *D. elavericus* and present in *Brachychampsa montana* Gilmore, 1911).

The topology presented here is similar to that in Martin *et al.* (2014), with some differences. Although the relationship between *D. deponiae* and *D. darwini* cannot be stabilized in analyses 1 and 2, they are recovered as the sister taxa to all other *Diplocynodon* species in analyses 3 and 4, as in Martin *et al.* (2014). Whereas in analysis 3, *D. deponiae* and *D. darwini* are successively nested species, which are sister to all other *Diplocynodon* species, in analysis 4 they form a sister pair to all other *Diplocynodon* species except *D. remensis* (see above). Unlike the earlier version of the analysis, *D. hantoniensis* is recovered as the sister species of *D. elavericus* and *D. ungeri*. The latter two species were not included in the analysis of Martin *et al.* (2014). Furthermore, we do not recover a clear sister taxon relationship between the two Spanish species, *D. muelleri* (early Oligocene) and *D. tormis* (middle Eocene). In analysis 1 their relationships are not resolved; in analysis 2 and 3 *D. tormis* is the sister to the group comprised of *D. ratelii*, *D. muelleri*

+ (*D. remensis* + (*D. hantoniensis* + (*D. elavericus* + *D. ungeri*))). Analysis 4 similarly does not support a sister relationship between *D. tormis* and *D. muelleri*. Here, *D. tormis*, *D. ratelii* and *D. muelleri* are recovered as successively nested species.

The analyses using equal weighting, implied weighting (k = 8) and extended implied weighting (k = 8), produced trees with the same stratigraphical incongruence observed by Martin *et al.* (2014). Here, the late Palaeocene species *Diplocynodon remensis* is recovered as the sister taxon to *D. hantoniensis* + (*D. elavericus* + *D. ungeri*). However, our fourth analysis, with the greatest downweighting of homoplastic characters, recovered *D. remensis* outside of *Diplocynodon,* basal to *Leidyosuchus*. This result is interesting considering the anatomical similarities between *Leidyosuchus* and *D. remensis* (Martin *et al.*, 2014); for example, in both taxa the splenial participates in the dentary symphysis, which is unknown in any other *Diplocynodon* species. However, Martin *et al.* (2014) stressed that the similarities between these taxa are non-exclusive and outlined several anatomical differences between them (as well as with *Borealosuchus*: see constrained analyses). Nonetheless, our results suggest that there is some uncertainty in the placement of *D. remensis* in *Diplocynodon*.

COMPARISONS OF *D. HANTONIENSIS* WITH OTHER *DIPLOCYNODON* SPECIES

Diplocynodon hantoniensis has a particularly broad rostrum, which among the known species of *Diplocynodon* is closest in shape to *D. darwini*, *D. deponiae, D. elavericus* and *D. muelleri*. In contrast, *D. ratelii*, *D. ungeri* and *D. tormis* have notably narrower, more pointed rostra. Furthermore, those taxa with a narrow rostrum appear to have a very modest canthus, which is absent in *D. hantoniensis*. The outline of the naris is square in *D. hantoniensis*, with straight, anteriorly diverging lateral margins. This contrasts with the strongly rounded narial margins seen in *D. ratelii*, *D. ungeri* and *D. tormis*. The presence of a deep notch situated lateral and slightly posterior to the external nares is characteristic of *Alligator*, but a similarly deep notch is observed in *D. hantoniensis* and *D. tormis*.

There is a large amount of inter- and intraspecific variation in cranial ornamentation in *Diplocynodon*. *Diplocynodon hantoniensis*, appears to be the only species with preorbital ridges (NHMUK OR 30392, CAMSM TN 907). These ridges are not as tall, narrow or elongate as those in some extant *Crocodylus* species, e.g. *C. porosus* Schneider, 1801. A small step immediately anterior to the orbits, and crossing the frontals, is absent or very weakly developed in

adult *D. hantoniensis*, as in *D. ratelii* (e.g. MNHN SG 539) and *D. darwini* (e.g. HLMD Me 7500). However, a step has been described in *D. remensis* (Martin *et al.*, 2014) and was figured in the description of *D. tormis* (Buscalioni *et al.*, 1992: fig. 2). A step was not described in *D. muelleri*, but figures in Piras & Buscalioni (2006: figs 2 and 3a) indicate its presence. The holotype of *D. deponiae* does not preserve the dorsal surface of the rostrum, and the best preserved referred specimens are broken along the frontal [e.g. SMF Me 2609, IRSNB R 261 (Delfino & Smith, 2012)]. A juvenile specimen (HLMD-Be-147) apparently lacks a step and so it is inferred to be absent in adult *D. deponiae* too.

Most species of *Diplocynodon* exhibit an ectopterygoid that contacts the walls of the posteriormost maxillary alveoli, which is the plesiomorphic condition in Crocodylia (Brochu, 1997) (Fig. 29C, D). Only *D. deponiae* (Delfino & Smith, 2012) and *D. tormis* (Buscalioni *et al.*, 1992) seem to express the alternative character state, whereby the maxilla separates the posteriormost alveoli from the ectopterygoid (Fig. 29B). Although *D. hantoniensis* also expresses the plesiomorphic condition, it shows a slight variation from other taxa. Here, the posteriormost maxillary alveolus is bordered medially by the ectopterygoid, but anteriorly the ectopterygoid narrows abruptly to an acute point, separated from the toothrow by the maxilla (Fig. 29E). This differs from other *Diplocynodon* species, e.g. *D. ratelii* (MNHN SG 539), whereby the ectopterygoid narrows gradually to an acute point (Fig. 29D). This condition resembles that seen in some *Caiman crocodilus chiapasius* (Bocourt, 1876) specimens (FMNH 73694, 73701, 73721) (Fig. 29F), which do not show the typical alligatoroid

condition. We regard this unique condition as a local autapomorphy of *D. hantoniensis*.

In all extant alligatorids, the squamosal and parietal have a large sutural contact on the posterior wall of the supratemporal fenestra, anterior to the orbitotemporal canal (Brochu, 1997) (Fig. 30A). In contrast, extant *Crocodylus*, *Tomistoma* and *Gavialis* express an alternative condition, in which the quadrate widely separates the squamosal and parietal, forming the floor of the orbitotemporal foramen (Fig. 30B). *Diplocynodon ratelii* possesses an intermediate condition, in which the squamosal approaches the parietal, but a narrow wedge of the quadrate separates them (Brochu, 1997) (Fig. 30C). Previously, this character was scored as unknown in *D. hantoniensis* (Brochu *et al.*, 2012; Martin *et al.*, 2014), but close inspection of the walls of the supratemporal fenestra in NHMUK OR 30393 reveals that the intermediate condition is also present in *D. hantoniensis* (Fig. 30D). This condition is now recorded in almost all *Diplocynodon* species, except *D. ungeri*, in which it is unknown, and *D. elavericus* (Martin, 2010), which seems to express the derived alligatorid condition. However, in the latter species, the supratemporal fenestra is poorly preserved. Outside of *Diplocynodon*, this condition is known only in *Brachychampsa montana*, so this feature could be a local autapomorphy of *Diplocynodon*.

Flexure of the ectopterygoid–pterygoid suture is retained into adulthood in *D. hantoniensis* (Fig. 8A). This feature was previously regarded as an unambiguous synapomorphy of crown caimans (Brochu, 1999) (Fig. 8B). However, it appears to occur more widely, as it is present in *Allodaposuchus precedens* (Martin *et al.*, 2016), *Thoracosaurus*
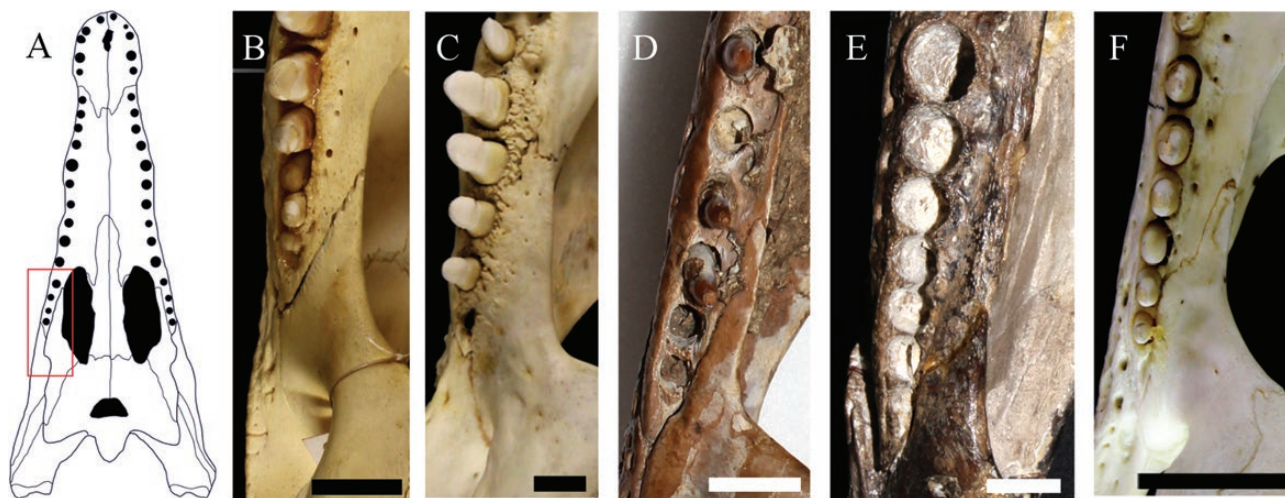

Figure 29. Comparison of the ectopterygoid–maxilla suture near the posterior maxillary toothrow in several crocodylians. A, generalized crocodylian skull in ventral view, showing the enlarged area in B–F; B, *Alligator mississippiensis* (Daudin, 1802) (AMNH 71621); C, *Crocodylus rhombifer* Cuvier, 1807 (AMNH R 154087); D, *Diplocynodon ratelii* (MNHN SG 539); E, *Diplocynodon hantoniensis* (NHMUK OR 30392); F, *Caiman crocodilus chiapasius* (FMNH 73694). Scale bar = 2 cm.

Figure 30. Comparisons of the posterior wall of the supratemporal fenestra in several crocodylians. A–C, enlarged left supratemporal fenestrae of *Alligator mississippiensis* (NHMUK uncatalogued) (A), *Crocodylus porosus* (NHMUK uncatalogued) (B) and *Diplocynodon ratelii* (MNHN SG 539) (C). D, both supratemporal fenestrae of *Diplocynodon hantoniensis* (NHMUK OR 30393). Abbreviations: pa, parietal; pr, prootic; qd, quadrate; sq, squamosal. White arrows indicate the position of the quadrate-parietal suture. Scale bar = 1 cm.

macrorhynchus de Blainville, 1855 [based on character scores in Brochu (1999)] and possibly in *D. deponiae* (Delfino & Smith, 2012). In the latter case, Delfino & Smith (2012) expressed some doubt that IRSNB 261, which formed the basis of their description, was a mature individual of *D. deponiae*. As a result, we cannot be confident that ectopterygoid–pteryoid flexure is retained into adulthood in *D. deponiae*, and thus we re-scored this character as missing in this taxon. All other species of *Diplocynodon* lack the ectopterygoid–pterygoid flexure. The condition in *D. hantoniensis* can only be confidently observed in a large isolated pair of pterygoids (NHMUK OR 30251). Here, the condition is slightly different to that of *Caiman*, which has a large lateral process of the pterygoid immediately posterior

to the suborbital fenestra. In contrast, *D. hantoniensis* also has an acute process of the ectopterygoid in the pterygoid, which we consider an autapomorphy of the species (Fig. 8A).

The choanae of *D. hantoniensis* are heart-shaped, resulting from a posterior projection of the pterygoid, which aligns with the recessed choanal septum (Figs 6B, 31A). Furthermore, they are ornamented with an anterolaterally directed ridge on each side. This ridge is even developed in juvenile specimens, becoming a prominent ventrally directed lamina bound by a sulcus at maturity. Heart-shaped choanae with anterolaterally developed ridges are also present in *D. remensis* (Martin *et al.*, 2014: fig 6K) and, tentatively, in *D. ratelii* (MNHN SG 539) (Fig. 31D). The lateral walls of
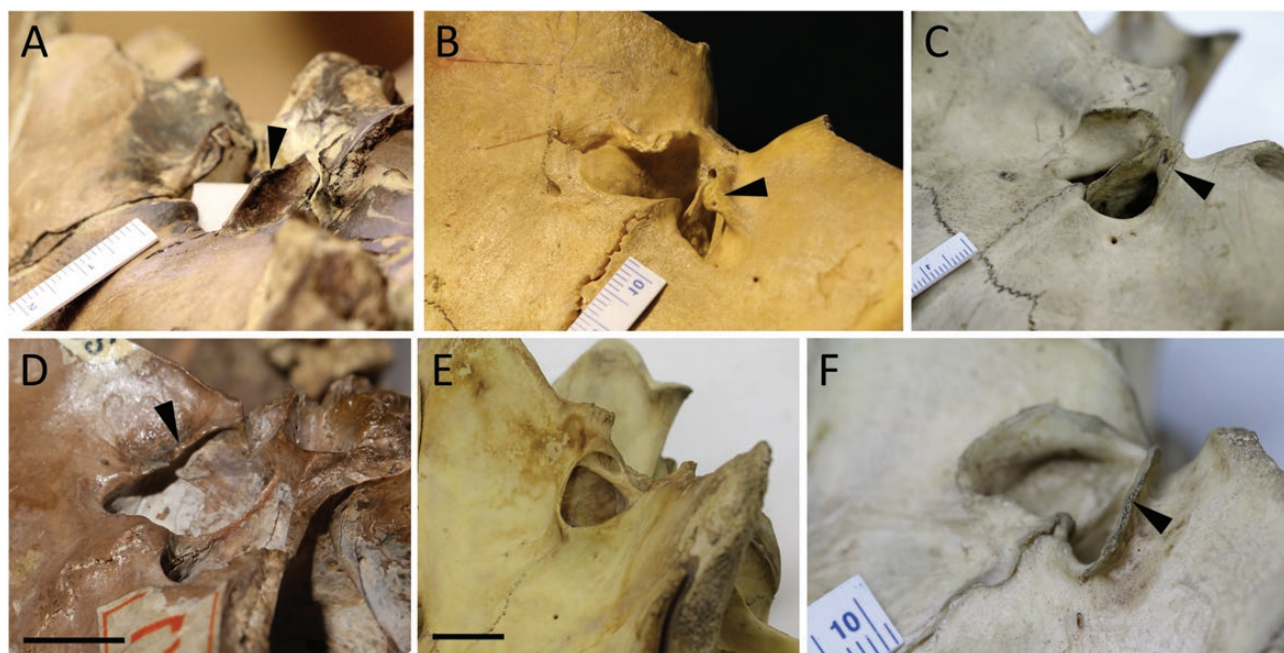
Figure 31. Comparisons between the structure of the choanae, in ventrolateral view, in: A, *Diplocynodon hantoniensis* (CAMSM TN 907); B, *Caiman yacare* (MACN I-15144-3603); C, *Alligator mississippiensis* (NHMUK 1873.2.21.1); D, *Diplocynodon ratelii* (MNHN SG 539); E, *Crocodylus intermedius* Graves, 1819 (NHMUK 1851.8.25.29); F, *Paleosuchus trigonatus* (Schneider, 1801) (NHMUK 1868.10.8.1). Scale bar = 2 cm.

the choana are broken off in the latter specimen, but deep sulci similar to *D. hantoniensis* are suggestive of a similar ridge. Wu *et al.* (2001) also described ridges lateral to the choana in *Leidyosuchus canadensis* Lambe, 1907, although restricted to some of the largest individuals. This contrasts with the condition in *D. hantoniensis*, in which they appear throughout ontogeny. The ridges in *D. hantoniensis*, *D. remensis* and *D. ratelii* appear homologous to those of several caimanines (Figs 31B, F), although the morphology is clearly different. In extant *Caiman* (Fig. 31B), these ridges are shorter, restricted to the posterolateral choanal margins and commonly folded medially into the choana. In *Paleosuchus* (Fig. 31F), ridges can encircle the choana and become almost completely everted. The ridges are also similar to those developed in *Alligator* (Fig. 31C), but in that taxon they form a near continuous posterior wall to the choana and do not extend very far anteriorly.

THE POTENTIAL FOR NEW PHYLOGENETIC CHARACTERS FROM THE POSTCRANIA

Postcranial character sampling is low in Crocodylia, as is the case for all of Crocodylomorpha (Godoy *et al.*, 2016; Mannion *et al.*, 2019). For example, in the data matrix used here, just 46 of 187 characters (25%) represent the postcranial skeleton. The dearth of postcranial

characters has been based on the assumption that the crocodylian postcranial skeleton is morphologically conservative, being less phylogenetically informative than cranial and mandibular components (see: Godoy *et al.*, 2016). However, recent studies of axial and appendicular skeletal components in extant crocodylians have demonstrated that there are broad differences in crocodylian postcrania, which have yet to be incorporated into phylogenetic studies (Chamero *et al.*, 2013; Iijima *et al.*, 2018). Furthermore, recent studies of notosuchian (Pol *et al.*, 2012; Godoy *et al.*, 2016), basal neosuchian (Martin *et al.*, 2016) and crocodylian (Iijima & Kobayashi, 2019) anatomy have started to demonstrate that there is a potentially richer suite of postcranial characters, and that these might impact upon crocodylomorph phylogenetic relationships.

The quantity and quality of preserved postcranial material belonging to *Diplocynodon hantoniensis* affords comparisons with extant and fossil taxa, and the identification of potential postcranial characters. In particular, the appendicular material is especially well preserved and represented by several ontogenetic stages, allowing us to distinguish between interspecific and ontogenetic variation. In addition to the recognition of numerous muscle scars (see Description), below we briefly outline a number of potential new characters pertaining to the appendicular skeleton.

Figure 32. Comparisons of humeral torsion and axial rotation of the proximal extremity of the humerus in Crocodylia, in medial (left) and ventral (right) views. The left humerus of *Crocodylus porosus* (QM J 48127) (A, B), *Kambara sp.* (mirror image of the right humerus) (QM F 56060) (C, D), *Diplocynodon hantoniensis* (NHMUK OR 30206) (E, F), *Borealosuchus sternbergii* (USNM 6533) (G, H), *Asiatosuchus germanicus* (SMF Me 1801) (I, J) and *Gavialis gangeticus* (Gmelin, 1789) mirror image of the right humerus (USNM 576261) (K, L). Abbreviations: dpc, deltopectoral crest. Arrows point to the apex of the deltopectoral crest. Vertical cross bars on arrows show the potion of the lateral edge of the humerus. All scale bars = 2 cm.

Only two humeral characters appear regularly in phylogenetic analyses of crown group crocodylians. These pertain to the shape of the deltopectoral crest and the presence of a separate or single common insertion for M. teres major and M. dorsalis scapulae (Brochu *et al.*, 2012: C27 and C28). In addition, character 36 in the matrix used herein describes the slenderness and relative length of the forelimb and hindlimb. Observations of *D. hantoniensis* and other crocodylians have led us to recognize two other potentially significant features in the humerus.

Stein *et al.* (2012) recognized differences in humeral torsion between the early Eocene Australian mekosuchine, *Kambara*, with that of *Crocodylus johnstoni* Krefft, 1873 and *C. porosus*. Humeral torsion describes the dorsoventral offset of the proximal and distal extremities (i.e. the metaphysis and epiphysis) of the humerus, which is most noticeable in medial view. A high degree of torsion results in a strongly sigmoidal outline of the humerus (Fig. 32A), whereas a low degree of torsion results in a relatively straight outline (Fig. 32C). Stein *et al.* (2012) noted that humeral torsion appears to be associated with a rotation of the lateral margin of the proximal extremity and resultant medial rotation of the deltopectoral crest (i.e. axial rotation of the proximal extremity). This results in movement of the apex of the deltopectoral crest from the lateral edge, to the centre of the humerus, when viewed ventrally (Fig. 32B). This also exposes the ventral surface of the proximal extremity in medial view. Whereas these two features appear to be linked to one another in *Crocodylus* and *Kambara*, an examination of a larger sample of crocodylians reveals that these features are not always associated. For example, *D. hantoniensis* exhibits a high degree of dorsoventral offset of the proximal and distal humeral extremities, without the axial rotation of the proximal end (Fig. 32E, F). This might be the plesiomophic condition in Crocodylia, as it is observed in the stem brevirostrine *Borealosuchus sternbergii* (Gilmore, 1910) (USNM 6533) (Fig. 32G, H) and the basal crocodyloid *Asiatosuchus germanicus* Berg, 1966 (SMF Me 1801) (Fig. 32I, J). The same condition is also observed in a number of other alligatoroids, e.g. *D. ratelii* (MNHN SG 628), *Alligator* (AMNH 71621) and *Caiman* (AMNH 97300). In contrast, *Gavialis* appears to lack significant dorsoventral offset of the proximal and distal extremities. When viewed medially, the distal half of the humerus of *Gavialis* is almost straight (Fig. 32K). However, the proximal end, beginning around the level of the deltopectoral crest, shows extreme axial rotation (Fig. 32L).

A comparison of the humeri of *C. porosus* at different ontogenetic stages reveals variation in the second character (axial rotation of the proximal extremity) (Fig. 33A, B). Humeral torsion appears relatively consistent in this growth series (Fig. 33C, D), but the juvenile specimens show less axial rotation of the proximal extremity than adult specimens. As a result, the latter should be compared only between adult specimens.
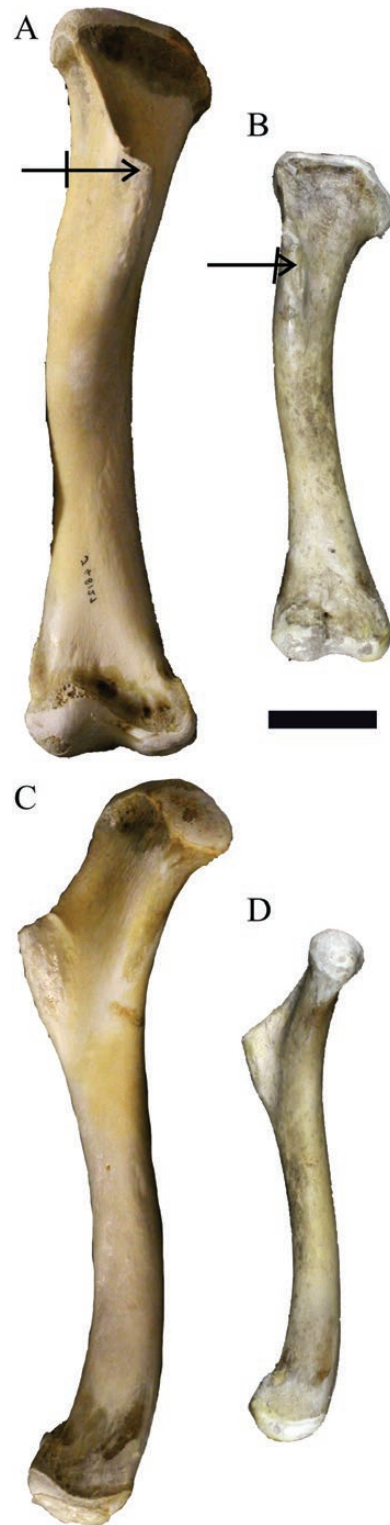

Figure 33. Comparisons between the humeri of adult *Crocodylus porosus* (QM J48127) (mirror image of left humerus) (A, C) and juvenile *Crocodylus porosus* (AMNH 7115) (B, D). Arrows point to the apex of the deltopectoral crest. Vertical cross bars on arrows show the potion of the lateral edge of the humerus. All scale bars = 2 cm.

CONCLUSIONS

The basal alligatoroid *Diplocynodon hantoniensis* from the late Eocene (Priabonian) of southern England is fully described for the first time in 150 years. This includes a detailed description of the often neglected postcranial skeleton, including a reconstruction of numerous muscle attachment sites, allowing future comparisons with other crocodylians. We also recognize humeral torsion and axial rotation of the proximal humeral extremity as two new independent characters, which show notable variation in Crocodylia that can be discretized in future phylogenetic analyses. *Diplocynodon hantoniensis* can be diagnosed by a unique combination of characters and its geographic range is currently restricted to the late Eocene of the UK. Using a revised phylogenetic data matrix, including all valid species of *Diplocynodon*, we show that implied and extended implied weighting improves tree resolution producing largely congruent tree topologies with equal weighted trees.

ACKNOWLEDEGEMENTS

REFERENCES

Benton MJ, **Spencer PS. 1995.** *Fossil reptiles of Great Britain*. London: Chapman & Hall, 386.

Blanco A, Fortuny J, Vicente A, Luján AH, García-Marçà JA, Sellés A. 2015. A new species of Allodaposuchus (Eusuchia, Crocodylia) from the Maastrichtian (Late Cretaceous) of Spain: phylogenetic and paleobiological implications. *PeerJ* **3**: e1171.

Bona P, **Desojo JB. 2011.** Osteology and cranial musculature of *Caiman latirostris* (Crocodylia: Alligatoridae). *Journal of Morphology* **272**: 780–795.

Bona P, Ezcurra MD, Barrios F, Fernandez Blanco MV. 2018. A new Palaeocene crocodylian from southern Argentina sheds light on the early history of caimanines. *Proceedings of the Royal Society B* **285**: 20180843.

Brazeau MD. 2011. Problematic character coding methods in morphology and their effects. *Biological Journal of the Linnean Society* **104**: 489–498.

Brinkmann W, **Rauhe M. 1998.** *Diplocynodon ratelii* POMEL, 1847 (Crocodylia, Leidyosuchidae) aus dem Unter-Oligozän von Céreste (Südfrankreich). *Neues Jahrbuch für Geologie und Paläontologie, Abhandlungen* **209**: 295–321.

Brochu CA. 1997. A review of '*Leidyosuchus*' (Crocodyliformes, Eusuchia) from the Cretaceous through Eocene of North America. *Journal of Vertebrate Paleontology* **17**: 679–697.

Brochu CA. 1999. Phylogenetics, taxonomy, and historical biogeography of Alligatoroidea. *Journal of Vertebrate Paleontology* **19**: 9–100.

Brochu CA. 2011. Phylogenetic relationships of *Necrosuchus ionensis* Simpson, 1937 and the early history of caimanines. *Zoological Journal of the Linnean Society* **163**: S228–S256.

Brochu CA, **Storrs GW. 2012.** A giant crocodile from the Plio-Pleistocene of Kenya, the phylogenetic relationships of Neogene African crocodylines, and the antiquity of Crocodylus in Africa. *Journal of Vertebrate Paleontology* **32**: 587–602.

Brochu CA, **Parris DC**, **Grandstaff BS**, **Denton RK Jr**, **Gallagher WB. 2012.** A new species of *Borealosuchus* (Crocodyliformes, Eusuchia) from the Late Cretaceous–Early Paleogene of New Jersey. *Journal of Vertebrate Paleontology* **32**: 105–16.

Buscalioni AD, **Sanz JL**, **Casanovas ML. 1992.** A new species of the eusuchian crocodile *Diplocynodon* from the Eocene of Spain. *Neues Jahrbuch für Geologie und Paläontologie, Abhandlungen* **187**: 1–29.

Chamero B, **Buscalioni AD**, **Marugán-Lobón J. 2013.** Pectoral girdle and forelimb variation in extant Crocodylia: the coracoid–humerus pair as an evolutionary module. *Biological Journal of the Linnean Society* **108**: 600–618.

Chandler MEJ. 1961. Flora of the Lower Headon Beds of Hampshire and the Isle of Wight. *Bulletin of the British Museum (Natural History), Geology Series* **5**: 93–157.

Chippindale PT, **Wiens JJ. 1994.** Weighting, partitioning, and combining characters in phylogenetic analysis. *Systematic Biology* **43**: 278–87.

Cray PE. 1973. Marsupialia, Insectivora, Primates, Creodonta and Carnivora from the Headon Beds (Upper Eocene) of southern England. *Bulletin of the British Museum (Natural History), Geology Series* **23**: 1–102.

Daley B. 1999. Palaeogene sections in the Isle of Wight. A revision of their description and significance in the light of research undertaken over recent decades. *Tertiary Research* **19**: 1–69.

Delfino M, **Smith T. 2012.** Reappraisal of the morphology and phylogenetic relationships of the Middle Eocene alligatoroid *Diplocynodon deponiae* (Frey, Laemmert, and Riess, 1987) based on a three-dimensional specimen. *Journal of Vertebrate Paleontology* **32**: 1358–1369.

Delfino M, **Codrea V**, **Folie A**, **Dica P**, **Godefroit P**, **Smith T. 2008.** A complete skull of *Allodaposuchus precedens* Nopcsa, 1928 (Eusuchia) and a reassessment of the morphology of the

taxon based on the Romanian remains. *Journal of Vertebrate Paleontology* **28:** 111–122.

Díaz Aráez JL, **Delfino M**, **Luján AH**, **Fortuny J**, **Bernardini F**, **Alba DM. 2017.** New remains of *Diplocynodon* (Crocodylia: Diplocynodontidae) from the Early Miocene of the Iberian Peninsula. *Comptes Rendus Palevol* **16:** 12–26.

Edwards N, **Daley B. 1997.** Stratigraphy of the Totland Bay Member (Headon Hill Formation, Late Eocene) at Hordle Cliff, Hampshire, southern England. *Tertiary Research* **18:** 35–50.

Farris JS. 1969. A successive approximations approach to character weighting. *Systematic Biology* **18:** 374–85.

Frey E, **Laemmert A**, **Riess J. 1987.** *Baryphracta deponiae* n. g. n. sp. (Reptilia, Crocodylia), ein neues Krokodil aus der Grube Messel bey Darmstadt (Hessen, Bundesrepublik Deutschland). *Neues Jahrbuch für Geologie und Paläontologie, Monatshefte* **1987:** 15–26.

Ginsburg L, **Bulot C. 1997.** Les *Diplocynodon* (Reptilia, Crocodylia) de l'Orléanien (Miocène inférieur à moyen) de France. *Geodiversitas* **19:** 107–128.

Godoy PL, **Bronzati M**, **Eltink E**, **Júlio CDA**, **Cidade GM**, **Langer MC**, **Montefeltro FC. 2016.** Postcranial anatomy of *Pissarrachampsa sera* (Crocodyliformes, Baurusuchidae) from the Late Cretaceous of Brazil: insights on lifestyle and phylogenetic significance. *PeerJ* **4:** e2075.

Goloboff PA. 1993. Estimating character weights during tree search. *Cladistics* **9:** 83–91.

Goloboff PA. 1995. Parsimony and weighting: a reply to Turner and Zandee. *Cladistics* **11:** 91–104.

Goloboff PA. 2014. Extended implied weighting. *Cladistics* **30:** 260–272.

Goloboff PA, **Carpenter JM**, **Arias JS**, **Esquivel DR. 2008.** Weighting against homoplasy improves phylogenetic analysis of morphological data sets. *Cladistics* **24:** 758–773.

Goloboff PA, **Torres A**, **Arias JS. 2018.** Weighted parsimony outperforms other methods of phylogenetic inference under models appropriate for morphology. *Cladistics* **34:** 407–437.

Gramann E. 1958. Der Crocodilide *Diplocynodon hantoniensis* (Wood) aus dem unteroligozänen Melanienton Niederhessens. *Notizblatt der Hessischen Landes-Amte Bodenforschung* **86:** 77–78.

Hastings AK, **Hellmund M. 2015.** Rare in situ preservation of adult crocodylian with eggs from the Middle Eocene of Geiseltal, Germany. *Palaios* **30:** 446–461.

Hastings, Marchioness of. 1848. On the freshwater Eocene beds of the Hordle Cliff, Hants. *Report of the British Association for the Advancement of Science* **17:** 63–64.

Hastings, Marchioness of. 1853. On the Tertiary Beds of Hordwell, Hampshire. *Philosophical Magazine and Journal of Science, Fourth Series* **6:** 1–11.

Haszprunar G. 1998. Parsimony analysis as a specific kind of homology estimation and the implications for character weighting. *Molecular Phylogenetics and Evolution* **9:** 333–339.

Hoffstetter R. 1942. Sur les restes de Sauria du Nummulitique Européen rapportés à la famille Iguanidae. *Bulletin du Muséum National d'Histoire Naturelle de Paris* **14:** 233–240.

Hoffstetter R, **Gasc JP. 1969.** Vertebrae and ribs of modern reptiles. In: Gans C, Bellairs A-d'A, Parsons TS, eds. *Biology of the Reptilia, Vol. 1. Morphology A*. London and New York: Academic Press, 201–310.

Holliday CM, **Tsai HP**, **Skiljan RJ**, **George ID**, **Pathan S. 2013.** A 3D interactive model and atlas of the jaw musculature of Alligator mississippiensis. *PLoS One* **8:** e62806.

Holman JA, **Harrison DL. 2003.** A new helmeted frog of the genus *Thaumastosaurus* from the Eocene of England. *Acta Palaeontologica Polonica* **48:** 157–160.

Holman JA, **Harrison DL**, **Ward DJ. 2006.** Late Eocene snakes from the Headon Hill Formation, southern England. *Cainozoic Research* **5:** 51–62.

Hooker JJ. 2014. New postcranial bones of the extinct mammalian family Nyctitheriidae (Paleogene, UK): primitive euarchontans with scansorial locomotion. *Palaeontologia Electronica* **17:** 47A.

Hooley RW. 1905. On a new tortoise from the Lower Headon Beds of Hordwell, *Nicoria headonensis* sp. nov. *Geological Magazine (Decade V)* **2:** 66–68.

Huxley T. 1859. On the dermal armor of *Crocodilus hastingsiae*. *Quarterly Journal of the Geological Society* **15:** 678–680.

Iijima M, **Kobayashi Y. 2019.** Mosaic nature in the skeleton of East Asian crocodylians fills the morphological gap between 'Tomistominae' and Gavialinae. *Cladistics* **0:** 1–10.

Iijima M, **Kubo T**, **Kobayashi Y. 2018.** Comparative limb proportions reveal differential locomotor morphofunctions of alligatoroids and crocodyloids. *Royal Society Open Science* **5:** 171774.

Kälin JA. 1936. *Hispanochampsa mülleri* nov. gen. nov. spec., ein neuer Crocodilide aus dem unteren Oligocaen von Tárrega (Catalonien). *Abhandlungen Schweizerischen Palaeontologischen Gesellschaft* **58:** 1–40.

Källersjö M, **Farris JS**, **Chase MW**, **Bremer B**, **Fay MF**, **Humphries CJ**, **Petersen G**, **Seberg O**, **Bremer K. 1998.** Simultaneous parsimony jackknife analysis of 2538rbcL DNA sequences reveals support for major clades of green plants, land plants, seed plants and flowering plants. *Plant Systematics and Evolution* **213:** 259–87.

Karl HV, **Müller A. 2008.** New fossil reptile material (Reptilia: Chelonii, Crocodylia) from the Lower Oligocene of Borken (Central Germany: Hesse). *Studia Geologica Salmanticensia* **44:** 41–58.

Klinkhamer AJ, **Wilhite DR**, **White MA**, **Wroe S. 2017.** Digital dissection and three-dimensional interactive models of limb musculature in the Australian estuarine crocodile (*Crocodylus porosus*). *PLoS ONE* **12:** e0175079.

Kotsakis T, **Delfino M**, **Piras P. 2004.** Italian Cenozoic crocodilians: taxa, timing and palaeobiogeographic implications. *Paleogeography, Paleoclimatology, Palaeoecology* **210:** 67–87.

Ludwig R. 1877. Fossile Crocodiliden aus der Tertiärformation des Mainzer Beckens. *Palaeontographica Supplement* **3:** 1–52.

Lydekker R. 1887. Note on the Hordwell and other crocodilians. *Geological Magazine* **4:** 307–312.

Lydekker R. 1888. *Catalogue of the fossil Reptilia and Amphibia in the British Museum (Natural History). Part I.* London: British Museum (Natural History), 309.

Mannion PD, **Chiarenza AA**, **Godoy PL**, **Cheah YN. 2019.** Spatiotemporal sampling patterns in the 230 million year fossil record of terrestrial crocodylomorphs and their impact on diversity. *Palaeontology*. Doi: 10.1111/pala.12419.

Martin JE. 2010. A new species of *Diplocynodon* (Crocodylia, Alligatoroidea) from the Late Eocene of the Massif Central, France, and the evolution of the genus in the climatic context of the Late Palaeogene. *Geological Magazine* **147:** 596–610.

Martin JE, **Gross M. 2011.** Taxonomic clarification of *Diplocynodon* Pomel, 1847 (Crocodilia) from the Miocene of Styria, Austria. *Neues Jahrbuch für Geologie und Paläontologie, Abhandlungen* **261:** 177–193.

Martin JE, **Smith T**, **Lapparent de Broin F**, **Escuillié F**, **Delfino M. 2014.** Late Palaeocene eusuchian remains from Mont de Berru, France, and the origin of the alligatoroid *Diplocynodon*. *Zoological Journal of the Linnean Society* **172:** 867–891.

Martin JE, **Delfino M**, **Smith T. 2016.** Osteology and affinities of Dollo's goniopholidid (Mesoeucrocodylia) from the Early Cretaceous of Bernissart, Belgium. *Journal of Vertebrate Paleontology* **36:** e1222534.

von Meyer H. 1857. Beiträge zur näheren Kenntniss fossiler Reptilien. *Neues Jahrbuch für Mineralogie, Geognosie, Geologie und Petrefaktenkunde* 532–543.

Meers M. 2003. Crocodylian forelimb musculature and its relevance to Archosauria. *The Anatomical Record Part A* **274**: 891–916.

Mook CC. 1960. Diplocynodon remains from the Bridger beds of Wyoming. *American Museum Novitates* **2007**: 1–4.

Mook CC, **Quackenbush LS. 2007.** *Diplocynodon* remains from the Bridger beds of Wyoming. *American Museum Novitates* **2007:** 1–4.

Norell MA, **Clark JM. 1990.** A reanalysis of *Bernissartia fagesii*, with comments on its phylogenetic position and its bearing on the origin and diagnosis of the Eusuchia. *Bulletin – Institut Royal des Sciences Naturelles de Belgique. Sciences de la Terre* **60:** 115–128.

Owen R. 1848. On the fossils obtained by the Marchioness of Hastings from the freshwater Eocene beds of the Hordle Cliffs. *Report of the British Association for the Advancement of Science* **17:** 65–66.

Owen R. 1850. Monograph on the fossil Reptilia of the London Clay, and of the Bracklesham and other Tertiary Beds. *Monograph of the Palaeontographical Society London* **3:** 1–50.

Pictet FJ, **Gaudin C**, **de La Harpe P. 1857.** Mémoire sur les animaux vertébrés trouvés dans le terrain sidérolitique du Canton de Vaud et appartenant à la faune Eocène. *Matériaux pour la Paléontologie Suisse, Ser. 1* **2:** 1–120.

Piras P, **Buscalioni AD. 2006.** *Diplocynodon muelleri* comb. nov., an Oligocene diplocynodontine alligatoroid from Catalonia (Ebro Basin, Lleida Province, Spain). *Journal of Vertebrate Paleontology* **26:** 608–620.

Pol D, **Leardi JM**, **Lecuona A**, **Krause M. 2012.** Postcranial anatomy of *Sebecus icaeorhinus* (Crocodyliformes, Sebecidae) from the Eocene of Patagonia. *Journal of Vertebrate Paleontology* **32:** 328–354.

Pomel A. 1847. Note sur les animaux fossiles découverts dans le département de l'Allier. *Bulletin de la Société Géologique de France* **4:** 378–385.

Pomel A. 1853. *Catalogue méthodique et descriptif des vértébres fossiles découverts dans le bassin hydrographique supérieur de la Loire et surtout dans la vallée de son affluent principal l´Allier*. Paris: J.-B. Bailliére, 193.

Prangner E. 1845. Über *Enneodon ungeri*, ein neues Genus fossiler Saurieraus den Tertiär-Gebilden zu Wies im Marburger Kreise Steiermark's. *Steiermärkische Zeitschrift, Neue Folge* **8:** 114–139.

Puértolas-Pascual E, **Blanco A**, **Brochu CA**, **Canudo JI. 2016.** Review of the Late Cretaceous–Early Paleogene crocodylomorphs of Europe: extinction patterns across the K–PG boundary. *Cretaceous Research* **57:** 565–590.

Roos J, **Aggarwal RK**, **Janke A. 2007.** Extended mitogenomic phylogenetic analyses yield new insight into crocodylian evolution and their survival of the Cretaceous–Tertiary boundary. *Molecular Phylogenetics and Evolution* **45:** 663–673.

Seeley HG. 1876. On remains of *Emys hordwellensis* (Seeley) from the Lower Hordwell Beds in the Hordwell Cliff, contained in the Woodwardian Museum of the University of Cambridge. *Quarterly Journal of the Geological Society* **32:** 445–450.

Stein M, **Salisbury SW**, **Hand SJ**, **Archer M**, **Godthelp H. 2012.** Humeral morphology of the Early Eocene mekosuchine crocodylian Kambara from the Tingamarra Local Fauna southeastern Queensland, Australia. *Alcheringa: an Australasian Journal of Palaeontology* **36:** 473–486.

Tschopp E, **Mateus O**, **Benson RB. 2015.** A specimen-level phylogenetic analysis and taxonomic revision of Diplodocidae (Dinosauria, Sauropoda). *PeerJ* **3:** e857.

Tschopp E, **Tschopp FA**, **Mateus O. 2018.** Overlap Indices: tools to quantify the amount of anatomical overlap among groups of incomplete terminal taxa in phylogenetic analyses. *Acta Zoologica* **99:** 169–176.

Tschopp E, Upchurch P. 2019. The challenges and potential utility of phenotypic specimen-level phylogeny based on maximum parsimony. *Earth and Environmental Science Transactions of The Royal Society of Edinburgh*. doi:10.1017/S1755691018000877

Tumarkin-Deratzian AR, **Vann DR**, **Dodson P. 2007.** Growth and textural ageing in long bones of the American alligator *Alligator mississippiensis* (Crocodylia: Alligatoridae). *Zoological Journal of the Linnean Society* **150:** 1–39.

Turner H, **Zandee R. 1995.** The behaviour of Goloboff's tree fitness measure F. *Cladistics* **11:** 57–72.

Vaillant L. 1872. Étude zoologique sur les crocodiliens fossiles tertiairesde Saint-Gérand-le-Puy. *Annales des Sciences Géologiques* **3:** 1–57.

Vignaud P, **Brunet M**, **Guevel B**, **Jehenne Y. 1996.** Un crâne de *Diplocynodon* (Crocodylomorpha, Alligatoridae) de l'Oligocène inférieur de Dordogne (France). *Comptes Rendus de l'Académie des Sciences Paris, Série 2a* **322:** 595–601.

Wang YY, **Sullivan C**, **Liu J. 2016.** Taxonomic revision of *Eoalligator* (Crocodylia, Brevirostres) and the paleogeographic origins of the Chinese alligatoroids. *PeerJ* **4:** e2356.

Weems RE, **Grimsley GJ. 1999.** Early Eocene vertebrates and plants from the Fisher/Sullivan site (Nanjemoy Formation) Stafford County, Virginia. *Commonwealth of Virginia, Department of Mines, Minerals and Energy, Division of Mineral Resources* **152:** 1–159.

Wood S. 1844. Record of the discovery of an alligator with several new Mammalia in the freshwater strata at Hordwell. *Annals and Magazine of Natural History* **14:** 349–351.

Wood S. 1846. On the discovery of an alligator and of several new Mammalia in the Hordwell Cliff; with observations upon the geological phenomena of that locality. *The London Geological Journal, and Record of Discoveries in British and Foreign Paleontology* **1:** 1–7.

Woodward AS. 1885. On the literature and nomenclature of British fossil Crocodilia. *Geological Magazine* **2:** 496–510.

Wu, X, Russell, AP, Brinkman, DB. 2001. A review of Leidyosuchus canadensis Lambe, 1907 (Archosauria: Crocodylia) and an assessment of cranial variation based upon new material. *Canadian Journal of Earth Sciences* **38**: 1665–1687.

Wright T. 1851. A stratigraphical account of the section at Hordwell, Beacon and Barton Cliffs, on the coast of Hampshire. *Annals and Magazine of Natural History (Series 2)* **7:** 433–446.

APPENDIX

Changes to the character scores of *Diplocynodon hantoniensis* from Martin *et al.* (2014) to this study: C7 (1→?), C9 (1→?), C17 (1→2), C22 (0→?), C40 (1→?), C43 (1→?), C49 (1→0), C62 (1→0), C65 (0→1), C66 (0→1), C84 (?→1), C86 (?→1), C90 (?→0), C94 (0→1), C96 (?→0), C125 (0→1), C144 (?→1), C146 (0→1), C147 (1→2), C162 (0→1), C173 (?→0).

SUPPORTING INFORMATION

Additional Supporting Information may be found in the online version of this article at the publisher's web-site.

Supporting Information 1. Character taxon matrix nex file.
Supporting Information 2. Character taxon matrix TNT file.
Supporting Information 3. Character list.